

DEVELOPMENT AND COMPARISON OF THE EXTENDED KALMAN FILTER  
AND UNSCENTED KALMAN FILTER FOR BOTH TIGHTLY COUPLED AND  
LOOSELY COUPLED INS/GNSS INTEGRATION BY USING MEMS IMU

A THESIS SUBMITTED TO  
THE GRADUATE SCHOOL OF NATURAL AND APPLIED SCIENCES  
OF  
MIDDLE EAST TECHNICAL UNIVERSITY

BY

ONUR GÜREŞ

IN PARTIAL FULFILLMENT OF THE REQUIREMENTS  
FOR  
THE DEGREE OF MASTER OF SCIENCE  
IN  
ELECTRICAL AND ELECTRONICS ENGINEERING

SEPTEMBER 2019



Approval of the thesis:

**DEVELOPMENT AND COMPARISON OF THE EXTENDED KALMAN  
FILTER AND UNSCENTED KALMAN FILTER FOR BOTH TIGHTLY  
COUPLED AND LOOSELY COUPLED INS/GNSS INTEGRATION BY  
USING MEMS IMU**

submitted by **ONUR GÜREŞ** in partial fulfillment of the requirements for the degree  
of **Master of Science in Electrical and Electronics Engineering Department,**  
**Middle East Technical University** by,

Prof. Dr. Halil Kalıpçılar  
Dean, Graduate School of **Natural and Applied Sciences**

\_\_\_\_\_

Prof. Dr. İlkay Ulusoy  
Head of Department, **Electrical and Electronics Engineering**

\_\_\_\_\_

Prof. Dr. Buyurman Baykal  
Supervisor, **Electrical and Electronics Engineering, METU**

\_\_\_\_\_

**Examining Committee Members:**

Prof. Dr. Engin Tuncer  
Electrical and Electronics Engineering Department, METU

\_\_\_\_\_

Prof. Dr. Buyurman Baykal  
Electrical and Electronics Engineering Department, METU

\_\_\_\_\_

Prof. Dr. Umut Orguner  
Electrical and Electronics Engineering Department, METU

\_\_\_\_\_

Prof. Dr. Kemal Leblebicioğlu  
Electrical and Electronics Engineering Department, METU

\_\_\_\_\_

Prof. Dr. Sinan Gezici  
Electrical and Electronics Eng. Dept., Bilkent University

\_\_\_\_\_

Date: 04.09.2019

**I hereby declare that all information in this document has been obtained and presented in accordance with academic rules and ethical conduct. I also declare that, as required by these rules and conduct, I have fully cited and referenced all material and results that are not original to this work.**

Name, Surname: Onur Güreş

Signature:

## **ABSTRACT**

### **DEVELOPMENT AND COMPARISON OF THE EXTENDED KALMAN FILTER AND UNSCENTED KALMAN FILTER FOR BOTH TIGHTLY COUPLED AND LOOSELY COUPLED INS/GNSS INTEGRATION BY USING MEMS IMU**

Güreş, Onur

M.S., Department of Electrical and Electronics Engineering

Supervisor: Prof. Dr. Buyurman Baykal

September 2019, 119 pages

Navigation technologies evolved with improvements for the last two decades. Navigation devices are easy to buy and satellite navigation is available all around the World. The key part for designing a navigation system is the algorithms used inside of it. This thesis focuses on the comparison between the proven reference unit and author designed navigation algorithms by using same IMU and GNSS inside of the reference unit with collected field data. In this thesis, both Extended and Unscented Kalman Filter estimation techniques were developed by applying tightly and loosely coupling methods in MATLAB. As the reference unit NovAtel SPAN IGM-A1 was selected. This unit is a self-proven unit which also has one of the market's best integration algorithm SPAN. The unit includes ADIS-16488 MEMS IMU and a NovAtel OEM6 GNSS Receiver with single antenna. The selected standalone units for developed algorithms' confirmation were also ADIS-16488 as MEMS IMU and NovAtel OEM6 GNSS receiver. Hence, a comparison between the reference unit and the author designed filters was made. Car navigation trial results were compared for

different estimation and integration methods. Results showed that tightly coupled EKF was the best among developed algorithms. The results also showed that tightly coupling integration outperformed both UKF and EKF loosely coupled INS/GNSS integration. The instability and effects of scale factors on UKF were also inspected.

Keywords: INS, GNSS, Kalman Filter, EKF, UKF, IMU Classification

## ÖZ

### **MEMS TİPİ AÖB KULLANILARAK SIKI BAĞLI VE GEVŞEK BAĞLI AÖB/KKS BÜTÜNLEŞTİRME TEKNİKLERİ İLE GENİŞLETİLMİŞ VE KOKUSUZ KALMAN FİLTRE ALGORİTMALARININ GELİŞTİRİLMESİ VE KARŞILAŞTIRILMASI**

Güreş, Onur

Yüksek Lisans, Elektrik Elektronik Mühendisliği Bölümü

Tez Yöneticisi: Prof. Dr. Buyurman Baykal

Eylül 2019 , 119 sayfa

Navigasyon teknolojileri son 20 yılda gerçekleşen teknolojik gelişmeler ile oldukça ilerlemiştir. Gerekli ekipmanların satın alımı ve erişim artık çok kolay olup ve uydu navigasyonu tüm dünyayı kapsamaktadır. Bu nedenle bir navigasyon sistemi tasarlanırken en önemli parçası içerisinde kullanılan algoritmalar olmaktadır. Bu tez kapsamında yapılan çalışmalar kendini kanıtlamış, bilinen referans bir ünite ile bu ünite yer alan aynı model AÖB ve KKS'den alınan verileri kullanan ve tez kapsamında geliştirilen navigasyon algoritmaları ile karşılaştırılmasına odaklanmıştır. Bu tez kapsamında, hem Genişletilmiş Kalman Filtresi (GKF) hem de Kokusuz Kalman Filtresi (KKF) kestirim teknikleri geliştirilmiş ve sıkı bağlı ile gevşek bağlı bütünleştirmek metodları uygulanmıştır. Referans ünite olarak NovAtel firmasına ait SPAN IGM-A1 seçilmiştir. Bu ünite kendini kanıtlamış ve içerisinde piyasada bulunan en iyi algoritmalarından biri olan SPAN yer alan bir üründür. Bu ünite içerisinde ADIS-16488 MEMS AÖB ve NovAtel'e ait tek antenli OEM6 KKS alıcısı yer almaktadır. Geliştirilen algoritmaların doğrulanması için seçilen bağımsız üniteler de ADIS-16488 ve

OEM6 KKS alıcısıdır. Bu nedenle, referans ünitesi ve geliştirilen algoritmalar arasında geçerli bir karşılaştırma gerçekleştirilmiştir. Araba testleri koşturulmuş ve elde edilen sonuçlar farklı kestirim ve bütünleştirme metotları için karşılaştırılmıştır. Elde edilen sonuçlar UKF ve EKF arasında büyük farklar oluşmadığını göstermektedir. Buna rağmen, UKF hata kestirim GNSS kaybı gibi durumlarda daha iyi performansa sahip olmuştur. Genişletilmiş Kalman Filtresi ise daha yönelim açılarının hesaplanmasında daha düşük hataya sahip olmuştur. Sıkı bağlı bütünleştirmenin gevşek bağlı bütünleştirmeye göre hem GKF hem de KKF için daha iyi performansa sahip olduğu görülmüştür. Son olarak her iki filtrenin kararlılığı ve KKF için kullanılan ölçek çarpanlarının etkisi incelenmiştir.

Anahtar Kelimeler: AÖB, KKS, Kalman Filtresi, Genişletilmiş Kalman Filtresi, Koksuz Kalman Filtresi, AÖB Sınıflandırması

*To the love of my life and the sun of my mind  
and  
To my beloved parents whom never stopped believing in me*

## ACKNOWLEDGMENTS

My sincerely acknowledge to all people who have supported me from the beginning to the end of this thesis:

- To Prof. Dr. Buyurman BAYKAL for his ever ending support and understanding from the first moment we met. You have provided me very nice background, equipment and answered my technical and personal questions. I am lucky to be able to work with you through my master degree. Thank you very much for all the patience and information you've given to me.
- To my former co-workers Levent CEVHER, Ali Onur BAYKAL, Erkut Ahmet SOLMAZ and İsmail Özdemir UZUNLAR and my college friend Görkem SARIKAYA for their continuous support and consultancy whenever I asked. Thank you for all the encouragement you've provided.
- To my all close friends for reminding me the importance of mental strength and my hunger for new information. Thanks to you I was always eager to make better.
- To NovAtel Inc. for making very nice documentation and manuals for their customers and navigation enthusiasts. Thank you for your clear and simple language in your documents.
- To my former company VESTEL Defence Industry for letting me explore navigation techniques and work with various devices. Thanks to you I've learnt how to test a navigation device and how to analyze test results.
- To my parents and brother for never stop believing in me. No matter what my situation is, I know that you will always be there for me. Thank you for your valuable life lessons and patience.
- To the love of my life and the sun of my mind. My dear wife, thanks to you I learned the true strength and power of determination. You are the strongest and

one of the smartest person I have ever known. I love you very much and thank you for being there at past, now and long future hopefully.

## TABLE OF CONTENTS

ABSTRACT . . . . .	v
ÖZ . . . . .	vii
ACKNOWLEDGMENTS . . . . .	x
TABLE OF CONTENTS . . . . .	xii
LIST OF TABLES . . . . .	xvii
LIST OF FIGURES . . . . .	xviii
LIST OF ABBREVIATIONS . . . . .	xxi
CHAPTERS	
1 INTRODUCTION . . . . .	1
1.1 Motivation and Problem Definition . . . . .	1
1.2 Objectives . . . . .	2
1.3 Previous Research and Limitations . . . . .	3
1.4 Contribution . . . . .	4
1.5 Outline . . . . .	4
2 BACKGROUND AND OVERVIEW OF GNSS AND INS . . . . .	7
2.1 Global Navigation Satellite Systems . . . . .	7
2.1.1 GNSS Overview . . . . .	7
2.1.2 GNSS Measurements and Errors . . . . .	9

2.1.2.1	Pseudorange Measurements . . . . .	9
2.1.2.2	Pseudorange Rate Measurements . . . . .	10
2.1.2.3	Carrier-Phase Measurements . . . . .	11
2.1.3	GNSS Navigation Solution . . . . .	13
2.1.4	GNSS Error Sources . . . . .	14
2.1.4.1	Ionospheric Errors . . . . .	15
2.1.4.2	Tropospheric Errors . . . . .	16
2.1.4.3	Clock Errors . . . . .	16
2.1.4.4	Orbital Errors . . . . .	17
2.1.4.5	Multipath . . . . .	17
2.1.4.6	Receiver Noise Error . . . . .	18
2.1.4.7	GNSS Error Summary . . . . .	18
2.1.5	Conclusions about GNSS . . . . .	20
2.2	Inertial Navigation Systems (INS) . . . . .	20
2.2.1	Reference Coordinate Frames . . . . .	21
2.2.1.1	Earth-Centered Inertial Frame (i-frame) . . . . .	22
2.2.1.2	Earth-Centered Earth-Fixed Frame (ECEF, e-frame) . . . . .	22
2.2.1.3	Local-Level Frame (LLF, l-frame) . . . . .	22
2.2.1.4	Body Frame (b-frame) . . . . .	24
2.2.1.5	IMU Enclosure Frame . . . . .	25
2.2.1.6	Computation Frame . . . . .	25
2.2.2	Coordinate Frame Transformations . . . . .	25
2.2.3	Inertial Navigation Systems Mechanization Equations . . . . .	28

2.2.3.1	Raw Measurements . . . . .	30
2.2.3.2	Attitude Update . . . . .	31
2.2.3.3	Acceleration Measurements Corrections and Frame Transformation . . . . .	32
2.2.3.4	Velocity and Position Update . . . . .	33
2.2.3.5	Computing Latitude, Longitude, Height and Roll, Pitch, Yaw . . . . .	34
2.2.4	INS Error Sources . . . . .	35
2.2.4.1	Bias . . . . .	37
2.2.4.2	Scale Factor . . . . .	38
2.2.5	Misalignment Errors . . . . .	38
2.2.5.1	Noise (Random Walk) . . . . .	38
2.2.6	Initial Alignment . . . . .	39
2.2.7	Classification of Inertial Navigation Systems . . . . .	42
2.2.8	Conclusions About INS . . . . .	42
3	ESTIMATION TECHNIQUES . . . . .	45
3.1	Estimation . . . . .	45
3.2	Kalman Filter . . . . .	48
3.2.1	Kalman Filter Algorithm . . . . .	49
3.2.1.1	Prediction . . . . .	50
3.2.1.2	Measurement Update . . . . .	51
3.3	Non-Linear Kalman Filtering . . . . .	53
3.3.1	Linearized Kalman Filter (LKF) . . . . .	55
3.3.2	Extended Kalman Filter (EKF) . . . . .	55

3.3.3	Unscented Kalman Filter (UKF)	56
3.3.3.1	Unscented Transform (UT)	58
3.3.3.2	Scaled Unscented Transform (SUT)	59
3.3.3.3	Kalman Filtering (UKF)	60
4	INTEGRATION OF INS/GNSS AND MODELING ERRORS BY LINEAR STATE EQUATIONS	65
4.1	Integration Techniques	65
4.1.1	Loosely Coupled Integration	66
4.1.2	Tightly Coupled Integration	67
4.1.3	Open Loop and Closed Loop Implementation	69
4.2	Lever Arm Effects on Integration	69
4.3	Modeling INS and GNSS Errors by Linear State Equations	71
4.3.1	System Process Model	71
4.3.1.1	General INS Error States	71
4.3.1.2	Sensor Error States	72
4.3.1.3	GNSS Error States	77
4.3.2	Measurement Model	77
4.3.2.1	Loosely Coupled Integration Method	78
4.3.2.2	Tightly Coupled Integration Method	78
4.4	Summary of Loosely and Tightly Coupled Integration	79
5	FIELD TEST AND RESULTS	83
5.1	Test Scenario and Setup	83
5.2	EKF Results with Collected Data	87

5.3	UKF Result with Collected Data . . . . .	93
5.4	Long Test Results . . . . .	99
5.5	Overall Results and Filtering Techniques Comparison . . . . .	106
5.6	Effects of Scale Parameters on Scaled UKF . . . . .	108
5.7	Stability of EKF and UKF . . . . .	109
6	CONCLUSIONS AND FUTURE WORK . . . . .	111
6.1	Conclusions . . . . .	111
6.2	Future Works . . . . .	113
	REFERENCES . . . . .	115

## LIST OF TABLES

### TABLES

Table 2.1	Summary of GNSS errors (adapted from [6, 11, 9, 5]) . . . . .	19
Table 2.2	IMU Quality Classification . . . . .	43
Table 5.1	NovAtel SPAN IGM-A1 IMU Specifications [28] . . . . .	84
Table 5.2	NovAtel SPAN IGM-A1 Navigation Performance [28] . . . . .	84
Table 5.3	RMS Error Comparison for Short Car Trial with high Satellite Availability . . . . .	107
Table 5.4	RMS Error Comparison of Long Car Trial with low Satellite Availability . . . . .	107
Table 5.5	Effects of $\alpha$ on the performance of UKF . . . . .	108

## LIST OF FIGURES

### FIGURES

Figure 2.1	GNSS Orbits and Segments [22] . . . . .	8
Figure 2.2	Carrier-Phase Measurement . . . . .	12
Figure 2.3	GNSS Multipath Error [22] . . . . .	17
Figure 2.4	ENU Frame and its relation with e-frame and i-frame [13] . . . . .	23
Figure 2.5	Vehicle Body Frame and Attitude Angles [13] . . . . .	24
Figure 2.6	LLF and ECEF Relation [13] . . . . .	27
Figure 2.7	INS Mechanization Summary . . . . .	35
Figure 2.8	INS Error Visualization [27] . . . . .	37
Figure 3.1	Kalman Filter Summary . . . . .	53
Figure 3.2	LKF and EKF Summary . . . . .	57
Figure 3.3	UKF Summary . . . . .	63
Figure 4.1	Loosely Coupled Integration . . . . .	67
Figure 4.2	Tightly Coupled Integration . . . . .	68
Figure 4.3	Summary of Loosely Coupled Integration . . . . .	80
Figure 4.4	Summary of Tightly Coupled Integration . . . . .	81
Figure 5.1	Car Trial Test Diagram . . . . .	85

Figure 5.2	Test Setup Placement Before Car Trial . . . . .	86
Figure 5.3	Car Trial Path . . . . .	87
Figure 5.4	EKF Tightly Coupled and Loosely Coupled Car Test Results . .	88
Figure 5.5	EKF Tightly Coupled and Loosely Coupled Latitude Performance	89
Figure 5.6	EKF Tightly Coupled and Loosely Coupled Longitude Performance . . . . .	90
Figure 5.7	EKF Tightly Coupled and Loosely Coupled Integration Positioning Errors . . . . .	91
Figure 5.8	EKF Tightly Coupled and Loosely Coupled Integration Velocity Errors . . . . .	92
Figure 5.9	EKF Tightly Coupled and Loosely Coupled Integration Roll and Pitch Errors . . . . .	92
Figure 5.10	EKF Tightly Coupled and Loosely Coupled Integration Heading Results . . . . .	93
Figure 5.11	UKF Tightly Coupled and Loosely Coupled Car Test Results . .	94
Figure 5.12	UKF Tightly Coupled and Loosely Coupled Latitude Performance	95
Figure 5.13	UKF Tightly Coupled and Loosely Coupled Longitude Performance . . . . .	96
Figure 5.14	UKF Tightly Coupled and Loosely Coupled Integration Velocity Errors . . . . .	97
Figure 5.15	UKF Tightly Coupled and Loosely Coupled Integration Roll and Pitch Errors . . . . .	98
Figure 5.16	UKF Tightly Coupled and Loosely Coupled Integration Heading Results . . . . .	98
Figure 5.17	Long Car Trial Path . . . . .	99

Figure 5.18	Long Car Trial Result of EKF and UKF . . . . .	100
Figure 5.19	Performance with Closer Look to Beginning . . . . .	100
Figure 5.20	Performance with Closer Look to Position with Turns and In- tense Trees/Buildings . . . . .	101
Figure 5.21	EKF and UKF Long Car Trial Test Results . . . . .	101
Figure 5.22	EKF and UKF Long Car Trial GNSS Satellite Availability . . . .	102
Figure 5.23	UKF and EKF Latitude Performance . . . . .	103
Figure 5.24	UKF and EKF Longitude Performance . . . . .	104
Figure 5.25	EKF and UKF Long Car Trial Positioning Errors . . . . .	105
Figure 5.26	EKF and UKF Long Car Trial Velocity Errors . . . . .	105
Figure 5.27	EKF and UKF Long Car Trial Roll and Pitch Errors . . . . .	106
Figure 5.28	EKF and UKF Long Car Trial Heading Results . . . . .	106

## LIST OF ABBREVIATIONS

### ABBREVIATIONS

AI	Artificial Intelligence
CDMA	Code Division Multiple Access
DR	Dead Reckoning
DCM	Direction Cosine Matrix
DOP	Dilution of Precision
ECEF	Earth-Centered Earth-Fixed Frame
EKF	Extended Kalman Filter
FDMA	Frequency Division Multiple Access
GNSS	Global Navigation Satellite System
GPS	Global Positioning System
IEEE	Institute of Electrical and Electronics Engineers
IMU	Inertial Measurement Unit
INS	Inertial Navigation System
LC	Loosely Coupled
LHU	Large Heading Uncertainty
LOS	Line of Sight
LKF	Linearized Kalman Filter
LLF	Local-Level Frame
MEMS	Micro-Electro Mechanical Systems
PCB	Printed Circuit Board
PPM	Pulse per Minute
RMS	Root Mean Square
RTK	Real Time Kinematic

RF	Radio Frequency
STM	State Transition Matrix
SUT	Scaled Unscented Transform
TC	Tightly Coupled
UERE	User Equivalent Range Error
UKF	Unscented Kalman Filter
UT	Unscented Transform

# CHAPTER 1

## INTRODUCTION

### 1.1 Motivation and Problem Definition

Today a few methods exist to calculate navigation data of a user, out of which two of them are used most commonly[6]. The first method uses Newton's Laws of Motion with gyroscope and accelerometer data. The main purpose is to compute the rate of change in position from epoch to epoch. This is done by integrating collected data from accelerometers twice to calculate the change in position and integrating data from gyroscopes once to get the change in rotation. This procedure requires initialization of position, velocity and attitude. Inertial Navigation System (INS) is the general name of devices which use explained procedure for calculation of navigation data. Inertial Measurement Unit (IMU) is the most important element in INS because it has gyroscopes and accelerometers for each reference axes inside[1].

The second method depends on receiving pre-defined Radio Frequency (RF) signals from navigation satellites. Original ideas to follow satellites from ground stations happened after the first satellite was placed in orbit in 1957. Scientists realized that satellites can be tracked by using "Doppler Affect" which enables calculation of the distance between satellite and ground station. Scientists used this information to track submarines with nuclear missiles by putting six satellites over the poles of world. However, the response time of these satellites could take minutes. To avoid latency and get accurate results, US Department of Defence accelerated its efforts and launched its first NAVSTAR satellite at 1978.[2] In 1993, there were 24 actively working Global Positioning System (GPS) satellites all around the world. Since then there have been additional constellations such as GLONASS, GALILEO, BEIDOU

and they are all called Global Navigation Satellite Systems (GNSS).

Both INS and GNSS have their lack of accuracy depending on their own error sources. INS has a drift in the solution that grows with time. It leads long term inaccuracy with the accumulation of systemic errors coming from inertial sensors. GNSS needs a line of sight (LOS) between the end-user and the corresponding satellite being used at each epoch. In obstructive environments where dense forests or high buildings exist, GNSS signal blockage can happen partially or completely. The following chapters will provide details about these error sources. In conclusion, other than some specific applications such as geo-referencing for INS and open area navigation for GNSS, these two technologies are not preferred for navigation as standalone system without aiding. Over the last two decades scientists and engineers made available using these two systems together and got superior navigation results especially when GNSS signal quality is low (urban environments) and price of the equipment is critical for upcoming applications.

## **1.2 Objectives**

Data fusion is a practical solution between INS and GNSS to compensate for errors of both systems. Kalman Filtering techniques are used for the combination. Kalman Filtering can be divided into two phases. At the first phase, position, velocity and attitude estimates are calculated by using INS mechanization equations. At the second stage, these estimates are updated with observed GNSS measurements by comparing to what mechanization equations estimated at the very same time. At the end of the second phase, the Kalman filter has enough information from both systems to compute their inaccuracies. Kalman Filter uses this information to find out the optimal navigation solution. The inertial navigation solution would diverge quickly in the absence of GNSS updates. GNSS solution limits inertial errors with its updates.

Extended Kalman Filter (EKF) is the most commonly used filtering technique in market for this purpose. On the other hand, the Unscented Kalman Filter (UKF) offers another characteristic for linearization. Both techniques have their disadvantages and the following chapters explain them in detail.

In the scope of this thesis, author designed filter algorithms were developed to show the performance differences between EKF and UKF compared with deeply coupled proven algorithm in the reference unit. MATLAB was used to develop algorithms and process data. For this purpose, well known and proven market INS/GNSS system NovAtel SPAN IGM-A1 is selected as reference unit. The subsystems of reference units are ADIS-16488 MEMS IMU and NovAtel OEM6 GNSS Receiver. Hence, the focused items in this thesis are the performance of developed filters and modelling system dynamics and measurement errors as linear states for Kalman filters.

IMU and GNSS receiver error models are created by autocorrelation analysis for the state transition matrix. To understand real performance differences with author-designed algorithms, the same IMU and GNSS receiver were selected. By collecting from standalone IMU and GNSS receiver raw data, author designed algorithm results were gathered. Differences of both filters compared with reference unit were computed and root-mean-square differences were used for error calculations. Results show that tightly coupled EKF is feasible for future works. With the results of this thesis, a single box INS/GNSS system can be developed and tests with land and aerial vehicles can be applied to this future system.

### **1.3 Previous Research and Limitations**

Solid scientific background has been created over the last two decades about integrating INS and GNSS systems thanks to the works such as [6, 5, 9, 4] and among others.

There are a lot of applications for INS/GNSS integration. Manned and unmanned aerial vehicles, ships, boats, submarine and agriculture are some of the most common applications. [14] For satellite navigation, a star tracker algorithm was used to improve attitude determination of INS while using GNSS as an update in the same Kalman Filter [3]. Other methods such as visual aided INS (VINS) was proposed instead of GNSS in [4] for Unmanned Aerial Vehicles by using a realistic camera model. In [5], author designed a loosely coupled Extended Kalman Filter for mobile phone navigation and compared it with higher grade proven INS/GNSS system.

The accuracy of an INS/GNSS system strongly relies on the quality of its sensors. Some of the applications need centimeter level accuracy such as unmanned aerial vehicles during landing. Some of them do not need very accurate results and 30 meter of accuracy is enough for their purpose such as personal car navigation [6].

To perform an integration, sensor errors inside an INS (accelerometers and gyroscopes) should be examined and classified. To prove designed INS/GNSS system performance, there should be a reference unit [5].

The integration methods also vary and should be investigated carefully concerning application. Filtering technique may vary such as Extended Kalman Filter and Unscented Kalman Filter [7, 8]. The selection of different filtering techniques with different integration strategy can affect navigation performance after mechanization equations are done in Inertial Navigation Systems. There are also error sources coming from GNSS and the robustness of the integration will reveal itself when GNSS outage happens. INS alignment is another case because if INS cannot be aligned correctly, navigation performance degrades very dramatically [21].

#### **1.4 Contribution**

This thesis aims to develop in a proven navigation algorithm in order to be used a single box real-time navigation system for future work. INS/GNSS algorithms with different integration methods and different filtering techniques were created to compare them with a qualified reference unit. For that purpose, all navigation algorithms were developed in MATLAB in compliance with real-time software. Field data were collected with car trials and root-mean-square technique were used to compute performance. At the end of this thesis, four different integration algorithms, two different Kalman Filter designs and two different system dynamics models are provided.

#### **1.5 Outline**

Chapter 2 describes INS and GNSS technologies in detail since, characteristics of two systems are important for understanding system dynamics and measurements.

The main topics are INS mechanization equations and INS error sources, GNSS measurements, position, velocity calculations and GNSS error sources and their effects on accuracy, alignment techniques and classification of INS sensors.

Chapter 3 describes Kalman processing methods by starting with linear Kalman Filter technique and exploring non-linear Kalman Filter techniques that includes both Extended (EKF), Unscented (UKF).

Chapter 4 describes author designed integration filters by presenting system process and measurement models. Chapter starts with the integration strategies and continues with integration filter details. At the end of the chapter, lever-arm effect and vehicle motion constraints are briefly explained.

Chapter 5 starts with the specifications of reference unit and continues with verification tests. Test results from car trials are given with figures and explained with respect to all filter output. General results are presented with respect to coupling methods. At the end of the chapter, scale parameters of UKF and stability of designed filters are provided.

Chapter 6 summarizes the conclusions of thesis and recommends future work.



## CHAPTER 2

### BACKGROUND AND OVERVIEW OF GNSS AND INS

#### 2.1 Global Navigation Satellite Systems

Global navigation satellite systems work in all environmental conditions and aim full coverage around the world. GNSS receivers need to track at least 4 satellites to compute 3D navigation information.

##### 2.1.1 GNSS Overview

U.S. Department of Defence kicked off GNSS with the launch of the Global Positioning System (GPS) in mid-1970s. Its main purpose was to provide sub-meter level positioning accuracy to submarines [9]. However, in today's modern world, almost all unmanned and manned applications use satellite navigation anywhere in the world. Ever since the launching of first navigation satellite, constellations such as GPS, GALILEO, GLONASS, BEIDOU led a robust satellite navigation network [22]. A general GNSS navigation architecture includes three main parts. These parts are the space segment, the control segment and the user segment.

The space segment is a cluster of satellites around Earth. These satellites orbit with a distance of nearly 20200 km [5]. Each satellite system has its own set of satellites, i.e. constellation. Each GNSS satellite in a constellation has same distance from each other with a nominal inclination angle  $55^\circ$  to equatorial plane [3].

The control segment includes ground equipment and facilities for monitoring and controlling entire the GNSS system. For GPS constellation, there are two master control stations (one primary and one backup), four navigation data uploading center

and sixteen monitor stations all around the world [22].

The user segment is the most crowded and dynamic part of the GNSS structure. Military purposes led GPS and GLONASS designs at first but from the start of the 2000s, civilian applications have become the major part of the user segment. There were around a few million users of the GNSS at the beginning but with the evolution of microchips and mobile phones, the GNSS application is everywhere today [6]. A user segment includes the receiver that includes a RF front-end with the GNSS antenna and a processor. The processor deals with measuring and decoding necessary information coming from a GNSS satellite.

A simple visualization of orbits and GNSS segments are given in Figure 2.1.

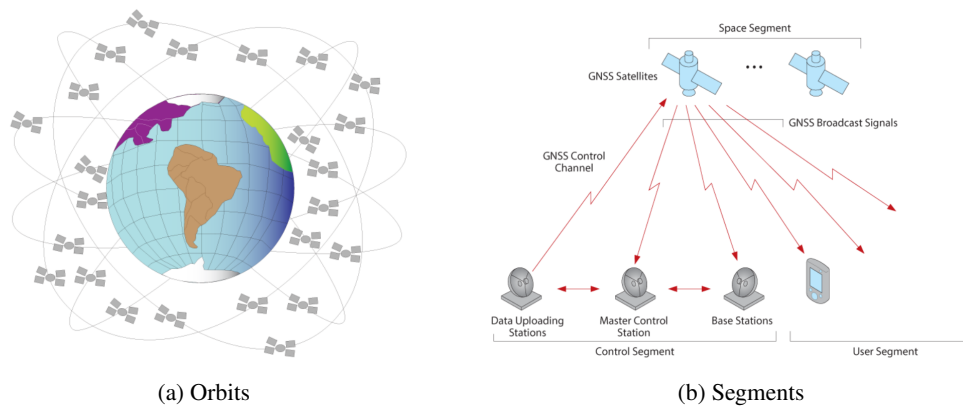


Figure 2.1: GNSS Orbits and Segments [22]

Today there are two GNSS constellations with full Earth coverage: GPS (USA) and GLONASS (Russia Federation). In addition to these constellations, there are ongoing works by the European Union (EU) and the Republic of China (RPC). EU's global navigation satellite system has been on development phase since 2004. The constellation is called GALILEO and there are currently 10 launched satellites at the space segment. However, these satellites are not open to public use and only have coverage around Europe for scientific developments and experiments. The key difference of GALILEO from others is that the constellation will serve only for civilian purposes. RPC's GNSS name is BEIDOU. BEIDOU constellation completed its regional coverage at the end of 2012 and started its service to China. China plans to launch 35 satellites including already launched, spared satellites and complete world coverage

by 2020 [10].

The addition of new constellations to current ones is important for end-users since it enables navigation alternatives for GNSS receivers with capability of working multi-frequency, multi-constellation. Especially for harsh environments and latitudes near both poles, increased satellite availability is crucial [21].

### **2.1.2 GNSS Measurements and Errors**

GNSS satellite sends navigation messages, which consist of the almanac, the ephemeris, timing, error correction and satellite status [11, 12]. Almanac and ephemeris are briefly explained below but a GNSS signal is much more complicated and requires a lot of detailed information to get familiar. In this thesis, only necessary information for navigation filter is focused. For more details on the GNSS signal, please refer to [2, 11, 15].

Satellite almanac data is a summary of orbital data for all the satellites. Master control stations send almanac data that is valid for weeks. Almanac data gives the receiver to have an idea about where the visible satellites might be. For this purpose, receivers usually keep Almanac data in their storage. Nevertheless, almanac data does not provide the necessary accuracy for the receiver to calculate the satellite's exact position. Ephemeris data provides the necessary accuracy. Ephemeris is a satellite specific data. It gives information that is much more accurate about the relevant satellite's position. Ephemeris has a shorter time of validation and satellites update ephemeris data more frequently than almanac data. [11].

With the explained information inside the GNSS signal, a receiver can gather three types of measurements to the end-user.

#### **2.1.2.1 Pseudorange Measurements**

For pseudorange measurements, the speed of signal propagating from satellite to user is equal to the speed of light. By using the time of arrival, receiver calculates the distance between itself and the relevant satellite. Calculated ranges are pseudoranges

because they contain errors, which come from the fact that satellite atomic clock and receiver clock synchronization is not perfect. This fact creates a bias and its name is clock bias [11].

Pseudorange measurements include the range with errors but clock bias is not the only error in real life. In addition to clock bias, random noise, various propagation, and system errors exist in real life. Hence, pseudorange measurement equation is written by Equation (2.1) [5, 6].

$$p = r + c\delta T - c\delta t + \delta_{ion} + \delta_{trop} + \delta_{orbit} + \delta_p \quad (2.1)$$

where

$p$  is the measured pseudorange between a satellite and an user in meters

$r$  is the true range between a satellite and an user in meters

$c$  is the speed of light in free space (m/s)

$\delta T$  is the receiver clock error in seconds

$\delta t$  is the satellite clock error in seconds

$\delta_{ion}$  is the ionospheric error in meters

$\delta_{trop}$  is the tropospheric error in meters

$\delta_{orbit}$  is the orbit prediction error in meters

$\delta_p$  is the combination of errors coming from multipath, receiver noise in meters.

### 2.1.2.2 Pseudorange Rate Measurements

Pseudorange rate measurements are the derivate of the pseudorange measurement [4].

Velocity observation is given in Equation (2.2).

$$\dot{p} = \dot{r} + c\dot{\delta T} - c\dot{\delta t} + \dot{\delta}_{ion} + \dot{\delta}_{trop} + \dot{\delta}_{orbit} + \dot{\epsilon} \quad (2.2)$$

where

$\dot{p}$  is the measured range rate in m/s

$\dot{r}$  is the true range rate in m/s

$\dot{\delta T}$  is the receiver clock drift in m/s

$\dot{\delta t}$  is the satellite clock drift in m/s

$\dot{\delta}_{ion}$  is the ionospheric error drift in m/s

$\dot{\delta}_{trop}$  is the tropospheric error drift in m/s

$\dot{\delta}_{orbit}$  is the orbital prediction error drift in m/s

$\dot{\epsilon}$  is the drift from multipath and noise in m/s.

In this thesis, incoming measurements from the reference unit receiver and the standalone GNSS receiver were pseudorange and pseudorange rate measurements. But there is another measurement which is not applicable to all GNSS receivers. It is told briefly in next section for information purposes.

### 2.1.2.3 Carrier-Phase Measurements

There is another measurement that depends on counting the carrier-phase for calculating pseudoranges. Centimeter-level accuracy is feasible with the usage of this method. It is feasible because it relies on counting the cycles of a GNSS signal. However, there is always a difference between measured and receiver generated ranges. This is the ambiguity and it is a combination of a fraction and an integer part. Calculation and elimination of the fraction part is easy but for the integer part, it is more complicated [23]. Therefore, the total carrier-phase can be written as a summation of measured carrier-phase and ambiguity. Carrier-phase visualization is given in Figure 2.2.

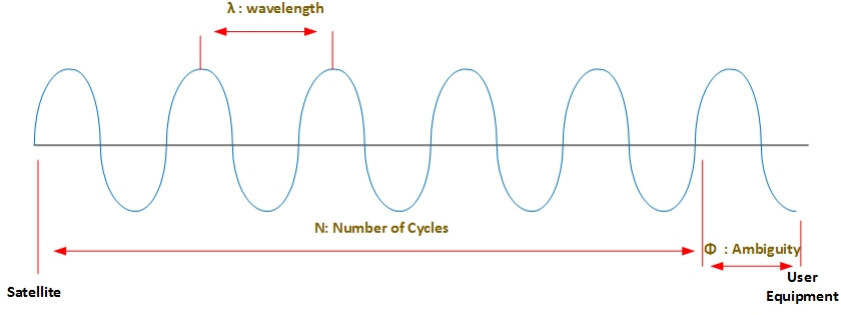


Figure 2.2: Carrier-Phase Measurement

Pseudorange from computed carrier-phase is a summation of measured carrier-phase and ambiguity as given in Equation 2.3.

$$p = (N + \Phi)\lambda \quad (2.3)$$

By using Equation 2.3, carrier-phase equation is provided as below.

$$p = r + c\delta T - c\delta t - \delta_{ion} + \delta_{trop} + \delta_{orbit} + \epsilon_c + \lambda\Phi \quad (2.4)$$

where

$\epsilon_c$  is the error in carrier measurement and multipath meters

$\Phi$  is the integer ambiguity in cycles and the rest of the parameters are same as given in Equation (2.1).

The carrier-phase measurement equation has the same errors with a slight difference. For carrier-phase measurement, the ionospheric effect has minus in front of it. Tropospheric effect creates additional cycles because delay in time causes advance in frequency. Readers can observe this difference in Equation (2.4) by comparing it with Equation (2.1). Another difference comes from the possible amount of errors affecting calculations. Since the accuracy is cm level, the multipath and system noise are much smaller by comparing same errors in pseudo-range measurements [2, 13].

### 2.1.3 GNSS Navigation Solution

Range between satellites and receivers are key information for calculation of the user position. There is also additional information from the navigation message such as the ephemeris data. For the details of the ephemeris data, readers can refer [11] and [14] and other GNSS textbooks.

A simple geometric range definition can be defined without errors as below:

$$r = \sqrt{(X_S - X_U)^2 + (Y_S - Y_U)^2 + (Z_S - Z_U)^2} \quad (2.5)$$

Calculation of range from pseudorange code or carrier-phase depends on the type of the receiver or application but results have same output.  $X_U, Y_U, Z_U$  are user coordinates and  $X_S, Y_S, Z_S$  are the known satellite coordinates coming from Ephemeris. The other unknown in addition to user position  $X_U, Y_U, Z_U$  in Equation 2.5 is the receiver clock bias  $\delta T$ .

Equation 2.5 is a non-linear equation. Taylor series expansion is used for linearization. For any pseudorange function  $f(X, Y, Z)$ , Taylor series expansion around  $i^{th}$  satellite is given in Equation 2.6.

$$f(X_i, Y_i, Z_i) = f(X_0, Y_0, Z_0) + \frac{\delta f(X_0, Y_0, Z_0)}{\delta X_0} \Delta X + \frac{\delta f(X_0, Y_0, Z_0)}{\delta Y_0} \Delta Y + \frac{\delta f(X_0, Y_0, Z_0)}{\delta Z_0} \Delta Z + HigherOrderTerms \quad (2.6)$$

where  $f(X_i, Y_i, Z_i)$  is equal to  $i^{th}$  satellite's range function.

By taking only first order terms and next taking the derivatives in 2.6, linearized pseudorange equation is computed as:

$$r_i = \rho_i - \frac{X_i - X_0}{p_i} \Delta X - \frac{Y_i - Y_0}{p_i} \Delta Y - \frac{Z_i - Z_0}{p_i} \Delta Z + c\delta T - c\delta t + \delta_{ion} + \delta_{trop} + \delta_{orbit} + \delta_p \quad (2.7)$$

where  $p_i = \sqrt{(X_i - X_U)^2 + (Y_i - Y_U)^2 + (Z_i - Z_U)^2}$

In matrix form, pseudorange equation becomes:

$$r_i = p_i + \begin{bmatrix} (-\frac{X_i-X_U}{p_i}) & (-\frac{Y_i-Y_U}{p_i}) & (-\frac{Z_i-Z_U}{p_i}) & 1 \end{bmatrix} \begin{bmatrix} \Delta X \\ \Delta Y \\ \Delta Z \\ c\Delta T \end{bmatrix} + \quad (2.8)$$

$$c\delta T - c\delta t + \delta_{ion} + \delta_{trop} + \delta_{orbit} + \delta_p$$

By using the standard LSE form which is  $Ax = b$  onto above equation for each satellite, pseudorange equation becomes as given in Equation 2.9 where the parameter  $n$  is the number of satellites and  $A$  is a  $(n \times 4)$  matrix.

$$\begin{bmatrix} (-\frac{X_1-X_U}{p_1}) & (-\frac{Y_1-Y_U}{p_1}) & (-\frac{Z_1-Z_U}{p_1}) & 1 \\ \dots & \dots & \dots & \dots \\ (-\frac{X_n-X_U}{p_n}) & (-\frac{Y_n-Y_U}{p_n}) & (-\frac{Z_n-Z_U}{p_n}) & 1 \end{bmatrix} \begin{bmatrix} \delta X \\ \delta Y \\ \delta Z \\ c\delta T \end{bmatrix} = \quad (2.9)$$

$$\begin{bmatrix} p_1 - r_1 + c(\delta T - \delta t_1) - \delta_{i1} - \delta_{t1} - \delta_{o1} - \epsilon_1 \\ \dots \\ p_n - r_n + c(\delta T - \delta t_n) - \delta_{in} - \delta_{tn} - \delta_{on} - \epsilon_n \end{bmatrix}$$

Next section will provide error sources and their mitigation methods to increase accuracy.

#### 2.1.4 GNSS Error Sources

For GNSS navigation, accuracy strongly depends on the location of the receiver and mitigating the error sources. Better accuracy comes with the well separated reference points in space. If the range measurements are relative to four satellites, which are very near to each other, results will become nearly equal and the effects of small relative errors will increase. The distribution of satellites may lead magnification of range error. Effect of satellite geometry over the GNSS solution uses the unitless dilution of precision (DOP) oarameter. For more details on DOP readers can refer to [11, 13].

DOP is a common parameter, which is a performance metric for GNSS receivers. It gives the user an idea of the possible GNSS quality of the current location.

Other errors affecting GNSS quality are summarized in the next subsections. Modeling or differential GNSS techniques can achieve the mitigation of these error sources with some exceptions. Differential GNSS uses either code or carrier-phase based methods. Carrier-phase method is referred as Real Time Kinematic (RTK).

There are also satellite correction networks and special softwares to provide correction of errors. If a receiver uses satellite network, corrections arrive from a set of geostationary satellites such as TerraSTAR, OmniSTAR. They have their trade-off but offer their subscribers less than a half meter accuracy. For details of differential GNSS and aided satellite corrections, readers can refer to [6] and [15].

#### **2.1.4.1 Ionospheric Errors**

Ionosphere covers between 50 to 1000 km distances from the surface of the Earth. It consists of ionized gases because of solar radiation. Ionized gases mean free electrons and ions. The existence of free electrons produced by ionization makes the ionosphere as acting a variable medium even during the daily cycle. A part of the ionosphere can be in shadow and other parts of the ionosphere can be under sunlight. This situation creates changes in the characterization of the ionosphere and makes it hard to model. The primary effect of the ionosphere onto the GNSS signal is relative speed degradation. Since a signal with speed of light enters a medium rather than free space, the relative speed of signals reduces below the speed of light.

The magnitude of the error related to the ionosphere is directly proportional to total electron content (TEC). Electrons do not spread homogeneously at the ionosphere. This leads reflection coefficient to change randomly and affecting GNSS frequency signals by delaying code measurements and advancing carrier-phase measurements [11, 15]. The mitigation of ionospheric errors is possible by using the differential GNSS methods. Ionosphere does not have same effects on different RF frequencies. Therefore, in the absence of differential GNSS methods, dual-frequency GNSS receiver can eliminate this error type. Today, most of the recent receivers support

dual-frequency and more than one constellation. However, in the case where one receiver does not support dual-frequency, this receiver uses Klobuchar Model from other satellites in order to decrease error [11, 15].

#### **2.1.4.2 Tropospheric Errors**

The troposphere is a layer which extends its upper limit to the stratosphere and lower limit to 9 km above Earth's surface. This layer is composed of dry gases and water vapour. Unlike ionosphere, the delay caused by this layer is same for all GNSS frequencies. That is why differential GNSS or multi-frequency GNSS receivers have no advantage in this error. Error sources reasoning from Tropospheric delays can be distributed around dry and wet parts of this layer. 90% contribution to refractive index of the troposphere comes from dry part and rest 10% comes from wet part. By modeling of dry part errors, mitigation down to 1-2% of the total is possible [11, 15]. The difficulty comes from predicting the wet part. However, since the percentage of wet part is small and can only affect a 5-30 cm error around mid-latitudes modelling is not crucial[11]. Finally, tropospheric errors below 5 cm is feasible by using differential GNSS techniques [6].

#### **2.1.4.3 Clock Errors**

As explained in pseudorange measurements section, the receiver's clock and a GNSS satellite's atomic clock are not perfectly synchronized with each other. Each side's clock has its own oscillator, and this leads noise around time information. The error is generally around a few meters and does not change much with time. If the receiver uses differential GNSS techniques, the error cancels out completely due to double differentiation. And if the receiver can see at least 4 satellites, the time error estimation by using GNSS computations is applicable [9].

#### 2.1.4.4 Orbital Errors

Satellites have pre-specified orbits for their missions but there are imperfections when the satellite moves. Wrong calculations for satellite's own location occurs and it leads wrong ephemeris data in navigation message. The ground segment compares the satellite's true location and calculated location. After that process, the ground segment send comparison results as correction messages to the satellites at least once a day. Satellite that receives correction message update its calculation and broadcasts updated ephemeris to receivers. Differential GNSS techniques can decrease this type of errors down to a few centimeters [15].

#### 2.1.4.5 Multipath

Multipath propagation of the GNSS signal is one of the dominant sources of error according to [11]. It really is a major problem especially around high buildings, obstructions, dense forests. GNSS signals can be reflected easily before coming to receiver and create secondary or multiple signals at the receiver as shown in Figure 2.3. Reflected signals always have longer propagation times and cause problems at the receiver side since it is waiting for only direct line of sight signal from relative satellite.

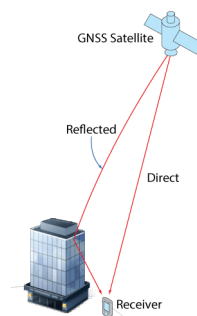


Figure 2.3: GNSS Multipath Error [22]

Multipath error mitigation is not feasible by using differential GNSS techniques. Antenna location strategy is the easiest and most effective mitigation method. Another simple protection is to use antennas with ground plane. Ground plane is a metallic disk centered at the base of the antenna and designed for attenuation of signals

reflected from ground. Another key aspect may be choosing a higher grade GNSS antenna which has capability of understanding the polarity of incoming signal. Since GNSS signals are right hand polarized, left hand polarized multipath signals eliminate directly with this type of antenna. It is also better to mention that using carrier-phase measurements rather than code measurements give lower multipath error according to [9].

Multipath error is hard to model and strongly depends on the receiver's environment. But there are methods of multipath mitigation which can be divided as Spatial Processing Techniques and Time-Domain Techniques [13]. However, mentioned methods increase the computational complexity of the GNSS solution.

#### **2.1.4.6 Receiver Noise Error**

Since GNSS signal levels are very low and the receiver's front-end is highly sensitive to receive weak signals, receiver noise is important for GNSS performance. Receiver noise is sum of the electromagnetic field created by receiver's cables, antennas. The random movement of electrons in a receiver's conductors has an effect which is called thermal noise. In the past by testing two same model receivers by connecting to one antenna by using a GNSS splitter, receiver noise became clear [14] and [6]. The results showed that differential GNSS cancels out all the major error sources but noise and multipath errors remain.

Combining all the possible receiver noise error together pseudorange code measurements can have minimum a 4 cm error while carrier-phase measurements can have mm level accuracy [25].

#### **2.1.4.7 GNSS Error Summary**

At the end of the GNSS error source discussions, a table which includes a summary of all errors and each error's level is given in Table 2.1.

User-equivalent-range-error (UERE) is the remaining GNSS error after mitigation of the above residual error. By using the assumption that is the remaining errors are

Table 2.1: Summary of GNSS errors (adapted from [6, 11, 9, 5])

Error Source	Single Point	Differential
Ionosphere	2 to 50 m	0.05 to 0.2 m
Troposphere	2 to 30 m	0.1 to 1 m
Clock (Receiver)	< 1 m	0 m
Clock (Satellite)	0 to 10 m	0 m
Orbital	< 1 m	~0 m
Multipath	0.2 to 500 m	0.2 to 500 m
Receiver (Code) Noise	~0.4 m	~0.4 m

uncorrelated, user equivalent range error (UERE) is easy to compute. A zero-mean Gaussian random variable that has a variance equal to the root-sum-square of each error source variances is equal to UERE variance as given below.

$$\sigma_{UERE} = \sqrt{\sigma_{eph}^2 + \sigma_{clk}^2 + \sigma_{ion}^2 + \sigma_{tro}^2 + \sigma_{mult}^2 + \sigma_{rec}^2} \quad (2.10)$$

where

$\sigma_{eph}$  is the range error due to ephemeris data

$\sigma_{clk}$  is the range error due to clocks

$\sigma_{ion}$  is the range error due to ionospheric conditions

$\sigma_{tro}$  is the range error due to tropospheric conditions

$\sigma_{mult}$  is the range error due to multipath

$\sigma_{rec}$  is the range error due to receiver noise.

According to [13] above equation is equal approximately to 5.3 m which is a typical expectation of single-point GNSS receiver with nice environmental conditions and 6 m is chosen for author designed measurement model based on this information.

### **2.1.5 Conclusions about GNSS**

GNSS is a very useful and accurate navigation system for a lot of applications. Under good conditions and with techniques such as differential GNSS, the accuracy of system can be mm level. However, as a standalone navigation system, GNSS has weaknesses. RF propagation is vulnerable to atmospheric conditions and signal speed decreases under speed of light. That causes delay for code-based measurements and advance for carrier-phase measurements. From the nature of RF propagation, it is also vulnerable to jamming and multipath. Under jamming conditions or loss of the line of sight signal between satellite and receiver, GNSS outages can occur. The reflection of signals can happen with environments where a lot of building and other obstructions exist. This will lead to multipath. Other error sources results from atomic clocks and receiver clocks of both sides. Most of the error sources can be eliminated by using differential GNSS techniques but not all the errors. It is also worth mentioning that differential GNSS techniques are not applicable to all navigation application and even if they exist, base stations cannot continuously give necessary information. They are dependent on the range of the radio-links of the communication system between base and rover.

As a conclusion, in applications where harsh reflection can occur or continuous and high accuracy navigation solution is necessity, standalone GNSS is not advised to be used. Therefore, it would be wiser to use an additional system to GNSS that does not affect from environment and weather conditions. On the other hand, INS is not vulnerable to environmental conditions but still has error sources. In the next section, details of an INS will be provided.

## **2.2 Inertial Navigation Systems (INS)**

As discussed in first chapter, ancient people tried to find their way by looking at their environments such as stars for their location and to sun for calculation of time. This form of navigation is called Dead Reckoning (DR). In modern times, after inventions of accelerometers and gyroscopes and other sensors, people started using these sensors to compute necessary information to be used for DR principle. An accelerometer

is a device usually with a proof mass,  $m$ , which is constant and at equilibrium position if the case is stable. If external force exists, the proof mass moves along its horizontal axis. If the rate of change is sensed and scaled correctly, the acceleration along this axis can be computed. On the other hand, a gyroscope senses the change in angular movements and measures angular rates with respect to reference frame.

An inertial measurement unit (IMU) includes three mutually orthogonal accelerometers and gyroscopes inside of it. Accelerometers measure linear motion and gyroscopes measure angular motion in three mutually orthogonal directions [13]. An inertial navigation unit (INS) consists of an IMU, a processor and a mechanization module. INS outputs position and attitude information which are calculated by using Newton's first and second law as a principle as a self-contained DR navigation system [6].

The basic working logic of INS can be summarized as sensing acceleration caused by an external force. By using Newton's law, force can be translated to acceleration. Integrating acceleration once provides change in velocity and twice provides change in position since the last calculated velocity and position. However, measured accelerations are in a coordinate frame which is different than the coordinate frames to be used in navigation calculations. Therefore, a translation between coordinate frames is required. This is achieved with angular rates coming from gyroscopes. Gyroscopes output necessary rotation information for coordinate translation. That is the main reason for using a gyroscope along with an accelerometer in an IMU. If the transformation of primary rotation of the accelerations into necessary coordinate frame fails, calculation of the true position will never occur. Therefore, INS quality strongly depends on the grade of gyroscopes to be used inside it.

### **2.2.1 Reference Coordinate Frames**

A set of transformations is necessary when working with INS. It is also important to have outputs with respect to Earth hence, further reference frames are necessary. This section explains briefly all reference frames relevant to inertial navigation systems used in this thesis. Most of the information was gathered from [13].

### **2.2.1.1 Earth-Centered Inertial Frame (i-frame)**

An inertial frame must be stationary in space or have a constant, non-accelerating velocity. All inertial sensor measurements are computed with respect to inertial navigation frame. In addition to that, GNSS receiver calculates satellite's position and velocity with respect to this frame originally.

*Origin*: Earth's center of mass

$Z^i$  axis: Parallel to the axis of Earth's rotation, pointing North Pole

$X^i$  axis: In equatorial plane towards the vernal equinox

$Y^i$  axis: Completes a right-handed system

### **2.2.1.2 Earth-Centered Earth-Fixed Frame (ECEF, e-frame)**

This frame has the same origin and z-axis with i-frame but rotates along with the Earth.

*Origin*: Earth's center of mass

$Z^e$  axis: Parallel to the axis of Earth's rotation, pointing North Pole

$X^e$  axis: In equatorial plane towards the mean Greenwich meridian

$Y^e$  axis: Completes a right-handed system

### **2.2.1.3 Local-Level Frame (LLF, l-frame)**

This frame is used to express the user's attitude and velocity when on or near the surface of Earth.

*Origin*: Navigation system's center of navigation

$Z^l$  axis: Upwards (Completes right-handed system)

$X^l$  axis: Points to east

$Y^l$  axis: Points to true north

This reference frame name is ENU since the directions of each axis. On the other hand, there is another LLF frame called NED (North, East, Down) which only differs from ENU with its z-axis pointing down. Hence, z-axis completes a left-handed system in this frame. Figure 2.4 shows the relation between i-frame, e-frame and l-frame.

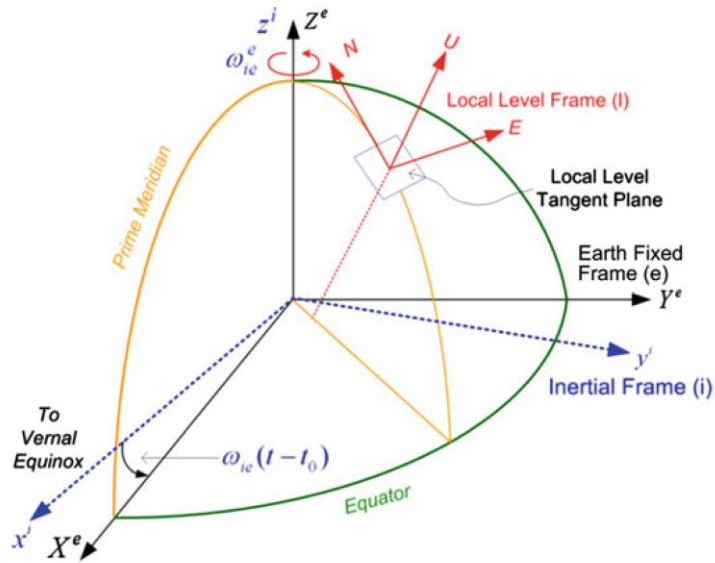


Figure 2.4: ENU Frame and its relation with e-frame and i-frame [13]

### 2.2.1.4 Body Frame (b-frame)

The body or vehicle frame is used for attitude calculations. There may be applications on the relevant vehicle which needs vehicle's attitude information. Therefore, attitude information on the e-frame or l-frame is converted to this frame. In this thesis, body-frame is aligned with navigation platform's attitude axes. Roll, pitch and yaw angles with respect to this frame are given at Figure 2.5.

*Origin:* Navigation system's center of navigation

$Z^b$  axis: Upwards (Completes right-handed system)

$X^b$  axis: Points to the right side of the vehicle

$Y^b$  axis: Points to the left side of the vehicle

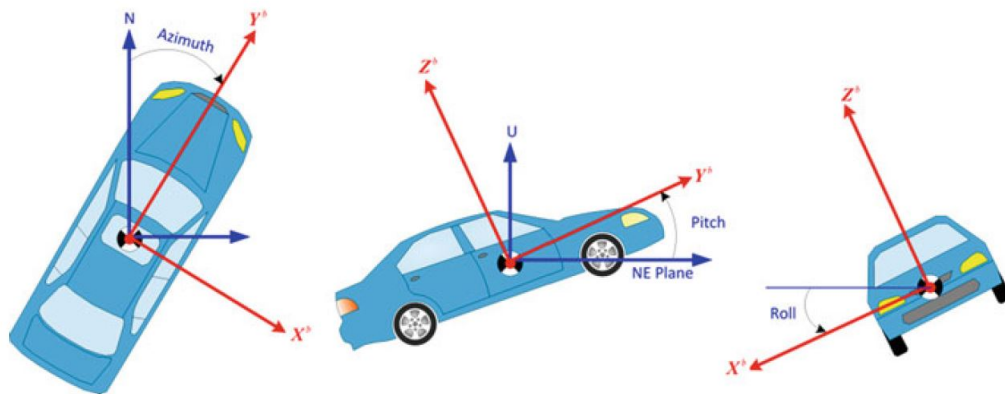


Figure 2.5: Vehicle Body Frame and Attitude Angles [13]

### 2.2.1.5 IMU Enclosure Frame

IMU enclosure frame is the physical distribution of sensors inside an IMU. It is useful especially for big systems to consider IMU enclosure firstly since matching enclosure frame with vehicle/system frame is the easiest way to reduce the number of frame translations. Otherwise, more translations would be required to get solution at desirable frame. IMU enclosure frame was aligned with test car's body frame in this thesis.

### 2.2.1.6 Computation Frame

This frame is the reference frame that INS computer assumes to be the true navigation frame. Whole equations of motion are implemented with respect to this frame on navigation solution module of INS algorithm in this thesis.

## 2.2.2 Coordinate Frame Transformations

The fundamental rotation matrix can be calculated by multiplying elementary rotation matrices around each axis as given in 2.11.  $R_a^d$  means a rotation matrix from a-frame to d-frame.  $R_c^d$  equals the rotation matrix around y-axis,  $R_b^c$  equals the rotation matrix around x-axis and  $R_a^b$  equals the rotation matrix around z-axis. Rotation starts with rotating from z-axis followed by x-axis and finally y-axis for correct alignment.

$$R_a^d = R_c^d R_b^c R_a^b \quad (2.11)$$

$$R_a^d = \begin{bmatrix} \cos\alpha & 0 & -\sin\alpha \\ 0 & 1 & 0 \\ \sin\alpha & 0 & \cos\alpha \end{bmatrix} \begin{bmatrix} 1 & 0 & 0 \\ 0 & \cos\beta & \sin\beta \\ 0 & -\sin\beta & \cos\beta \end{bmatrix} \begin{bmatrix} \cos\gamma & \sin\gamma & 0 \\ -\sin\gamma & \cos\gamma & 0 \\ 0 & 0 & 1 \end{bmatrix} \quad (2.12)$$

Inertial calculations used in this thesis often include coordinate frame transformations. Each transformation involves a rotation matrix which is called direction cosine matrix (DCM). The basis vectors of rotation matrix are normalized in length and cosine of angle between them is equal to dot product of them. This is the motivation of

calling rotation matrices as direction cosine matrices [5]. Some useful properties of DCM's are presented in Equation 2.13.

$$\begin{aligned} R_d^a &= (R_a^d)^{-1} = (R_a^d)^T = (R_c^d R_b^c R_a^b)^T \\ &= (R_a^b)^T (R_b^c)^T (R_c^d)^T \end{aligned} \quad (2.13)$$

The transformation between inertial frame and ECEF frame depends on the knowledge of the angular velocity vector between these two frames. The angular velocity between of those two vectors is equal to rotation of the Earth. From Figure 2.4, for a transformation from i-frame to e-frame is equal to a rotation about the z-axis by the angle  $\omega_e$  which denotes the Earth's rotation rate [13]. Notice that, the DCM for this transformation is equal to third matrix in Equation 2.12.

$$R_i^e = \begin{bmatrix} \cos\omega_e t & \sin\omega_e t & 0 \\ -\sin\omega_e t & \cos\omega_e t & 0 \\ 0 & 0 & 1 \end{bmatrix} \quad (2.14)$$

The inverse of the matrix  $R_i^e$  is equal to transformation from the e-frame to the i-frame as given in 2.15:

$$R_e^i = (R_i^e)^{-1} = (R_i^e)^T \quad (2.15)$$

Transformation from LLF to ECEF is applied by rotating x-axis with  $\varphi-90$  degrees first and next by a rotation around z-axis with  $\lambda+90$  degrees as shown in Figure 2.6.

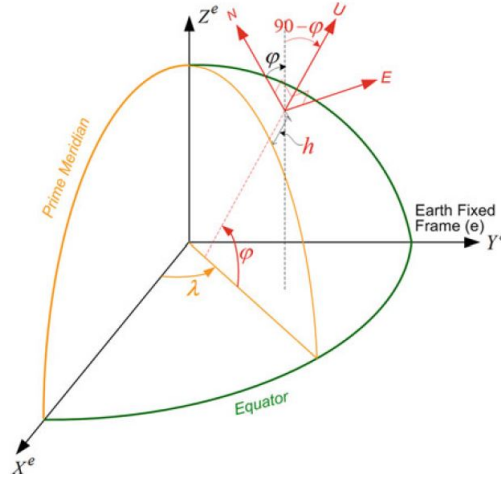


Figure 2.6: LLF and ECEF Relation [13]

The DCM  $R_l^e$  for this transformation is calculated as given in Equation 2.16 and its matrix form is given in 2.17.

$$R_l^e = [(R_a^b)(90 + \lambda)][(R_b^c)(\varphi - 90)] \quad (2.16)$$

$$R_l^e = \begin{bmatrix} \cos(-\lambda - 90) & \sin(-\lambda - 90) & 0 \\ -\sin(-\lambda - 90) & \cos(-\lambda - 90) & 0 \\ 0 & 0 & 1 \end{bmatrix} \begin{bmatrix} 1 & 0 & 0 \\ 0 & \sin(\varphi) & -\cos(\varphi) \\ 0 & \cos(\varphi) & \sin(\varphi) \end{bmatrix} \quad (2.17)$$

In geographical manner, the angle  $\varphi$  is the latitude and the angle  $\lambda$  is the longitude. The reverse transformation is given in Equation 2.18.

$$R_e^l = (R_l^e)^{-1} = (R_l^e)^T \quad (2.18)$$

The final transformation, which is done from body frame to local level frame, is used frequently during mechanization equations in the INS navigation solution process. It is done by rotating all three axes. The rotation sequence is first making a rotation around z-axis, then a rotation about x-axis and finally a rotation about y-axis. The

angles which apply all three sequential rotation are called Euler angles roll, pitch and yaw respectively. The process is given in 2.19.

$$\begin{aligned}
R_b^l &= (R_l^b)^{-1} = (R_l^b)^T = (R_c^d R_b^c R_a^b)^T \\
&= (R_a^b)^T (R_b^c)^T (R_c^d)^T \\
&= R_Z(-\psi) R_X(-\xi) R_Y(-\eta)
\end{aligned} \tag{2.19}$$

The rotation angle around x, y, z axes are pitch, roll and yaw respectively. If DCM  $R_b^l$  is known accurately, Euler angles can be calculated easily [13].

Since this thesis deals with navigation equations and attitude outputs should have roll, pitch and heading, Equation 2.19 should be modified as below:

$$R_b^l = (R_l^b)^{-1} = (R_l^b)^T = (R_c^d R_b^c R_a^b)^T = R_Z(\psi) R_X(-\xi) R_Y(-\eta) \tag{2.20}$$

The transformation from body frame to ECEF and the i-frame can be computed with already found rotation matrices above.

b-frame to e-frame is calculated as follows where  $R_{le}$  was given is Equation 2.17 and  $R_b^l$  was given in Equation 2.20:

$$R_b^e = R_l^e R_b^l \tag{2.21}$$

b-frame to i-frame is calculated as follows where  $R_{ei}$  was given is Equation 2.15 and  $R_b^e$  was given in Equation 2.21:

$$R_b^i = R_e^i R_b^e \tag{2.22}$$

### 2.2.3 Inertial Navigation Systems Mechanization Equations

An INS uses the dead reckoning method for the position, velocity, and attitude calculations as mentioned earlier sections. Calculations are done by using IMU's raw

data inside. The IMU's raw data includes angular rates and accelerations or velocity changes from epoch to epoch. Mechanization starts with a set of initial values and iterations are done recursively from the beginning with the prior epoch's output. The mechanization equations written in this section is implemented with respect to ECEF.

As mentioned above there are two kinds of data coming from an IMU. Mechanization is done by integrating these two data set with proper transformations. For the IMU used in this thesis, the body frame is the same as the inertial frame. Therefore, raw observations are collected in body frame. With this information at first step, a rotation matrix for transformation from b-frame to e-frame is computed by using IMU's angular rates in each axis. To get real angular data, Earth rotation should also be considered which is sensed in e-frame. Earth's rotation rate is rotated to b-frame and compensated from gyroscope's raw data. After finding angular rates relative to body frame, rotation matrix from b-frame to e-frame can be calculated.

At the next stage, the calculated rotation matrix is used for rotation of acceleration's measurements from b-frame to e-frame. Notice that the Earth's gravity is also measured with accelerometers so, this effect should be removed from measurements. After removing gravity and integrating accelerations created by external forces, velocity of the vehicle is computed. Finally, with the integration of velocity, position is computed.

INS error sources such as biases, scale factors should be removed before starting mechanization. The details of INS error sources and methods to mitigate them are discussed in the next section.

As a summary, the mechanization equations are given by Equation 2.23. The mechanization equations are the results of the derivative of position, velocity and attitude equations.

$$\begin{bmatrix} \dot{r}^e \\ \dot{v}^e \\ \dot{R}_b^e \end{bmatrix} = \begin{bmatrix} v^e \\ R_b^e f^b - 2\Omega_{ie}^e v^e + \gamma^e \\ R_b^e (\Omega_{ei}^b + \Omega_{ib}^b) \end{bmatrix} \quad (2.23)$$

where 'dots' implies derivative, 'b' and 'e' letter imply the b-frame and e-frame re-

spectively. The symbols,

$r^e$  is a three-dimensional position vector  $(x^e, y^e, z^e)$ ,

$v^e$  is a three-dimensional velocity vector  $(v_x^e, v_y^e, v_z^e)$ ,

$\gamma^e$  is a three-dimensional velocity vector  $(\gamma_x^e, \gamma_y^e, \gamma_z^e)$ ,

$R_b^e$  is the rotation matrix from b-frame to e-frame,

$\Omega_{ei}^b$  is the skew-symmetric matrix of the rotation rate  $\omega_{ei}^b$ ,

$\Omega_{bi}^b$  is the skew-symmetric matrix of the rotation rate  $\omega_{bi}^b$ ,

$f^b$  and  $\Omega_{ib}^b$  are the measurements taken from IMU. Mechanization equation given here for e-frame is solved in the next sub-section . Most of the calculations gathered from [13].

### 2.2.3.1 Raw Measurements

Raw measurements coming from an IMU tend to have errors that grow with time additively if not compensated. Details of these errors and how to obtain their values such as biases, scale factors and others are given in Section 2.2.4. Below is a method to correct these errors after obtaining their values,

$$\theta_{ib}^b = \frac{(\tilde{\theta}_{ib}^b - b_g \Delta t)}{(1 + S_g)} \quad (2.24)$$

$$v_f^b = \frac{(\tilde{v}_f^b - b_a \Delta t)}{(1 + S_a)} \quad (2.25)$$

where  $\tilde{\theta}_{ib}^b$  is the angular rates from gyroscope. Subscript implies rotation from i-frame to b-frame and superscript implies that the measurement is done in b-frame.  $\Delta \tilde{v}_f^b$  is the acceleration increments from the accelerometer. Superscript implies that the measurement is done in b-frame.  $b_g$  and  $b_a$  are gyroscope and accelerometer biases and  $S_g$  and  $S_a$  are gyroscope and accelerometer scale factors respectively.

### 2.2.3.2 Attitude Update

The measured rotation rate from the gyroscope includes Earth's mean rotation rate. In order to find vehicle's rotation accurately, Earth's rotation should be removed from gyroscope's measurements. Since vehicle's measurements are done in body frame, Earth's rotation rate is transformed from e-frame to b-frame. After transformation, it is subtracted from total measurements taken from gyroscope. The equations for this process are given in Equation 2.26 and Equation 2.27.

$$\theta_{ie}^b = (R_i^b \omega_{ie}^e) \Delta t \quad (2.26)$$

$$\theta_{eb}^b = \theta_{ib}^b - \theta_{ie}^b \quad (2.27)$$

$\omega_e$  is the Earth's rotation rate which is equal to approximately  $15.041^\circ/h$  and  $\theta_{eb}^b$  is the angular rotation in the b-frame.

After computing angular measurements in the b-frame, current epoch's rotation matrix  $R_e^b$  is created by using these measurements. A quaternion approach is proposed for this purpose because it provides a convenient representation and it is easy to place found angular measurements with a quaternion method. It also has the advantage of having fewer differential equations than a rotation matrix. This method also adds a cover for singularities, which can be occurred at edges of roll and pitch values [5]. Hence, the rotation matrix can be created by using measurements  $\theta_{eb}^b$  ( $\theta_x^b, \theta_y^b, \theta_z^b$ ) as given in the following equations.

Update quaternion [6]:

$$\begin{bmatrix} q_1 \\ q_2 \\ q_3 \\ q_4 \end{bmatrix}_{k+1} = \begin{bmatrix} q_1 \\ q_2 \\ q_3 \\ q_4 \end{bmatrix}_k + 0.5 \begin{bmatrix} c & s\theta_z^b & -s\theta_y^b & s\theta_x^b \\ -s\theta_z^b & c & s\theta_x^b & s\theta_y^b \\ s\theta_y^b & -s\theta_x^b & c & s\theta_z^b \\ -s\theta_x^b & -s\theta_y^b & -s\theta_z^b & c \end{bmatrix} \begin{bmatrix} q_1 \\ q_2 \\ q_3 \\ q_4 \end{bmatrix}_k \quad (2.28)$$

where

$$s = \frac{2}{\theta} \sin \frac{\theta}{2} \quad (2.29)$$

$$c = 2 \cos \left( \frac{\theta}{2} - 1 \right) \quad (2.30)$$

$$\theta = \sqrt{(\theta_x^b)^2 + (\theta_y^b)^2 + (\theta_z^b)^2} \quad (2.31)$$

After obtaining the quaternion at current epoch, rotation matrix  $R_e^b$  at current epoch can be calculated as given in Equation 2.32.

$$(R_e^b)_{k+1} = \begin{bmatrix} (q_1^2 - q_2^2 - q_3^2 + q_4^2) & 2(q_1q_2 - q_3q_4) & 2(q_1q_3 + q_2q_4) \\ 2(q_1q_2 + q_3q_4) & (q_2^2 - q_1^2 - q_3^2 + q_4^2) & 2(q_2q_3 - q_1q_4) \\ 2(q_1q_3 - q_2q_4) & 2(q_2q_3 + q_1q_4) & (q_3^2 - q_1^2 - q_2^2 + q_4^2) \end{bmatrix} \quad (2.32)$$

The new rotation matrix is used to calculate roll, pitch and heading after calculation of position in geodetic coordinates.

### 2.2.3.3 Acceleration Measurements Corrections and Frame Transformation

Coriolis Effect is named after the effects of pseudo-forces from Earth's rotation since IMU can be assumed to be at the surface of the Earth. It can be computed by using the previous epoch velocity as given in Equation 2.33 [5].

$$\alpha^e = 2\Omega_{ie}^e v_e \quad (2.33)$$

Gravity correction should also be applied to velocity increments. This can be calculated by using the latest position. After calculating these values, Coriolis and gravity corrections can be applied to acceleration measurements as given in Equation 2.34.

$$\Delta v = \Delta v_f^e - \alpha^e \Delta t + \gamma^e \Delta t \quad (2.34)$$

The third term on the right of the above equation is gravity correction that is calculated from latest position. First term on the right is the acceleration measurements rotated to e-frame. Hence, velocity increments,  $\Delta v_f^b$  measured by accelerometer in b-frame shall be rotated to e-frame. It is done by using the prior epoch's rotation matrix  $R_b^e$  and corrected angular measurements from gyroscopes as given Equation 2.35.

$$\Delta v_f^e = (R_b^e)_{k+1} \left( I - \frac{1}{2} S^b \right) \Delta v_f^b \quad (2.35)$$

where  $S^b$  is the skew-symmetric matrix of angular measurements and  $I$  is the identity matrix.

#### 2.2.3.4 Velocity and Position Update

The velocity and position at the current epoch can be computed by using previous epoch's velocity and average of both previous and current epochs corrected velocity measurements of as given in Equation 2.36.

$$v_{k+1}^e = v_k^e + \frac{1}{2} (\Delta v_{k+1}^e + \Delta v_k^e) \quad (2.36)$$

Calculation of the current epoch's position uses same methodology as velocity as given in Equation 2.37.

$$r_{k+1}^e = r_k^e + \frac{\Delta t}{2} (v_{k+1}^e + v_k^e) \quad (2.37)$$

### 2.2.3.5 Computing Latitude, Longitude, Height and Roll, Pitch, Yaw

Latitude and longitude are the most common output form of position. Increments of position can be calculated by using the computed velocities in the local frame [4]. In order to have geodetic positions latitude, longitude and height, rotation from e-frame to geodetic coordinates should be applied. It is given in Equations 2.38, 2.39, 2.40:

Latitude:

$$\dot{\varphi} = \frac{v_n}{R_M + h} \quad (2.38)$$

Longitude:

$$\dot{\lambda} = \frac{v_e}{(R_N + h) \cos \varphi} \quad (2.39)$$

Height:

$$\dot{h} = v_u \quad (2.40)$$

where  $v_e, v_n, v_u$  are the components of the velocity in east, north and up directions in order.  $R_M$  and  $R_N$  are the meridian and normal radius of the accepted Earth model WGS-84. Details about calculation of  $R_M$  and  $R_N$  can be found in [11].

$R_b^e$  was already found in Equation 2.32. Therefore, the rotation matrix from b-frame to l-frame is found as given by Equation 2.41.  $R_e^l$  was computed by using geodetic latitude and longitude.

$$R_b^l = R_e^l R_b^e \quad (2.41)$$

From  $R_b^l$ , Euler angles i.e. roll, pitch and yaw are computed as given in Equations 2.42, 2.43, 2.44.

$$\xi = -\tan^{-1} \left( \frac{(R_b^l)_{3,1}}{(R_b^l)_{3,3}} \right) \quad (2.42)$$

$$\eta = \sin^{-1} \left( (R_b^l)_{3,2} \right) \quad (2.43)$$

$$\psi = \tan^{-1} \left( \frac{(R_b^l)_{1,2}}{(R_b^l)_{2,2}} \right) \quad (2.44)$$

The complete mechanization equation is summarized in Figure 2.7.

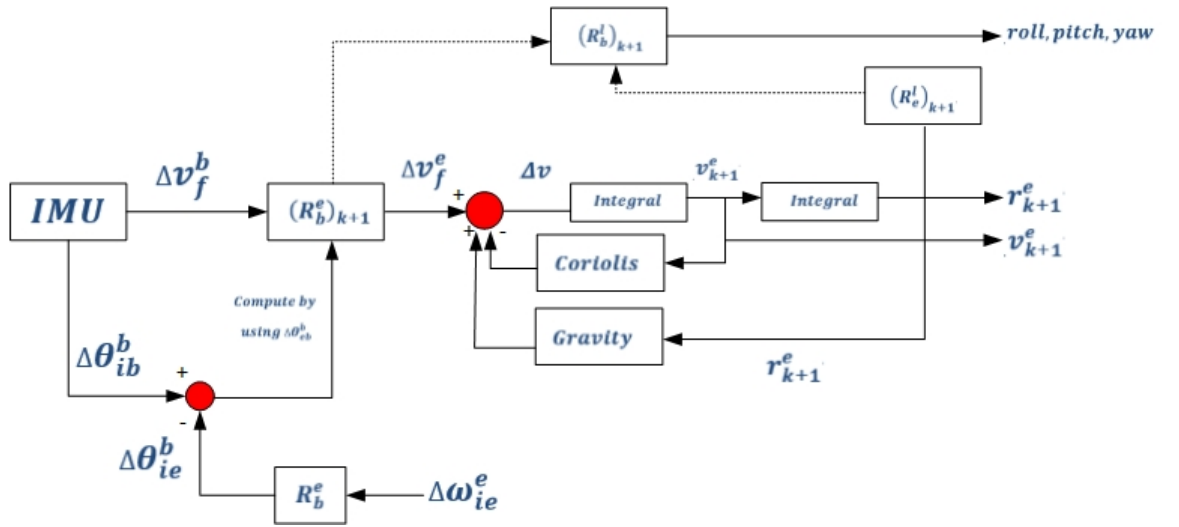


Figure 2.7: INS Mechanization Summary

## 2.2.4 INS Error Sources

INS measurements accuracy strongly depends on correct computation of position, velocity and attitude information of vehicle or user before starting navigation. As mentioned earlier, there are some error sources coming from the nature of accelerometers and gyroscopes such as bias, scale factor. In addition to these error sources, there are Earth gravity and Coriolis effects. There are other errors and special arrangements should be done to cancel their effects on inertial navigation. Three criteria for the performance or classification of an IMU is given below [27].

- **Repeatability:** The quality of an IMU in a manner by looking at the differences between each output under the same conditions. It refers on the product sheets

as the maximum variation between same measurements under same conditions over multiple trials.

- **Stability:** The quality of an IMU is measured by evaluating the same output over time with the same input. Stability is decided by single run with longer time.
- **Drift:** The rate of change occurred at the output when the input remains constant i.e. changes in outputs without an input.

Both gyroscopes and accelerometers have errors that are generally defined by bias stability, bias drift, scale factors, noise and misalignment of the axes. Accelerometer and gyroscope measurement model with all possible error sources are given in Equation 2.45 and Equation 2.46.

$$\tilde{\omega} = \mathbf{w} + b_g + \mathbf{w}.S_g + \mathbf{w}.N_g + \varepsilon_g \quad (2.45)$$

$$\tilde{f} = \mathbf{f} + b_a + \mathbf{f}.S_a + \mathbf{f}.N_a + \varepsilon_a \quad (2.46)$$

where '*tilda*' means measurement made by relevant sensor, subscript 'a' means accelerometer errors and 'g' means gyroscope errors and

$\mathbf{w}$  is the angular rate (deg/h),

$\mathbf{f}$  is the specific force,

$b$  is the bias,

$S$  is the scale factor,

$N$  is the non-orthogonality of relevant sensor triad,

$\varepsilon$  is the relevant sensor random noise.

Modeling an INS with certain error constraints results removal of errors partially or

completely. In these sections, important errors affecting sensors inside an IMU are provided. Visualizing of common INS errors are provided in Figure 2.8.

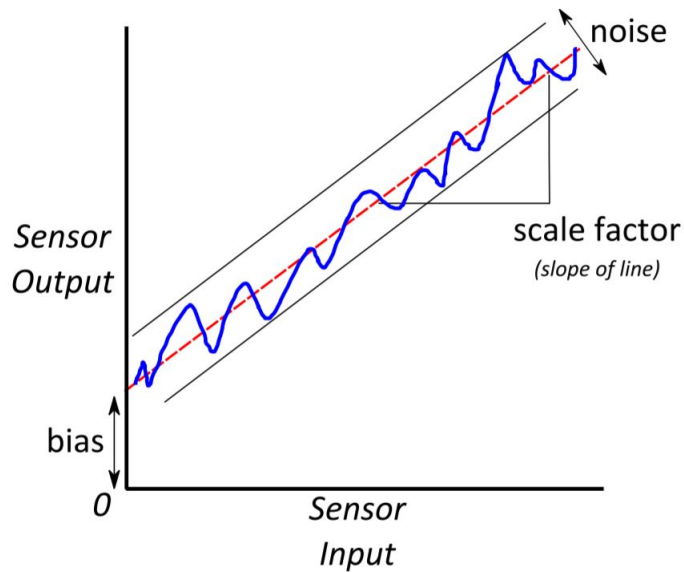


Figure 2.8: INS Error Visualization [27]

#### 2.2.4.1 Bias

Bias is the average difference between the expected output and the measured output when the IMU is turned on. It has  $^{\circ}/h$  (or  $\text{rad/s}$ ) unit for gyroscopes and  $m/s^2$  ( $\text{mg}$ ) unit for accelerometers. Bias characteristics of an IMU are important since a repeatable bias can be compensated easily and a stable bias is a key to minimizing error in measurement. Therefore, bias can be divided into two parts as bias repeatability and bias stability.

Bias repeatability is generally referred to as turn-on bias because, it evaluates the consistency of bias generated at each IMU power-up. It is found deterministically by taking average of many measurements under same conditions. Calibration processes such as six-position test or the turntable calibration enable computation of bias repeatability. For high-grade IMUs, bias repeatability is negligible [6]. For lower-grade IMUs, bias repeatability cannot be decided in certain since on the each power-up, biases can result in big differences. For this class of sensors a turn-on bias should be calculated at each power-up and it causes longer estimation period and longer align-

ment [27].

Bias stability is the change on the bias from the power-up until the end of the measurement. It is also referred as in-run bias. It depends on the temperature, time and sensor type. Bias stability is estimated by INS filter constantly and it is well-compensated error source for all low and high grade IMUs [16].

#### **2.2.4.2 Scale Factor**

Scale factor is the deviation of the input-output gradient as shown in Figure 2.8. Scale factor errors are provided in PPM. For high grade IMUs, scale factor is negligible but for low grade IMUs (MEMS) a calibration procedure is required. Since scale factor is deterministic, it can be calculated by using six-position test or turntable calibration procedures just like turn-on bias. If the scale factor errors are variable, they can also be modeled stochastically by using any random process [6, 16].

#### **2.2.5 Misalignment Errors**

Misalignment errors occur mainly during the manufacturing processes of an IMU. The axis orthogonality is broken and the measurements of each axes become dependent to other axes measurements. This error can be removed by calibration methods given above section or modeled by a random process just like in this thesis [16].

##### **2.2.5.1 Noise (Random Walk)**

There is an additive noise in each gyroscope and accelerometer measurements. Sensor dynamics or electronics, cabling around sensor create noise. It is also referred to as random walk. Random walk is an effective error within alignment and GNSS outages and depends mainly on the quality of gyroscope. It is generally modeled as zero-mean white Gaussian process but can also be calculated deterministically. Calculation is done by collecting only a few seconds measurements from IMU sensors between different time cycles and finding the mean standard deviation value from

these measurements [16, 27]. In this thesis, chosen method was to model it as random noise.

### 2.2.6 Initial Alignment

As mentioned in the beginning of this section, INS needs initial position, velocity and attitude information before starting navigation. After taking an initial information, INS can start mechanization by using accelerations and rotation rates measurements. For in-run situations, there is already information about the prior epoch. However, for the very first initialization INS needs this information externally. The process of providing this information includes position, velocity, and attitude alignment.

For the initialization process, position and velocity information is supplied from the aiding system. GNSS was the aiding system for this thesis. Velocity is also available with other aiding equipment such as odometer (for land applications) or air computer (for aerial applications) but in this thesis, only aiding system was GNSS.

Roll and pitch angles are only dependent on acceleration measurements. Under static conditions, the accelerations measured on the x-axis and y-axis of body frame can be used to compute roll and pitch angles as given below equations [14].

$$\xi = -\sin^{-1}\left(\frac{\Delta\bar{v}_x^b}{\gamma\Delta t}\right) \quad (2.47)$$

$$\eta = \sin^{-1}\left(\frac{\Delta\bar{v}_y^b}{\gamma\Delta t}\right) \quad (2.48)$$

'bar' above equations means time average. In this thesis time to calculate first roll and pitch was 60 seconds.

Accelerometer bias magnitude is an indication of the accuracy for roll and pitch estimation. They are calculated as given in Equations 2.49 and 2.50 [6]:

$$\delta\xi = \frac{(b_a)_x}{\gamma} \quad (2.49)$$

$$\delta\eta = \frac{(b_a)_y}{\gamma} \quad (2.50)$$

The final part of the attitude information is the toughest part of alignment. The quality of an IMU or the type of application can decide the alignment method. The quality of an IMU for heading initialization depends on the gyroscope. The gyroscope inside an IMU must have capability of measuring rotation rate of Earth in order to find heading statically. It requires that gyroscope shall have total gyro-bias less than 15.04 deg/h. High-grade IMUs have highly sensitive gyroscope inside of them. They can achieve static heading alignment. Since static alignment strongly depends on gyroscope, it is also referred as gyro compassing [21].

Heading is computed statically by rotating body frame angular rate measurements to the horizontal frame. Rotation angles are applied according to computed initial roll and pitch angles as given in Equation 2.51. Finally heading is calculated by taking inverse tangent of angular measurements. Before doing that, rotation to horizontal plane should be applied for roll and pitch.

$$\psi = -\tan^{-1} \left( \frac{(\Delta\bar{\theta}_{ib}^h)_x}{(\Delta\bar{\theta}_{ib}^h)_y} \right) \quad (2.51)$$

Static alignment can take time between a minute or a few minutes. It strongly depends on the environment since the sensors inside IMUs are sensitive and no movements should be done during static alignment.

With lower grade IMUs such as used in this thesis, gyroscopes are not that sensitive. In order to evaluate heading information in such systems the kinematic alignment procedure is applied. This procedure is called kinematic alignment because, it uses GNSS velocity measurements.

$$\psi = \tan^{-1} \left( \frac{v_{GNSS}^E}{v_{GNSS}^N} \right) \quad (2.52)$$

where  $v_E$  and  $v_N$  represents the velocities computed from GNSS measurements. This procedure generally needs at least 5 m/s speed in the horizontal plane because the accuracy of calculated heading depends on the amount of movement or velocity as given in Equation 2.53. As velocity or acceleration get higher, accuracy of initial heading estimation gets higher.

$$\sigma_{\psi_{GNSS}}^2 = \frac{(V_{GNSS}^E)^2}{(v_{GNSS}^E)^2 + (v_{GNSS}^N)^2} \sigma_{v_{GNSS}^N}^2 + \frac{(V_{GNSS}^N)^2}{(v_{GNSS}^E)^2 + (v_{GNSS}^N)^2} \sigma_{v_{GNSS}^E}^2 = \frac{\sigma_{v_{GNSS}}^2}{v_{GNSS}^2} \quad (2.53)$$

where sigmas are the standard deviation of GNSS computed velocities and  $V_{GNSS}$  is the GNSS computed velocity.

The other and application dependable method for heading alignment is using an external aiding. By using either a magnetometer or a Dual-Antenna GNSS receiver. A magnetometer is very sensitive to the electromagnetic variations around it and needs soft and hard iron calibrations. In a complex system, placement of a magnetometer is hard. On the other hand, Dual-Antenna GNSS receivers can provide heading and pitch information by using dual measurements taking from both antennas ends. This solution adds extra price and another GNSS antenna to be placed, which requires at least a meter distance in order to provide accurate heading information [8].

Finally, it would be nice to mention that kinematic heading alignment has some conditions. For most of the land applications, east and north components of l-frame velocities are horizontal to the vehicle's direction of motion. However, for applications such as marine and aerospace, there may exist both horizontal and vertical velocity components due to motion or environmental conditions. For this type of applications, alignment should be computed analytically based on there is large uncertainty on heading. The method is referred as Large Heading Uncertainty (LHU) [8].

In this thesis, first heading was given manually to filter and kinematic method was

used to provide more accurate heading due to the grades of IMU's inside of both reference and developed systems. The summary on the quality of IMUs depending on type and amount of errors is provided in the next section.

### **2.2.7 Classification of Inertial Navigation Systems**

IMU's quality depends on the bias, the noise, the measurement rate, gyroscope technologies and their capability of the output data in one second. The IMU grades in Table 2.2 are taken from [28] and classified as high, mid and entry performance. The key element which determines the accuracy and quality of an IMU is gyroscope. Accelerometer technology is more mature and even if the high-level IMUs have more accurate acceleration measurements, they do not create the real difference. Most of the accelerometers are very accurate at measuring gravity and roll/pitch values estimations are accurate enough even with entry-level IMUs.

As mentioned in the previous section, gyroscopes that can measure Earth rotation rate can make static heading alignment. In general the heading needs kinematics to be accurate. Therefore, there will be drifts over heading for level flight or straight route. The amount of the drifts on heading strongly depend on the quality of gyroscope.

Finally, with high-level IMUs, system can estimate IMU errors more accurately and this will reduce the possibility of unexpected drifts or unacceptable navigation solutions. As can be seen from Table 2.2, the IMUs used in this thesis are entry-level IMUs. Therefore, there shall be special arrangements to prevent performance degradation for developed INS/GNSS systems while using IMU data.

### **2.2.8 Conclusions About INS**

Inertial navigation is a solid method for computing position, velocity and attitude of a vehicle since it does not depend on the external or environmental conditions like GNSS. It is a self-contained navigation method. However, inertial navigation solution have errors and the accuracy strongly depends on the error characteristics and accuracy of gyroscopes used.

Table 2.2: IMU Quality Classification

<b>IMU Level</b>	<b>Entry Perf.</b>	<b>Mid Perf.</b>	<b>High Perf.</b>
<u>Gyro Bias</u> (deg/hr)	20 to 700	2 to 6	$\leq 2$
<u>Angular Random Walk</u> (deg/rt-hr)	0.0667 to 0.3	0.012 to 0.125	0.07 to 0.125
<u>Acc. Bias</u> (mg)	$\geq 4$	1 to 3	$\leq 1$
<u>Meas. Rate</u> (Hz)	100 to 200	100 to 200	$\geq 200$
<u>Gyro Tech.</u>	MEMS	RLG,FOG, MEMS	FOG, RLG
<u>Some COTS Sensors</u>	STIM300, ADIS16488, EPSON EG320N	HG1900, uIMU-IC, KVH1750	LN200, ISA-100, HG1700

As given in Table 2.2, errors are worse for MEMS sensors and they can grow quickly as the solution becomes unacceptable. There are always errors in the measurements made by gyroscopes and accelerometers. Hence, integration on these measurements will add these errors to calculated velocity, position and attitudes. Rapid growth in error is caused by these integration methods mainly and main elements of errors are biases in accelerometers and gyroscopes.

In order to have an accurate attitude measurements, accurate computation of velocity components is required. There are a few aiding systems such as GNSS for position and velocity, dual-antenna GNSS for heading and pitch additionally, air data computers for airspeed and barometric altitude, magnetometer for heading and odometer for velocity updates [17].

To estimate errors and update INS computations, there are techniques such as Kalman filtering, particle filtering, federated filter, and artificial intelligence (19). The most frequently used technique is Kalman filtering. Both INS and GNSS have weakness in their nature, integration of both technologies is common nowadays for accurate navigation solution. This thesis uses GNSS as aiding to a MEMS IMU. Estimation techniques and integration details of INS and GNSS are discussed in next chapters.

## CHAPTER 3

### ESTIMATION TECHNIQUES

#### 3.1 Estimation

Estimation can be explained as using the knowledge coming from various observations to calculate unknown parameters. Fundamentally if the number of known parameters is equal to the number of unknown parameters, unknown parameters can be found perfectly. Additionally, if the system that has been dealing with is linear, knowledge from measurements can be written as Equation 3.1.

$$z = Hx + \eta \quad (3.1)$$

where,

$z$  is the measurement vector,

$H$  is the observation,

$\eta$  is the measurement noise.

Measurement noise comes from the imperfections due to measurement equipment or technique or environmental conditions and random errors. As told above, if the number of known measurements is equal, there is no problem but if the number of measurements is more than unknowns, there should be an optimal solution to the problem. This is where the least square estimation enters estimation process. Least square estimation computes the optimal state which has the minimum residual. Residuals are the differences between measurements and estimation of unknowns. This method gives

most probable, most precise and most accurate estimate by choosing the state with minimum residual [18].

In order to compute an estimate from measurements by using least squares estimation, below computations should be done. Assume that an estimate with minimum residual is found as given in Equation 3.2:

$$v = z - H\hat{x} \quad (3.2)$$

where  $\hat{x}$  is the least square estimated vector of unknown parameters. Optimal solution is not possible for conditions where the number of measurements is less than the number of unknowns. Additionally, if unknown parameters are not time invariant, measurements are not enough to make an optimal estimation. In this situation, the system needs to know dynamic behaviour of the system in the defined time interval. INS/GNSS integrated systems are good example of this type of calculations. With the information to understand dynamic behaviour of the systems, better estimations are feasible. Limitations coming from the number of measurements are cancelled hence it will be possible to make estimation in conditions where there are fewer measurements than the unknowns. A linear time-variant system dynamics and measurement models are given as in Equation 3.3 and Equation 3.4:

$$\dot{x}(t) = F(t)x(t) + G(t)w(t) \quad (3.3)$$

$$z(t) = H(t)x(t) + \eta(t) \quad (3.4)$$

where, 'dot' represents time derivative and

$F(t)$  is the system dynamics matrix,

$G(t)$  is the shaping matrix of system noise,

$w(t)$  is the process noise with covariance  $Q(t)$ ,

Equations 3.3 and 3.4 are the basis for Kalman Filtering which uses both measurements and dynamics of the system to get optimal result.

It would be better to go forward with discrete-time equations since computations were done discretely on a computer in this thesis. Discrete Equations 3.3 and 3.4 are given below:

$$x_{k+1} = \Phi_{k+1,k}x_k + G_k w_k \quad (3.5)$$

$$z_k = H_k x_k + \eta_k \quad (3.6)$$

where,

$x_{k+1}$  is the state vector at epoch k+1,

$x_k$  is the state vector at epoch k,

$\Phi_{k+1,k}$  is the state transition matrix computed from system dynamics matrix from epoch k to k+1,

$G_k$  is the shaping matrix of system noise at epoch k,

$w_k$  is the process noise at epoch k with covariance  $Q_k$ ,

$z_k$  is the measurement vector at epoch k,

$H_k$  is the measurement matrix at epoch k,

$\eta_k$  is the measurement noise at epoch k with covariance  $R_k$ .

With the assumption that the system dynamics do not change from epoch  $k$  to epoch  $k + 1$ , computation of the state transition matrix (STM) is applicable with a Taylor expansion on system dynamics as given by Equation 3.7 [6]:

$$\Phi \approx e^{F\Delta t} = I + F\Delta t + \frac{(F\Delta t)^2}{2!} + \frac{(F\Delta t)^3}{3!} + \dots \quad (3.7)$$

where  $I$  is the identity matrix and  $\Delta t$  is the time interval between two epochs. First order Taylor expansion uses first two terms of the Equation 3.7 as STM with the assumption that higher order terms are negligible.

The process noise matrix is a diagonal matrix where each diagonal element has the expected value of process noise at that time epoch. It is calculated as in Equation 3.8:

$$Q_k = \int_{t_k}^{t_{k+1}} \Phi_{k+1,\tau} G(\tau) Q(\tau) G^T(\tau) \Phi_{k+1,\tau}^T d\tau \quad (3.8)$$

Using the assumption of constant process noise between epochs  $t_k$  and  $t_{k+1}$ , process noise becomes as in Equation 3.9 [8]:

$$Q_k \approx \frac{1}{2} [\Phi_k G_{t_k} Q_{t_k}^T + G_{t_k} Q_{t_k} G_{t_k}^T \Phi_k^T] \Delta t_{k+1} \quad (3.9)$$

### 3.2 Kalman Filter

Kalman filter is a recursive algorithm and is used for compensation of INS sensor errors with updates from GNSS in this thesis. Kalman filtering is an optimal least mean-variance estimator and also has the advantage of giving valuable statistical information about error characteristics of relevant systems. It does that by using all knowledge without looking at their precision. It is very useful for error analysis. Kalman filtering uses below information to make an optimal estimation [13]:

1. Information about the system and its measurements.
2. Statistical knowledge of the noise characteristics of system, measurements and uncertainty in system model.
3. Knowledge coming from initial conditions to be estimated system states.

An inertial system outputs navigational data with high data rates. But the error arising from its sensor characteristics grows with time. KF takes low frequency data

from GNSS to compensate errors coming from INS high frequency data. There are alternative systems for aiding purposes such as microwave radar (LORAN), air data computer for air speed, an odometer for land applications, set of images with a geographical database [37]. GNSS is the most common method for land, marine and air applications since it has a global coverage, good accuracy, low cost and high availability of receivers where they can be purchased over internet or off-line data sets can be found on-line. This thesis uses a GNSS receiver with one antenna as an aiding source to be integrated with an entry-level MEMS inertial navigation system.

### 3.2.1 Kalman Filter Algorithm

Kalman filter has three main stages in which two of them are prediction and measurement updates. Before starting the process, an initialization should be applied. With a wrong initialization, the filter can diverge to a whole different result than it should do. There are also assumptions for KF algorithm used in thesis which are summarized below:

1. KF is optimal for linear systems hence both process and measurements must be described as linear models.
2. KF assumes that process to be estimated and measurements occur at discrete points and both measurements and process are modeled as given in Equation 3.3 and 3.4.
3. The system (process) noise  $w_k$  and the measurement noise  $\eta_k$  are uncorrelated zero-mean white noise processes where their auto covariance functions  $Q_k$ ,  $R_k$  are known.  $Q_k$  is a positive definite matrix that represents the process noise related with INS sensor errors and  $R_k$  is a positive definite matrix that represents the measurement noise related to aiding sensor error and constraints.
4. As mentioned above, initialization is also crucial for KF performance hence an initial state vector is assumed to be a random vector that is uncorrelated with measurement and process noises.

5. Finally, the initial state vector  $x_0$  and its covariance matrix  $P_0$  are known prior to initialization.

KF is a recursive sequential algorithm. After initialization is completed, a prediction is made about the next state vector. Measurement from aiding system is used to correct predicted state vector.

### 3.2.1.1 Prediction

In the prediction stage of KF, the best estimate of last epoch is used with the state transition matrix given in Equation 3.7. Since the process noise is zero-mean, the predicted state vector is computed as given in Equation 3.10:

$$\hat{X}_{k+1}^- = \Phi_{k+1,k} \hat{x}_k^+ \quad (3.10)$$

where the 'hat' describes the estimated parameter, the superscript '-' describes the predicted parameter before measurement and the superscript '+' describes the quantity that updated with measurement at last epoch. Note that predicted state vector depends only on the state transition matrix i.e. system dynamics and the last known updated state.

Computation of a priori error covariance matrix is similar. This matrix represents the error propagation contributed from the process noise (i.e. INS sensor errors) from epoch  $k$  to  $k + 1$ .

$$P_{k+1}^- = \Phi_{k+1,k} P_k^+ \Phi_{k+1,k}^T + Q_k \quad (3.11)$$

where  $P_k^+$  is the updated estimate of the last epoch with the measurement at epoch  $k$ . Note that predicted error covariance matrix depends on system process noise and a posteriori error covariance.

### 3.2.1.2 Measurement Update

Whenever aiding system measurement is available, it is used to correct errors in predicted state. The new information coming from aiding system should be weighted by using predicted error covariance matrix  $P_{k+1}^-$  and measurement noise covariance  $R_{k+1}$ . The computation of Kalman gain aims minimizing the mean squared error of the estimate [13].

$$K_{k+1} = P_{k+1}^- H_{k+1}^T (H_{k+1} P_{k+1}^- H_{k+1}^T + R_{k+1})^{-1} \quad (3.12)$$

Kalman gain is the key parameter in deciding the amount of correction from new measurement about the predicted estimation. Equation 3.12 shows that if new measurement is noisy then the measurement noise covariance is expected to be higher or if the predicted error covariance is lower than KF will trust the predicted estimations rather than new measurement. On the contrary, if new measurement is accurate and have less noise or if predicted error covariance is higher, KF will trust on the measurement. This logic determines the amplitude of Kalman gain parameter. In this thesis, if GNSS measurements are accurate;  $K$  has large amplitude and measurement noise covariance matrix  $R_{k+1}$  gets smaller.

The comparison between predicted state vector and measurement is done by using Kalman gain as given in Equation 3.13:

$$\hat{x}_{k+1}^+ = \hat{x}_{k+1}^- + K_{k+1} (z_{k+1} - H_{k+1} \hat{x}_{k+1}^-) \quad (3.13)$$

where  $H_{k+1} \hat{x}_{k+1}^-$  is the predicted measurement  $\hat{z}_{k+1}$ .  $z_{k+1}$  is the actual measurement made at epoch  $k + 1$ . They both create the innovation sequence  $v_{k+1}$  as given in Equation 3.14:

$$v_{k+1} = z_{k+1} - \hat{z}_{k+1} = z_{k+1} - H_{k+1} \hat{x}_{k+1}^- \quad (3.14)$$

Innovation sequence is the amount of new information coming from the measurement and is weighted with Kalman gain as explained earlier.

Finally, error covariance is updated by using predicted error covariance matrix and Kalman Gain for a current epoch as given in Equation 3.15. Error covariance matrix is useful for error analysis and next epoch's initialization before prediction.

$$P_{k+1}^+ = I - K_{k+1}H_{k+1}P_{k+1}^- \quad (3.15)$$

Updated error covariance matrix implies the level of reliability on the updated (corrected) estimated a posteriori state vector  $\hat{x}_{k+1}^+$  for the next state.

A summary of general Kalman filtering is provided in Figure 3.1 with explanations.

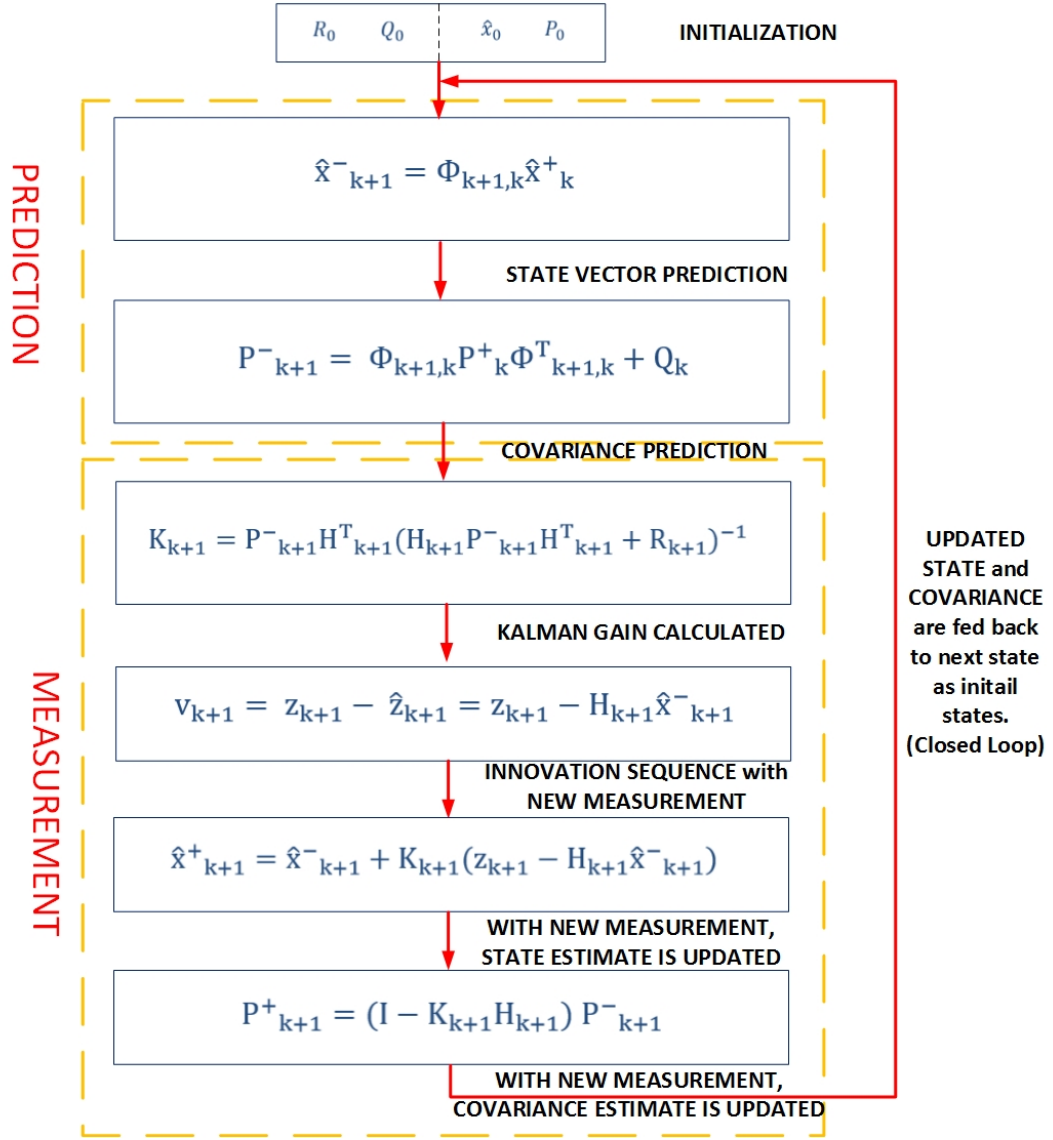


Figure 3.1: Kalman Filter Summary

### 3.3 Non-Linear Kalman Filtering

One of the assumptions was made previous section about KF optimality is that the process and measurement models must be described as linear models. However, in real-world, there are no linear systems at all. Applications such as INS and GNSS integration and their equations are non-linear. First known trial and application was Apollo space missions in 1960s for linearization according to [37]. The basic idea was to linearise a non-linear system and apply KF algorithm as given in previous

section. A non-linear process and measurement models are presented by Equations 3.16 and 3.17:

$$x_{k+1} = f(x_k, k) + w_k \quad (3.16)$$

$$z_{k+1} = h(x_{k+1}, k + 1) + \eta_{k+1} \quad (3.17)$$

where  $f$  and  $h$  are the non-linear, known system and observation matrices. Linearisation to these functions means the differences of them from the nominal trajectory.

$$x_{k+1} = x_{k+1}^* + \delta x_{k+1} \quad (3.18)$$

where '\*' means that the value to be used as reference ' $\delta$ ' means the perturbation from the reference value. Hence, when dealing non-linear systems, KF estimates error states rather than whole states. Error states represent the difference between predicted states and measurement states. Then the system and measurement equations are represented as Equations 3.19 and 3.20:

$$\delta x_{k+1} = \phi_{k+1,k} \delta x_k + w_k \quad (3.19)$$

$$\delta z_{k+1} = H_{k+1,k} \delta x_{k+1} + \eta_{k+1} \quad (3.20)$$

There are three methods to be explained which are used for linearisation non-linear systems in the next sub-sections. The first two of them use derivatives or Jacobian for the linearisation of system and process models. The third one uses a different method which focuses on the Gaussian distribution properties and making a linearisation by selecting sigma points from distribution. Methods are named Linearised Kalman Filtering (LKF), Extended Kalman Filtering (EKF) and Unscented Kalman Filtering (UKF) in order.

### 3.3.1 Linearized Kalman Filter (LKF)

With the assumption of perturbations calculated in Equations 3.19 and 3.20, the first-order Taylor series expansion can be applied to calculate system transition  $\Phi_{k+1,k}$  and measurement  $H_{k+1}$  matrices. As given in Equation 3.7, if a non-linear state dynamics matrix  $F$  is differentiable, it can be linearised with Jacobian matrix. Hence,  $\Phi_{k+1,k}$  can be represented as linearised system model with the Jacobian of system dynamics. Similarly, if a non-linear observation matrix  $H$  is differentiable, it can be linearised with Jacobian matrix. Hence,  $H_{k+1}$  can be represented as linearised measurement (sensor) model with the Jacobian of observations.

For the evaluation of Jacobian matrices, LKF uses a known trajectory. LKF is used commonly during for a system's design beginning phase or in applications where a reference trajectory can be created without breaking the assumption of little perturbations for linearisation to be realized. These applications are the flying route of an air-plane or a satellite that will orbit around world with same trajectory for years. It is also used for INS/GNSS applications. In INS/GNSS applications, mechanization equations output is accepted as reference trajectory for current epoch.

LKF is an open-loop configuration where calculated perturbations from KF is directly subtracted from reference trajectory and calculated perturbations are not fed back to inertial navigation system [11], [19].

### 3.3.2 Extended Kalman Filter (EKF)

For most of the real-time navigation applications where random trajectories occur frequently, finding a reference trajectory is not possible. There is also a possibility that the difference between reference trajectory and calculated estimates can grow in time and the assumption of small perturbations is not held.

There is another linearization method where Jacobian matrices are calculated with respect to the best state estimate rather than reference trajectory. In this method, best estimates initialize KF and estimated value is used as reference trajectory for current epoch-to-epoch Jacobian matrix calculations. This method creates a closed-loop

configuration where the inertial navigation system are updated with last calculated perturbations before calculating its output. By updating on reference trajectory with best estimates, growth of error due to big difference between reference and estimated states is limited. However, there is still a possibility of divergence from filter estimates if initial values are highly erroneous and noisy according to [20].

In this thesis one of the KF filters developed for INS/GNSS integration was EKF. In Figure 3.2, LKF and EKF equations and implementations are summarized. EKF part was implemented exactly same in MATLAB for designing EKF in this thesis.

### **3.3.3 Unscented Kalman Filter (UKF)**

The other linearization method is applicable by using Unscented Transform (UT). It is applicable by carefully sampling several points from the given mean and covariance of the PDF and making linearization with respect to these selected samples. Linearized points create transformed mean and covariance. In EKF, predictions depend only on the a priori mean value from last epoch without taking any expectation. Also for EKF, Covariance is calculated same as linear Kalman filter equations. However, if the approximations on first-order terms have high errors, the Kalman filter may not work optimally and may even diverge completely from true mean and covariance [29].

There have been researches and works done about UKF in the past. The first proposal for Unscented Transform (UT) was presented by [30] and authors of [31] worked on adaptations of UT to UKF and observed its performance on INS/GNSS integrated systems. Even though there were better results in some cases comparing with EKF, singularities occurred from Euler angle calculations according to [8]. This problem was solved by using quaternions [34]. Also in [32], authors worked on UKF non-linear estimation and presented their algorithm and comparisons with EKF.

The biggest concern of applying UKF rather than EKF in nonlinear estimation is the computation burden in real-time applications. For systems with a large number of sigma points may lead to a significant computational burden according to [8]. Every extra transformation which is not done in EKF brings additional burden. Hence there

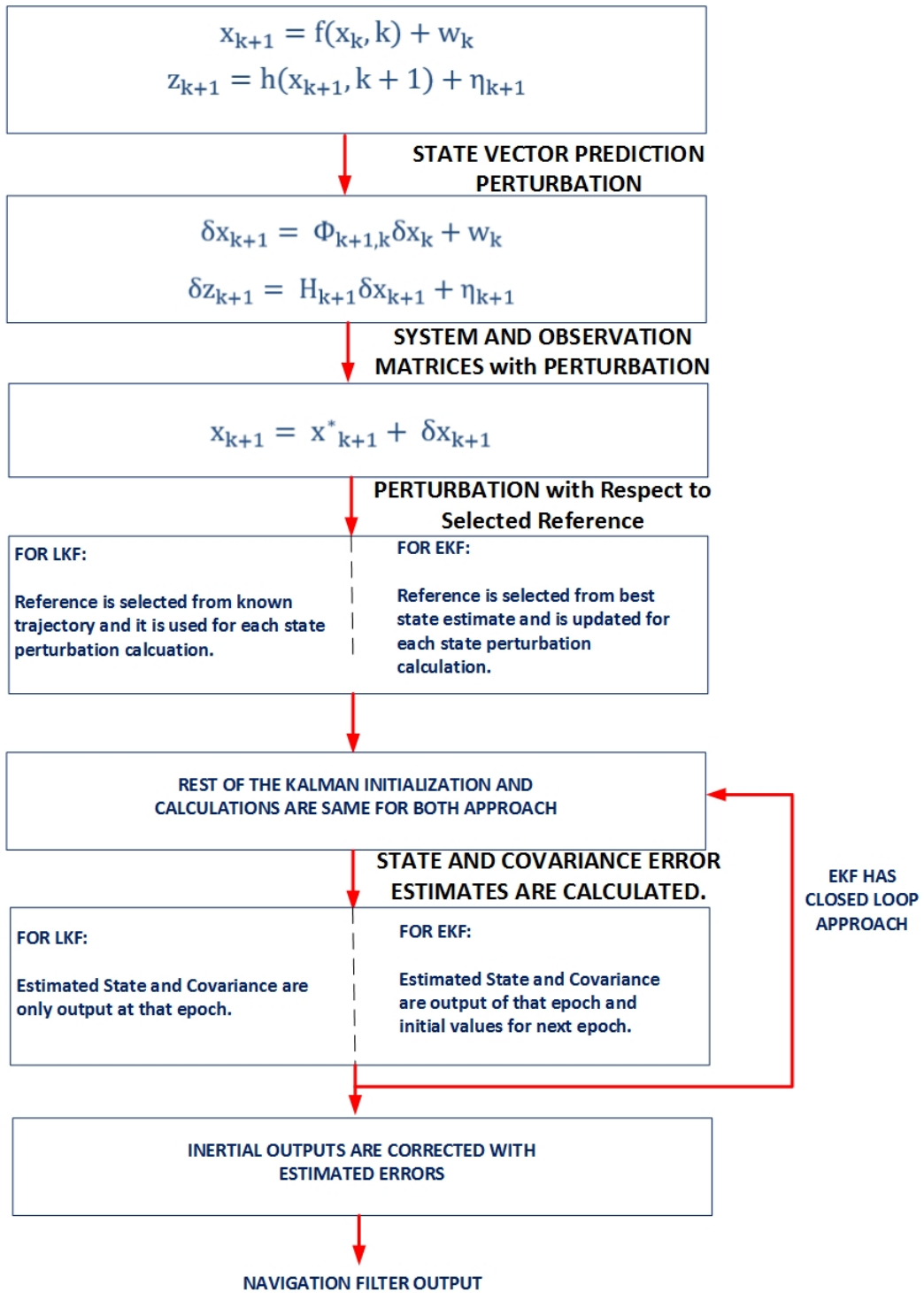


Figure 3.2: LKF and EKF Summary

have been works on that issue additionally. In [33], authors offered a method of using square root UKF besides Cholesky update algorithms as provided in [8]. In [30], authors made trials and presented a method for reducing sigma points.

In the next sections, the basics of UT is given and Scaled UT is explained. After transformation is done, Kalman Filtering by using unscented transformed mean and covariance is explained. At the end of this section, there will be a summary about calculating sigma points, weights, UKF prediction and measurement updates in author generated UKF. Mathematical explanations and equations are mostly taken from [8].

### 3.3.3.1 Unscented Transform (UT)

The UT is a procedure which depends on sampling a set of weights and sigma points with respect to given mean and covariance. Selected weights and sigma points satisfy below conditions:

$$\begin{cases} \sum_{i=0}^{p-1} w_i = 1 \\ \sum_{i=0}^{p-1} w_i X_i = \hat{x} \\ \sum_{i=0}^{p-1} w_i (X_i - \hat{x})(X_i - \hat{x})^T = P \end{cases} \quad (3.21)$$

where  $w_i$ 's are weights,  $X_i$ 's are sigma points,  $p$  is the number of sigma points,  $\hat{x}$  and  $P$  are the given mean and covariance in order. Equation 3.21 gives the idea about the realization of UT. There are two constraints about selecting weights in order to overcome the possibility of being sampled far from uncertainty level. These constraints were presented by [34].

1. The  $0^{\text{th}}$  weight is a free parameter. It can be chosen by designer freely and all other weights have the same magnitude.
2. The  $0^{\text{th}}$  weight is equal to mean and all other weights lie on a hypersphere where they are all centered at the mean.

The summarized UT is given in Equations 3.22 and 3.23:

$$X_i = \begin{cases} \bar{x}, & i=0 \\ \bar{x} + \sqrt{n + \kappa P_x}, & i=1, \dots, N \\ \bar{x} - \sqrt{n + \kappa P_x}, & i=N+1, \dots, 2N \end{cases} \quad (3.22)$$

$$w_i = \begin{cases} \frac{\kappa}{n+\kappa}, & i=0 \\ \frac{1}{2(n+\kappa)}, & i=1, \dots, N \end{cases} \quad (3.23)$$

where  $\kappa$  is a scaling parameter which is used to adjust higher-order non-linearities such as fourth and higher; and  $P$  is the covariance matrix for given PDF.  $\kappa$  is assigned as zero commonly as stated in [33].

With standard UT even if the above constraints are applied, there may be large uncertainty for attitude angles especially. Therefore, [35] represented an updated UT method that scales sigma points and this method is called Scaled UT (SUT).

### 3.3.3.2 Scaled Unscented Transform (SUT)

Sigma points and weights given by Equation 4.19 can be scaled by using below equations. For sigma points [8]:

$$X_i = \begin{cases} \bar{x}, & i=0 \\ \bar{x} + \alpha\sqrt{n + \kappa P_x}, & i=1, \dots, N \\ \bar{x} - \alpha\sqrt{n + \kappa P_x}, & i=N+1, \dots, 2N \end{cases} \quad (3.24)$$

where  $\alpha$  is a small positive scale factor which takes values between  $10^{-4}$  and 1. In SUT, weights are also scaled but they are scaled differently for mean and variance as

given in Equations 3.25 and 3.26:

$$w_i^m = \begin{cases} \frac{w_0-1}{\alpha^2} + 1, & i=0 \\ \frac{w_i}{\alpha^2}, & i=1,\dots,2N \end{cases} \quad (3.25)$$

$$w_i = \begin{cases} \frac{w_0-1}{\alpha^2} + 2 + \beta - \alpha^2, & i=0 \\ \frac{w_i}{\alpha^2}, & i=1,\dots,2N \end{cases} \quad (3.26)$$

where  $w_i^m$ 's are scaled weights for transformed mean and  $w_i^c$ 's are scaled weights for transformed covariance.  $\beta$  is another parameter to reduce higher-order effects which has the optimum value 2 for Gaussian distributions [35]. Note that the weights and sigma points given above are true for three conditions given at the beginning of this section. The calculations are not given here but they can be found in [8].

### 3.3.3.3 Kalman Filtering (UKF)

Details of Unscented Kalman Filtering step by step are given next.

With the assumption that there is a non-linear system dynamics matrix and a measurement matrix with additive Gaussian noise as given below:

$$x_{k+1} = f(x_k, k) + w_k, \text{ where } Q_k = E [w_k w_k^T] \quad (3.27)$$

$$z_{k+1} = h(x_{k+1}, k+1) + \eta_{k+1}, \text{ where } R_{k+1} = E [\eta_{k+1} \eta_{k+1}^T] \quad (3.28)$$

First step is initialization:

$$\hat{x}_0 = E [x_0] \quad (3.29)$$

$$P_0 = E [(x_0 - \hat{x}_0)(x_0 - \hat{x}_0)^T] \quad (3.30)$$

Next step is to calculate weights and sigma points according to SUT equations given in Equations 3.25 and 3.26. After this step, Kalman filter can start its prediction state based on INS output.

Transformation of calculated sigma points are done through non-linear system dynamics matrix:

$$\hat{X}_{k+1,k} = f(X_k) \quad (3.31)$$

where  $\hat{X}_{k+1,k}$  is transformed sigma points from epoch k to k+1.

Computation of mean and covariance from transformed sigma points is done:

$$\hat{X}_{k+1}^- = \sum_{i=0}^{p-1} w_i^m \hat{X}_{i,k+1,k} \quad (3.32)$$

$$P_{k+1}^- = \sum_{i=0}^{p-1} w_i^c \left( \hat{X}_{i,k+1,k} - \hat{X}_{k+1}^- \right) \left( \hat{X}_{i,k+1,k} - \hat{X}_{k+1}^- \right)^T + Q_k \quad (3.33)$$

For measurement update, measurement prediction should be done. For this to happen, transformed sigma points in Equation 3.31 are transformed again through the non-linear measurement matrix:

$$\hat{Z}_{k+1,k} = h\left(\hat{X}_{k+1,k}\right) \quad (3.34)$$

Predicted measurement can be computed from above information:

$$\hat{z}_{k+1}^- = \sum_{i=0}^{p-1} w_i^m \hat{Z}_{i,k+1,k} \quad (3.35)$$

The covariance between the predicted state and measurement is calculated as follows:

$$P_{xz,k+1} = \sum_{i=0}^{p-1} w_i^c \hat{X}_{i,k+1,k} - \hat{x}_{k+1}^- \hat{Z}_{i,k+1,k} - \hat{z}_{k+1}^-^T \quad (3.36)$$

The covariance of innovation sequence is also calculated as follows:

$$P_{zz,k+1} = \sum_{i=0}^{p-1} w_i^c \dot{Z}_{i,k+1,k} - \hat{z}_{k+1}^- \dot{Z}_{i,k+1,k} - \hat{z}_{k+1}^-^T + R_k \quad (3.37)$$

Kalman gain is calculated with these covariances as follows:

$$K_{k+1} = P_{xz,k+1} P_{zz,k+1}^{-1} \quad (3.38)$$

After Kalman gain is calculated, measurement update finalizes with corrected state vector eliminates as following two equations:

$$\hat{x}_{k+1}^+ = \hat{x}_{k+1}^- + K_{k+1} (z_{k+1} - \hat{z}_{k+1}) \quad (3.39)$$

$$P_{k+1}^+ = P_{k+1}^- - (K_{k+1} P_{zz,k+1} K_{k+1}^T) \quad (3.40)$$

The corrected or updated state vector and covariance which is an indicator of how reliable this estimated value is then fed back as initial values for the next epoch and they are used for calculation of sigma points and weights. The algorithm used in the thesis for UKF is given in Figure 3.3.

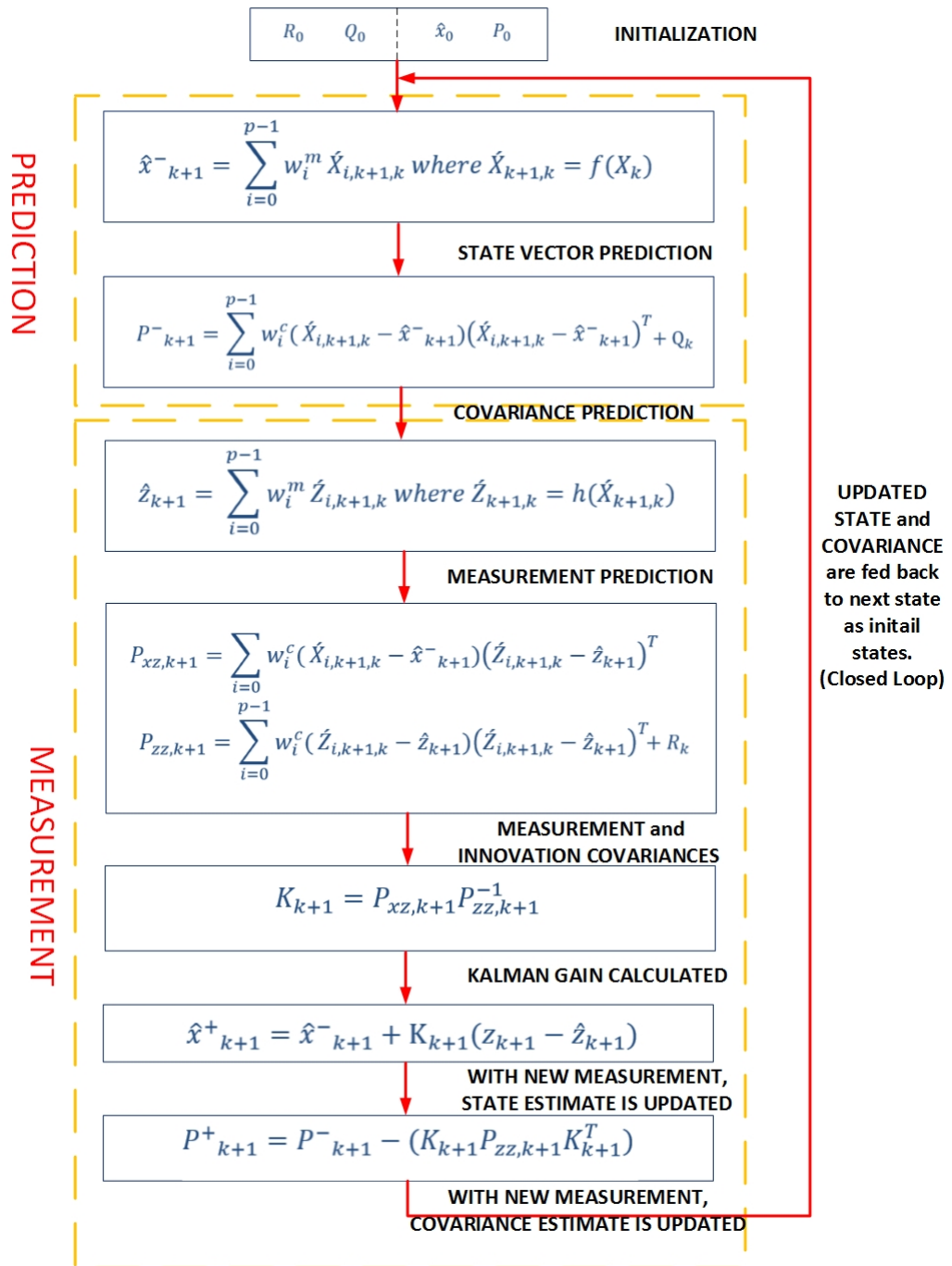


Figure 3.3: UKF Summary



## CHAPTER 4

### INTEGRATION OF INS/GNSS AND MODELING ERRORS BY LINEAR STATE EQUATIONS

#### 4.1 Integration Techniques

As mentioned earlier, both INS and GNSS have flaws in their nature and advantages compared to each other. To overcome both system flaws, there are different methods at the level of sharing information and usage of estimated errors at Kalman filter. The methods can be chosen according to the application, environmental conditions (such as Urban or Open Area), quality and accuracy of chosen INS sensor and GNSS receiver.

There are four methods for integration purposes. The main difference between these methods comes from the types of information used to compute navigation data. With this aspect, methods can be named as uncoupled, loosely coupled, tightly coupled and deeply coupled integration. The most common methods used in user level are loosely coupled and tightly coupled integration methods [13, 19].

In some applications of INS/GNSS integration, estimated errors are only used for current state's INS navigation solution error compensation. This implementation approach is defined as *open loop*. The second approach uses these estimated errors to compute better navigation solution from INS-only solution in addition to current state's error compensation. Hence, this method is named as *closed loop*.

In the uncoupled integration, systems work independently from each other and both INS and GNSS systems compute their positions differently. In this method, when GNSS starts to compute navigation solution, INS stops computing or INS outputs are

not used during this period. In this method, INS and GNSS become a backup system for each other. This method requires the least computational load since it does not include any Kalman filter. However, since both systems work independently from each other, their navigational accuracy is not improved at all. In addition to this fact, attitude information such as roll, pitch and heading is not computed during GNSS period if chosen GNSS receiver is a single antenna GNSS receiver like the one in this thesis.

On the other hand, deeply coupled integration method requires both systems to work cooperatively. At this method, integration is called deeply since integration is done at the GNSS receiver tracking loops level. Rather than using GNSS as an aiding source only, deeply coupling uses INS to improve GNSS tracking loops accuracy when GNSS signals is degraded or GNSS accuracy is low additionally. However, integration at this level requires designer to manipulate firmware of the receiver and to sample in-phase and quadrature of GNSS correlators. Hence, this type of integration is not commonly used by designers other than receiver manufacturer [4, 7].

The most common methods for INS/GNSS integration are loosely and tightly coupled since they can be applied to most of the equipment on market.

#### **4.1.1 Loosely Coupled Integration**

Context of loosely coupled integration comes from the fact that error corrections are only done by aiding GNSS position and velocity as measurement to Kalman Filter. It means, GNSS position and velocity are computed separately by a GNSS filter and computed GNSS position and velocity are subtracted from position and velocity computed by INS. The difference then becomes the input for navigation filter.

The main advantage of this method is that even if one of the systems fail, other system can keep on computing navigational data on itself. Hence, system becomes robust to failures. Another advantage of this system will be seen in next sections where loosely coupled integration requires less states than tightly coupled integration method at Kalman filter design. However, this method requires using two system's output and this leads a high probability on increasing noise at system. In addition, to compute

accurate GNSS position and velocity, receiver needs at least four satellites on sight. Otherwise GNSS accuracy becomes corrupted and lead low accuracy solution.

The loosely coupled integration method block diagram is given in Figure 4.1. It can be seen from this figure there are two Kalman filters. Hence, [6] named this method as decentralized integration strategy.

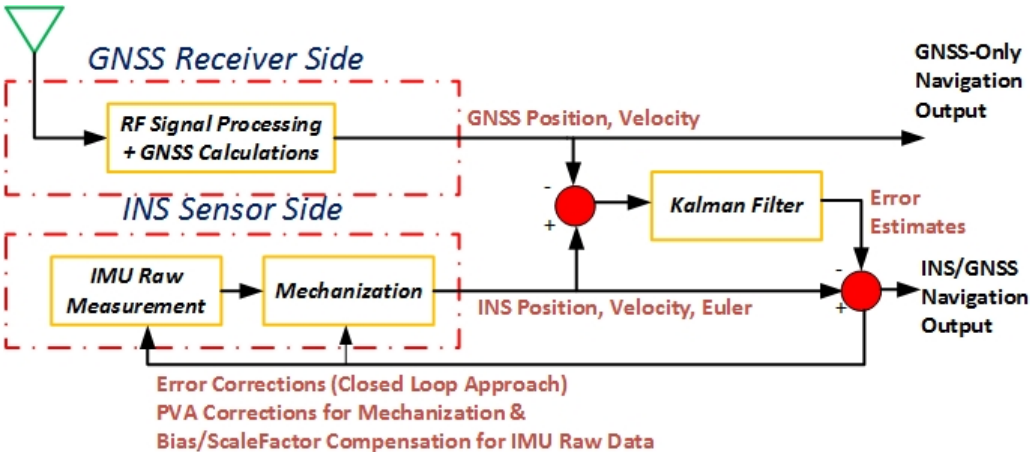


Figure 4.1: Loosely Coupled Integration

As discussed in the beginning of this chapter, application does matter for choosing right integration method. The cost, computational load and ease of implementation need to be compared with the environmental conditions where system will work commonly. For aerial applications or open area application, there are no obstruction to lead multipath or corruption on GNSS signals, loosely coupled INS/GNSS integrated products are used commonly. However, if the application is critical and blockage of GNSS signals may happen frequently, tightly coupled integration method is chosen. Details of this method is given in the next section.

**4.1.2 Tightly Coupled Integration**

In this integration method, GNSS and INS work together where each can be referred as a sub-system of a system. Tightly coupled integration uses raw GNSS measurements such as pseudorange, carrier-phase measurements and Doppler measurements are used rather than GNSS computed position and velocity. Perturbations are com-

puted by finding difference between GNSS raw measurements and INS predictions. The rest of the navigation algorithm is same with loosely coupled integration. Navigation filter takes perturbations and outputs estimated errors. The block diagram of tightly coupled integration is given in Figure 4.2 where it can be observed that if GNSS ambiguities are solved, system needs only one Kalman Filter [7].

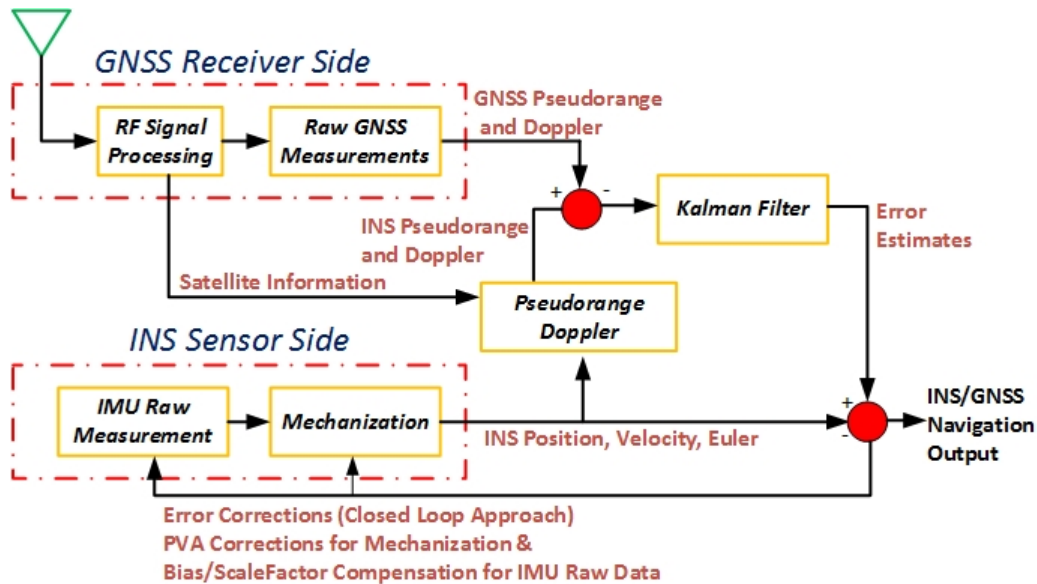


Figure 4.2: Tightly Coupled Integration

Tightly coupled integration can still compute INS/GNSS solution even under low number of visible satellites. As given in Chapter 2, GNSS receiver needs at least 4 satellites to compute position and velocity. Since raw measurements are used for tightly coupling, even with 2 satellites, accurate navigation solution can be computed continuously. However, system process model should be modified for tightly coupled integration method. System transition matrix (STM) have larger dimensions comparing with loosely coupled STM. Hence, additional states increase computational load. Today, for urban areas or city center where blockage of GNSS systems happen frequently, tightly coupled integration is a common choice.

Since both methods are the most common integration methods in market today, INS/GNSS integration is applied by using both methods with different Kalman Filtering techniques on same sensors in this thesis.

### 4.1.3 Open Loop and Closed Loop Implementation

At the both loosely coupled and tightly coupled integration block diagrams given in Figure 4.1 and Figure 4.2, computed error estimates are fed back to INS mechanization process. This type of implementation is named Closed Loop. This implementation type is a necessity when low-cost IMU sensors exist in INS/GNSS integration since this type of sensors tend to have drift and growth on their errors. These errors propagate largely in a short time [6]. Feedback of error estimates corrects this type of sensor error sources and improve Kalman Filter performance.

For *Open Loop* implementation, INS mechanization equations do not aware of the estimated errors by Kalman filter because errors are not fed back to INS. Estimated errors are only used for error correction of INS navigation output. This type of implementation is valid if system have high-grade IMU sensors. This type of sensors tends to behaviour more stable than low-grade sensors and do not propagate large errors in short time intervals [6].

For this thesis, *Closed Loop* implementation is adapted for both tightly coupled and loosely coupled integration methods since a low-cost MEMS IMU is used in INS mechanization process.

## 4.2 Lever Arm Effects on Integration

Beside INS/GNSS integration techniques above, there is another critical parameter which affects the accuracy of system. GNSS receiver makes calculations with respect to antenna phase center. INS makes its measurement with respect to intersection of three orthogonal axes. The distance vector between the antenna phase center and the center of INS measurements is called lever arm. Lever arm is a three-dimensional vector and differences between INS and GNSS centers at each axis are taken account. Mathematical equations for lever arm effect are taken from [14].

The difference in position and velocity depending on the lever arm vector is found by

following Equations 4.1 and 4.2:

$$\Delta r^e = R_b^e l^b \quad (4.1)$$

$$\Delta v^e = \Omega_{ie}^e R_b^e l^b + R_b^e \Omega_{ib}^b l^b \quad (4.2)$$

where  $l_b$  is lever arm vector in b-frame. To compute the effect of lever arm at each calculation, above equations are perturbed as given Equations 4.3 and 4.4 with the assumptions of errorless gyro measurements and perfectly known rotation matrix.

$$\delta \Delta r^e = R_b^e \delta l^b \quad (4.3)$$

$$\delta \Delta v^e = \Omega_{ie}^e R_b^e \delta l^b + R_b^e \Omega_{ib}^b \delta l^b \quad (4.4)$$

From Equation 4.3, in order to cancel lever-arm effect on position, lever-arm must be known with the same accuracy as position. There is another fact from Equation 4.4 which shows the effect of lever-arm on velocity depends on the rotation rate in addition to position. In this case, lever-arm should be known with better accuracy than position since only 1 cm error in velocity can cause 5 mm/s velocity error [14].

As a result, lever-arm must be known with very high accuracy (less than 1 cm) in order to cancel its effect in each measurement update. To measure lever-arm, proved common measurement techniques are used such as laser total station with mm accuracy. Another method of measuring lever-arm is estimating it by IMU mechanization process with enough accuracy. However, under bad GNSS coverage and low dynamics conditions, the filter may diverge from the truth [38]. Lever-arm estimation with error decreases the accuracy on horizontal plane for single-antenna GNSS receiver. Lever-arm error with respect to secondary antenna for dual-antenna GNSS receiver leads a biased computation of lever-arm [36]. Finally, lever-arm inaccuracies lead growth of error in position, velocity and heading. Hence, it should be noted for hardware integration of an INS/GNSS system, lever-arm measurement should be done with enough accuracy.

### 4.3 Modeling INS and GNSS Errors by Linear State Equations

This section explains the system dynamics and measurement models developed for this thesis. It starts with the augmentation of INS error sources for system transition matrix and measurement matrix.

As discussed earlier, Kalman filter calculates error states of the navigation. Augmented states need to be added to system model for accurate navigation. On the other hand, measurement states need to be modified according to integration techniques given in previous section.

#### 4.3.1 System Process Model

General navigation filter for INS contains nine error states which are defined as three positions, three velocities and three attitude error states. This is only possible where all the error sources and their characteristics are completely known hence it is not possible in real life. As explained in Chapter 2, there are quality differences among IMUs because of the inertial sensors inside of them. In this thesis an entry performance MEMS IMU ADIS-16488 was used for development. This led system dynamics model needs to be augmented with additional error states. All states and complete system dynamics model will be explained in following sub-sections.

##### 4.3.1.1 General INS Error States

The INS mechanization output position, velocity and attitude vectors. For compliance, Equation 4.5 is represented again:

$$\begin{bmatrix} \dot{r}^e \\ \dot{v}^e \\ \dot{R}_b^e \end{bmatrix} = \begin{bmatrix} v^e \\ R_b^e - 2\Omega_{ie}^e v^e + \gamma^e \\ R_b^e (\Omega_{ei}^b \Omega_{ib}^b) \end{bmatrix} \quad (4.5)$$

Kalman filtering uses perturbed system model. Hence, Equation 4.6 needs to be perturbed. This process includes a series of complex derivation hence details of this

derivation are not given here. Readers can find details of derivation in [40] and [8] and [13].

$$\begin{bmatrix} \delta \dot{r}^e \\ \delta \dot{v}^e \\ \dot{\varepsilon}^e \end{bmatrix} = \begin{bmatrix} \delta v^e \\ -2\Omega_{ie}^e \delta v^e + N^e \delta r^e - F^e \varepsilon^e \\ -\Omega_{ei}^e \varepsilon^e \end{bmatrix} + \begin{bmatrix} 0 \\ R_b^e \delta f^b \\ R_b^e \delta w^b \end{bmatrix} \quad (4.6)$$

where  $\delta$  sign means perturbed quantity and '*dots*' denote time derivatives and the superscripts '*b*' and '*e*' denote body and ECEF frames in order. Other symbols:

$\delta r$  is three-dimensional position error state vector,

$\delta v$  is three-dimensional velocity error state vector,

$\varepsilon$  is misalignment error state vector in three dimensions,

$F$  is the skew-symmetric matrix of specific force in three dimensions,

$R_b^e$  is the rotation matrix from b-frame to e-frame,

$\Omega_{ie}$  is the skew-symmetric matrix of rotation rate from i-frame to e-frame,

$N$  is the gravity gradient coefficient matrix,

$\delta f$  is the accelerometer sensor errors in three dimensions,

$\delta w$  is the gyroscope sensor errors in three dimensions.

According to [6] and [8], this error model is named as the  $\phi$ -angle error model in the literature.

#### 4.3.1.2 Sensor Error States

IMU sensors have different quality grades and their error characteristics differ in accordance with sensor quality. For high-quality IMUs, turn-on bias (bias repeatability), scale factor and axes misalignment errors can be ignored since they are all calculated with calibration methods explained in Chapter 2 easily. The remaining errors for high-quality IMUs are bias stability (in-run bias) and sensor noise. Given these facts,

there were two different filters designed for this thesis. First one included the sensor error states with bias stability error and sensor noise. As a result, accelerometer and gyroscope error equation can be written as Equation 4.7 and Equation 4.8 [6, 14]:

$$\delta f = \tilde{f} - f = \delta b_a + \eta_a \quad (4.7)$$

$$\delta w = \tilde{w} - w = \delta b_g + \eta_g \quad (4.8)$$

Sensor noise spectral densities  $\eta_a$  and  $\eta_g$  were computed by computing the standard deviation by using a few seconds of static data. Standard deviations were computed after removing the mean and by selecting random periods in static data. By taking mean of these standard deviation, noise spectral densities,  $q_a$  and  $q_g$  were computed.

The general method for modelling bias stability,  $\delta b_i$ , is to use First order Gauss-Markov process. It can also be modeled as zero-mean white Gaussian but as presented in [41] and [42], for engineering application it is more realistic to use Gauss-Markov process [5]. The first order Gauss-Markov process model for bias stability is given in Equation 4.9:

$$\delta \dot{b}_i = -\frac{1}{\tau_i} \delta b_i + \eta_{bi} \quad (4.9)$$

where 'i' is equal to 'a' for accelerometer and 'g' for gyroscope and

$\tau_i$  is the selected correlation time,

$\eta_{bi}$  is the Gauss-Markov process driving noise with spectral density  $q_{bi}$ .

Hence, the Gauss-Markov process includes parameters  $\tau_i$ ,  $q_i$  and these parameters were computed from autocorrelation function of the raw data collected in user-selected correlation time [6, 41]. The general rule for collecting static data from IMU was to collect as much as possible for required accuracy. As told in [5] for 10 percent accuracy in an hour, amount of static data to be collected can be up to 200 hours. Previous researches showed that even with the less static data, there is still enough accuracy for this thesis. Hence, as [14] and [5] authors did in their researches, as much as static

data was collected for this purpose. For this thesis, ten hours of static data is used in order to compute the Gauss-Markov model parameters.

$$q_{bi} = \sqrt{\frac{2\sigma_i^2}{\tau_i}} \quad (4.10)$$

where  $\sigma_i$  is the computed standard deviation.

Computing temporal variance and using Equation 4.10 for both accelerometer and gyroscope bias stability model, augmented bias stability error states were ready.

After auto-correlation processes is done and Gauss-Markov process model parameters are computed, the system dynamics model can be written with bias stability error and sensor noise parameters as below which results in a 15-State system dynamics model:

$$\begin{bmatrix} \delta \dot{r}^e \\ \delta \dot{v}^e \\ \dot{\varepsilon}^e \\ \delta \dot{b}_a \\ \delta \dot{b}_g \end{bmatrix} = \begin{bmatrix} 0_{3 \times 3} & I_{3 \times 3} & 0_{3 \times 3} & 0_{3 \times 3} & 0_{3 \times 3} \\ N_{3 \times 3}^e & -2(\Omega_{ie}^e)_{3 \times 3} & -F_{3 \times 3}^e & (R_b^e)_{3 \times 3} & 0_{3 \times 3} \\ 0_{3 \times 3} & 0_{3 \times 3} & -(\Omega_{ie}^e)_{3 \times 3} & 0_{3 \times 3} & (R_b^e)_{3 \times 3} \\ 0_{3 \times 3} & 0_{3 \times 3} & 0_{3 \times 3} & \left(\frac{-1}{\tau_a}\right)_{3 \times 3} & 0_{3 \times 3} \\ 0_{3 \times 3} & 0_{3 \times 3} & 0_{3 \times 3} & 0_{3 \times 3} & \left(\frac{-1}{\tau_g}\right)_{3 \times 3} \end{bmatrix} \begin{bmatrix} \delta r^e \\ \delta v^e \\ \varepsilon^e \\ \delta b_a \\ \delta b_g \end{bmatrix} + \begin{bmatrix} 0_{3 \times 3} & 0_{3 \times 3} & 0_{3 \times 3} & 0_{3 \times 3} \\ (R_b^e)_{3 \times 3} & 0_{3 \times 3} & 0_{3 \times 3} & 0_{3 \times 3} \\ 0_{3 \times 3} & (R_b^e)_{3 \times 3} & 0_{3 \times 3} & 0_{3 \times 3} \\ 0_{3 \times 3} & 0_{3 \times 3} & I_{3 \times 3} & 0_{3 \times 3} \\ 0_{3 \times 3} & 0_{3 \times 3} & 0_{3 \times 3} & I_{3 \times 3} \end{bmatrix} \begin{bmatrix} \eta_a \\ \eta_g \\ \eta_{ba} \\ \eta_{bg} \end{bmatrix} \quad (4.11)$$

System dynamics noise spectral density matrix is given below which is created with the information gained from auto-correlation:

$$Q = \begin{bmatrix} (q_a)_{3 \times 3} & 0_{3 \times 3} & 0_{3 \times 3} & 0_{3 \times 3} \\ 0_{3 \times 3} & (q_g)_{3 \times 3} & 0_{3 \times 3} & 0_{3 \times 3} \\ 0_{3 \times 3} & 0_{3 \times 3} & (q_{ba})_{3 \times 3} & 0_{3 \times 3} \\ 0_{3 \times 3} & 0_{3 \times 3} & 0_{3 \times 3} & (q_{bg})_{3 \times 3} \end{bmatrix} \quad (4.12)$$

The above system dynamics model was valid for systems with high-quality IMUs.

However, for applications with lower grade IMUs such as the one which is used for this thesis, scale factor, non-orthogonality and turn-on biases should also be compensated through Kalman filter. In Chapter 2, these errors were told as deterministic in their nature but can have rapid changes from one turn-on to next turn-on for entry-level IMUs. Both errors were modeled as bias stability and noise. Modeling all error sources can lead instabilities in filter and weaken accuracy of navigation solution [14].

Scale factor error can be modeled as the Gauss-Markov process in order to compensate error through the Kalman filter. It requires computation of parameters such as correlation time and noise spectral density which has same procedure with bias stability. Other methods can be found in [5]. In this thesis Gauss-Markov process model was chosen and correlation time was selected as 10 hours. The Gauss-Markov process model for scale factor was given in Equation 4.13:

$$\dot{S}_i = \frac{-1}{\tau_{si}} S_i + \eta_{si} \quad (4.13)$$

where 'i' is equal to 'a' for accelerometer and 'g' for gyroscope.

With the assumption of slow variation, static data from both gyroscope and accelerometer was collected for 10 hours and the temporal standard deviation was computed by using technical specifications provided by IMU company.

Turn-on biases was assumed to be constant for each power-up cycle. Hence, for both accelerometer and gyroscope, it was modelled as random constant processes [6]. Other methods for computing or modelling turn-on biases can be found in [5]. Turn-on bias processes are given in Equation 4.14:

$$\dot{b}_{i,turnon} = 0 \quad (4.14)$$

where 'i' is equal to 'a' for accelerometer and 'g' for gyroscope.

Combining the above error states results in a 27-State augmented system process model as given in Equation 4.15:

$$\begin{bmatrix} \delta \dot{r}^e \\ \delta \dot{v}^e \\ \dot{\varepsilon}^e \\ \delta \dot{b}_a \\ \delta \dot{b}_g \\ \dot{b}_{a,ton} \\ \dot{b}_{g,ton} \\ \dot{S}_a \\ \dot{S}_g \end{bmatrix} = (\Phi)_{27 \times 27} \begin{bmatrix} \delta r^e \\ \delta v^e \\ \varepsilon^e \\ \delta b_a \\ \delta b_g \\ b_{a,ton} \\ b_{g,ton} \\ S_a \\ S_g \end{bmatrix} + \begin{bmatrix} 0_{3 \times 3} & 0_{3 \times 3} & 0_{3 \times 3} & 0_{3 \times 3} & 0_{3 \times 3} & 0_{3 \times 3} & 0_{3 \times 3} & 0_{3 \times 3} & 0_{3 \times 3} \\ (R_b^e)_{3 \times 3} & 0_{3 \times 3} & 0_{3 \times 3} & 0_{3 \times 3} & 0_{3 \times 3} & 0_{3 \times 3} & 0_{3 \times 3} & 0_{3 \times 3} & 0_{3 \times 3} \\ 0_{3 \times 3} & (R_b^e)_{3 \times 3} & 0_{3 \times 3} & 0_{3 \times 3} & 0_{3 \times 3} & 0_{3 \times 3} & 0_{3 \times 3} & 0_{3 \times 3} & 0_{3 \times 3} \\ 0_{3 \times 3} & 0_{3 \times 3} & I_{3 \times 3} & 0_{3 \times 3} & 0_{3 \times 3} & 0_{3 \times 3} & 0_{3 \times 3} & 0_{3 \times 3} & 0_{3 \times 3} \\ 0_{3 \times 3} & 0_{3 \times 3} & 0_{3 \times 3} & I_{3 \times 3} & 0_{3 \times 3} & 0_{3 \times 3} & 0_{3 \times 3} & 0_{3 \times 3} & 0_{3 \times 3} \\ 0_{3 \times 3} & 0_{3 \times 3} & 0_{3 \times 3} & 0_{3 \times 3} & I_{3 \times 3} & 0_{3 \times 3} & 0_{3 \times 3} & 0_{3 \times 3} & 0_{3 \times 3} \\ 0_{3 \times 3} & 0_{3 \times 3} & 0_{3 \times 3} & 0_{3 \times 3} & 0_{3 \times 3} & I_{3 \times 3} & 0_{3 \times 3} & 0_{3 \times 3} & 0_{3 \times 3} \\ 0_{3 \times 3} & 0_{3 \times 3} & 0_{3 \times 3} & 0_{3 \times 3} & 0_{3 \times 3} & 0_{3 \times 3} & I_{3 \times 3} & 0_{3 \times 3} & 0_{3 \times 3} \\ 0_{3 \times 3} & 0_{3 \times 3} & 0_{3 \times 3} & 0_{3 \times 3} & 0_{3 \times 3} & 0_{3 \times 3} & 0_{3 \times 3} & I_{3 \times 3} & 0_{3 \times 3} \end{bmatrix} \begin{bmatrix} \eta_a \\ \eta_g \\ \eta_{ba} \\ \eta_{bg} \\ \eta_{sa} \\ \eta_{sg} \end{bmatrix} \quad (4.15)$$

where  $(\Phi)_{27 \times 27}$  is given in Equation 4.16 where each elements presented below is  $3 \times 3$  matrix:

$$\begin{bmatrix} 0 & I & 0 & 0 & 0 & 0 & 0 & 0 & 0 \\ N^e & -2(\Omega_{ie}^e) & -F^e & (R_b^e) & 0 & 0 & 0 & 0 & 0 \\ 0 & 0 & -(\Omega_{ie}^e) & 0 & (R_b^e) & 0 & 0 & 0 & 0 \\ 0 & 0 & 0 & \left(\frac{-1}{\tau_a}\right) & 0 & 0 & 0 & 0 & 0 \\ 0 & 0 & 0 & 0 & \left(\frac{-1}{\tau_g}\right) & 0 & 0 & 0 & 0 \\ 0 & 0 & 0 & 0 & 0 & 0 & 0 & 0 & 0 \\ 0 & 0 & 0 & 0 & 0 & 0 & 0 & 0 & 0 \\ 0 & 0 & 0 & 0 & 0 & 0 & 0 & \left(\frac{-1}{\tau_{sa}}\right) & 0 \\ 0 & 0 & 0 & 0 & 0 & 0 & 0 & 0 & \left(\frac{-1}{\tau_{sg}}\right) \end{bmatrix} \quad (4.16)$$

Corresponding system process noise spectral density matrix for 27-State is given in

Equation 4.17:

$$Q = \begin{bmatrix} (q_a)_{3 \times 3} & 0_{3 \times 3} & 0_{3 \times 3} & 0_{3 \times 3} & 0_{3 \times 3} & 0_{3 \times 3} \\ 0_{3 \times 3} & (q_g)_{3 \times 3} & 0_{3 \times 3} & 0_{3 \times 3} & 0_{3 \times 3} & 0_{3 \times 3} \\ 0_{3 \times 3} & 0_{3 \times 3} & (q_{ba})_{3 \times 3} & 0_{3 \times 3} & 0_{3 \times 3} & 0_{3 \times 3} \\ 0_{3 \times 3} & 0_{3 \times 3} & 0_{3 \times 3} & (q_{bg})_{3 \times 3} & 0_{3 \times 3} & 0_{3 \times 3} \\ 0_{3 \times 3} & 0_{3 \times 3} & 0_{3 \times 3} & 0_{3 \times 3} & (q_{sa})_{3 \times 3} & 0_{3 \times 3} \\ 0_{3 \times 3} & 0_{3 \times 3} & 0_{3 \times 3} & 0_{3 \times 3} & 0_{3 \times 3} & (q_{sg})_{3 \times 3} \end{bmatrix} \quad (4.17)$$

It would be nice to mention the fact that, INS bias is the summation of bias repeatability and turn-on bias. Since they were modeled separately, four different error state matrices were occurred in Equation 4.16 and Equation 4.17.

There are other modeling techniques for augmented error states for low-cost, low-quality IMUs. Readers are invited to read [4], [11] and [8].

#### 4.3.1.3 GNSS Error States

In a tightly coupled integration, GNSS pseudorange and pseudorange rate measurements are used in calculations. Hence, their error sources should be augmented to system process model for compensation. Two additional error states which are clock offset and clock drift error states [6] are the additional two states for tightly coupled integration method. In this situation, 15-State and 27-State system process matrix becomes 17-State and 29-State for tightly coupled method.

#### 4.3.2 Measurement Model

The measurement models for loosely coupled and tightly coupled integration methods are different since measurements taken from aiding sensors are different. For compliance, the loosely coupled measurement model is given first and it is followed by tightly coupled measurement model.

### 4.3.2.1 Loosely Coupled Integration Method

In this integration method, the difference between INS computed position/velocity and GNSS derived position/velocity is used for the innovation sequence. A comparison is done between measurements and INS predictions at this step and at the next step, this comparison is weighted according to the uncertainty of current measurements and predictions. Thus, the measurement design matrix for loosely coupled integration is written easily in Equation 4.18:

$$H = \begin{bmatrix} I_{3 \times 3} & 0_{3 \times 3} & 0_{3 \times (n-6)} \\ 0_{3 \times 3} & I_{3 \times 3} & 0_{3 \times (n-6)} \end{bmatrix} \quad (4.18)$$

where 'n' is the number of states used in the system dynamics model.

Measurement noise covariance matrix R for this thesis was computed by calculating measurement's standard deviation at zenith and scale it according to elevation angle  $e$  with  $\sin\left(\frac{1}{e}\right)$  [14].

The measurement noise is only composed of GNSS components. INS noises is already processed before innovation sequence in Kalman filtering. Hence, INS error states have no effect on innovation and, after first 6 columns, rest of the columns are equal to zero.

### 4.3.2.2 Tightly Coupled Integration Method

In this integration method GNSS pseudorange and pseudorange rate measurements are used for innovation sequence of Kalman filtering. The pseudorange and pseudorange rate rows in design matrix are given in Equations 4.19 and 4.20:

$$h_p = \sqrt{(X_i - X_U)^2 + (Y_i - Y_U)^2 + (Z_i - Z_U)^2} + ct \quad (4.19)$$

$$h_{\dot{p}} = \sqrt{(V_{x_i} - V_{x_u})^2 + (V_{y_i} - V_{y_u})^2 + (V_{z_i} - V_{z_u})^2} + c\delta t \quad (4.20)$$

where  $X_i, Y_i, Z_i$  and  $V_{x_i}, V_{y_i}, V_{z_i}$  are the  $i^{th}$  satellites's position and velocity in ECEF and  $X_U, Y_U, Z_U$  and  $V_{x_u}, V_{y_u}, V_{z_u}$  are the user's position and velocity in ECEF,  $t$  is the clock offset error and  $\delta$  is clock drift error.

Since clock offset and drifts error states are augmented into the system process model and other error states are processed by system process matrix, the design matrix  $H$  can be written as in Equation 4.21 [6]:

$$H = \begin{bmatrix} H(\rho)_{Nx3} & 0_{Nx3} & 0_{Nx(m-8)} & -1_{Nx1} & 0_{Nx1} \\ 0_{Nx3} & H(\dot{\rho})_{Nx3} & 0_{Nx(m-8)} & 0_{Nx1} & -1_{Nx1} \end{bmatrix} \quad (4.21)$$

where  $N$  is the number of visible satellites and  $m$  is the number of states.  $H(\rho)$  and  $H(\dot{\rho})$  are given in Equations 4.22 and 4.23:

$$H(\rho) = \begin{bmatrix} \frac{\partial p^1}{\partial r_x} & \frac{\partial p^1}{\partial r_y} & \frac{\partial p^1}{\partial r_z} & 0 & 0 & 0 & 1 & 0 \\ \dots & \dots & \dots & \dots & \dots & \dots & \dots & \dots \\ \frac{\partial p^N}{\partial r_x} & \frac{\partial p^N}{\partial r_y} & \frac{\partial p^N}{\partial r_z} & 0 & 0 & 0 & 1 & 0 \end{bmatrix} \quad (4.22)$$

$$H(\dot{\rho}) = \begin{bmatrix} \frac{\partial \dot{p}^1}{\partial r_x} & \frac{\partial \dot{p}^1}{\partial r_y} & \frac{\partial \dot{p}^1}{\partial r_z} & \frac{\partial \dot{p}^1}{\partial v_x} & \frac{\partial \dot{p}^1}{\partial v_y} & \frac{\partial \dot{p}^1}{\partial v_z} & 0 & 1 \\ \dots & \dots & \dots & \dots & \dots & \dots & \dots & \dots \\ \frac{\partial \dot{p}^N}{\partial r_x} & \frac{\partial \dot{p}^N}{\partial r_y} & \frac{\partial \dot{p}^N}{\partial r_z} & \frac{\partial \dot{p}^N}{\partial v_x} & \frac{\partial \dot{p}^N}{\partial v_y} & \frac{\partial \dot{p}^N}{\partial v_z} & 0 & 1 \end{bmatrix} \quad (4.23)$$

Measurement noise covariance matrix for this thesis was computed by calculating measurement's standard deviation at zenith and scale it according to elevation angle  $e$  with  $\sin\left(\frac{1}{e}\right)$  [14] for tightly coupled measurement model too.

#### 4.4 Summary of Loosely and Tightly Coupled Integration

In this section, the summary of loosely and tightly coupled integration developed for this thesis are provided separately. They are provided in Figure 4.3 and Figure 4.4:

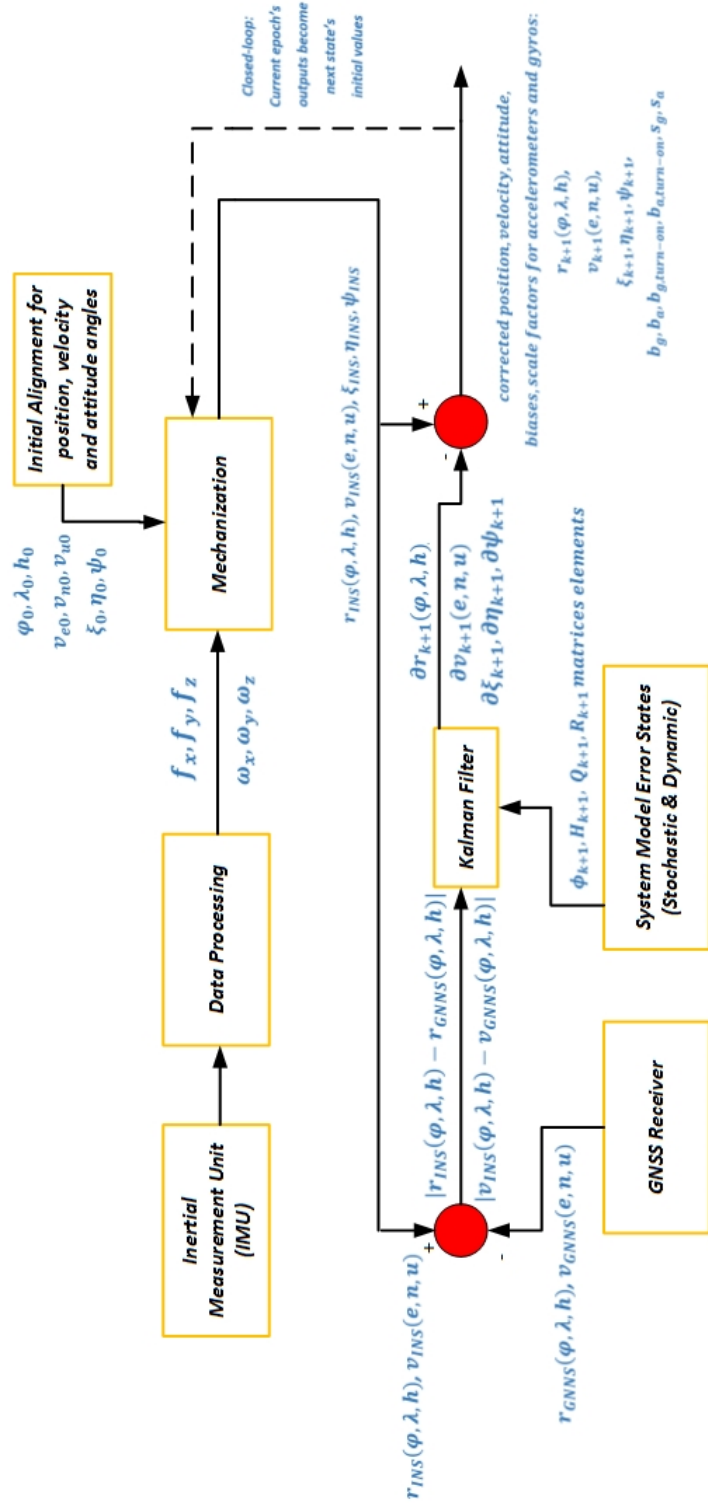


Figure 4.3: Summary of Loosely Coupled Integration

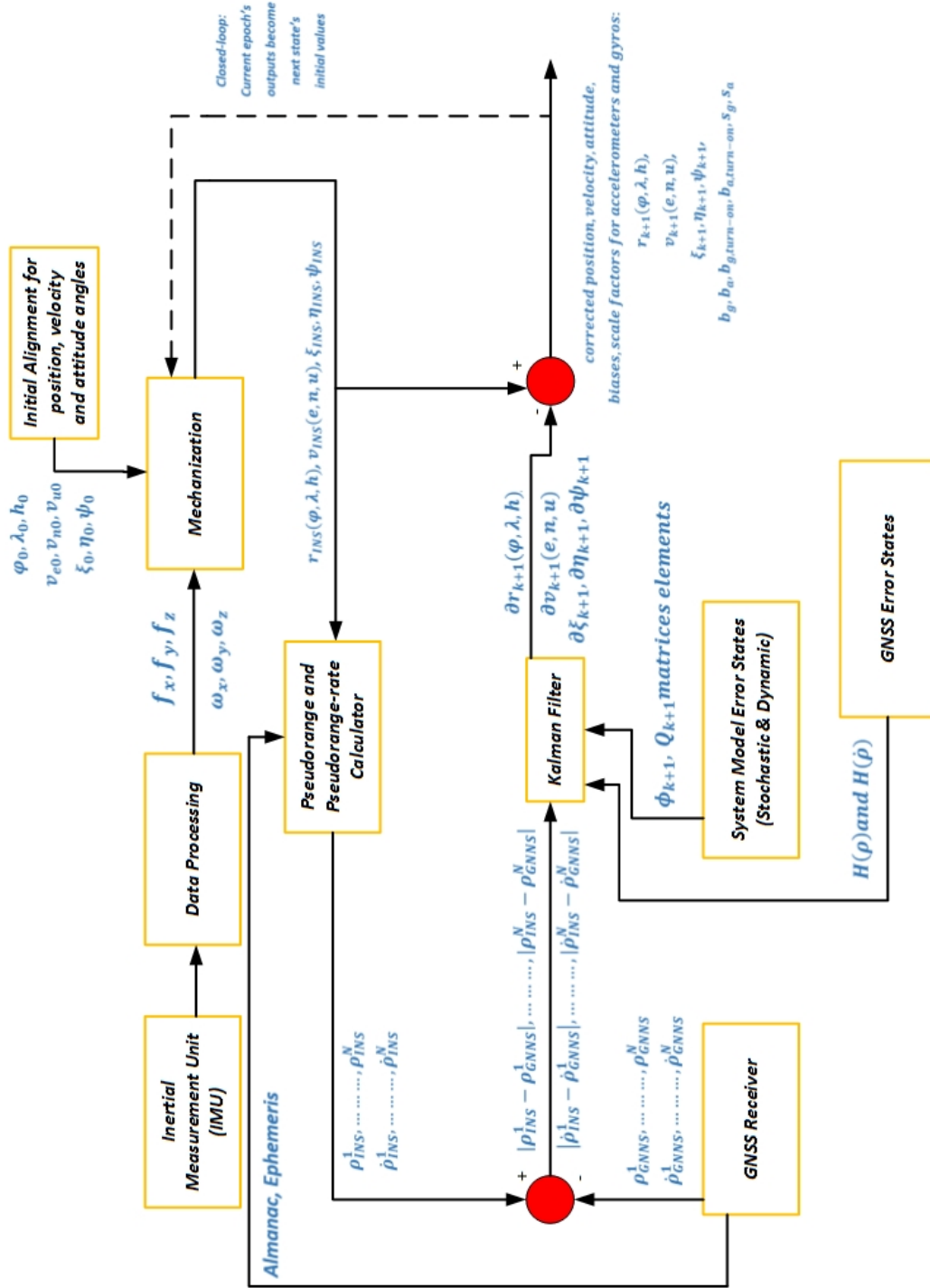


Figure 4.4: Summary of Tightly Coupled Integration



## CHAPTER 5

### FIELD TEST AND RESULTS

#### 5.1 Test Scenario and Setup

In this chapter, all test results with the author designed INS/GNSS integrated systems are presented. Results starts with selected path and reference unit specifications. After this section, results for loosely and tightly couple EKF and results for loosely and tightly coupled UKF is presented in different sections. Comparison between UKF and EKF is done with respect to both loosely and tightly coupled integration methods in general and GNSS outage. Effects of scale parameters on designed UKF are presented. Finally, stability for two filters are compared.

Data collection from standalone ADIS-16488 IMU and Novatel OEM-6 GNSS receiver is done at the same time with reference unit Novatel SPAN IGM A1 unit. The difference of this thesis comes from the fact that the reference unit IMU and GNSS receiver elements are the same with the standalone units used for author designed filter confirmation. Hence, results will enable a real comparison between a self-proved high technological integration algorithm of a INS/GNSS unit at market and author-designed algorithm's performance.

The reference unit has a deeply coupled INS/GNSS filter which is called NovAtel SPAN. It is a proven technology that has been used in various applications [26]. Novatel also offers Dual Antenna options which enables heading and pitch improvements at overall performance but since the GNSS unit selected for this thesis can make single point positioning, reference unit was selected to have single point solution too. The overall performance of reference unit presented by [28] is given in Table 5.1:

Table 5.1: NovAtel SPAN IGM-A1 IMU Specifications [28]

Gyro Input Range	+/-450 deg/s
Rate Bias Stability	2 to 50 m
Angular Random Walk	0.3 deg/sqrt(hr)
Acc. Input Range	+/-18 g
Bias Stability	0.1 mg
Velocity Random Walk	0.029 m/s/sqrt(hr)
Dimensions	152x142x51 mm
Weight	515 gr
Power Input / Consumption	10-30 VDC / 4W

The coarse alignment of the reference unit is done by entering initial heading or kinematically with speeds higher than 5 m/s [21]. The accuracy of reference unit is also presented by Novatel for both normal and two different GNSS outage time intervals are given in Table 5.2:

Table 5.2: NovAtel SPAN IGM-A1 Navigation Performance [28]

Outage Duration	Position Mode	Pos (M) RMS		Vel (M/S) RMS		Att (deg) RMS		
		<u>H</u>	<u>V</u>	<u>H</u>	<u>V</u>	<u>R</u>	<u>P</u>	<u>H</u>
GNSS OK	SP	1	0.6	0.02	0.01	0.035	0.035	0.015
10s Outage	SP	1.41	0.7	0.1	0.021	0.072	0.072	0.21

where,

'SP' means Single Positioning i.e. without differential GNSS,

'H' and 'V' mean horizontal and vertical,

'R', 'P', 'H' mean roll, pitch and heading.

Standalone ADIS-16488 IMU has MEMS technology and very easy to integrate it to any system with proper interface [39]. Raw and compensated data can be collected from IMU but the compensation should be applied by Kalman Filter since MEMS IMU's tend to have variate error characteristics from day to day as discussed earlier.

Standalone GNSS receiver was also selected the same within reference unit and bought from Novatel. It provided position, velocity and pseudorange measurements.

The visuals of elements and test setup block diagram is provided in Figure 5.1:

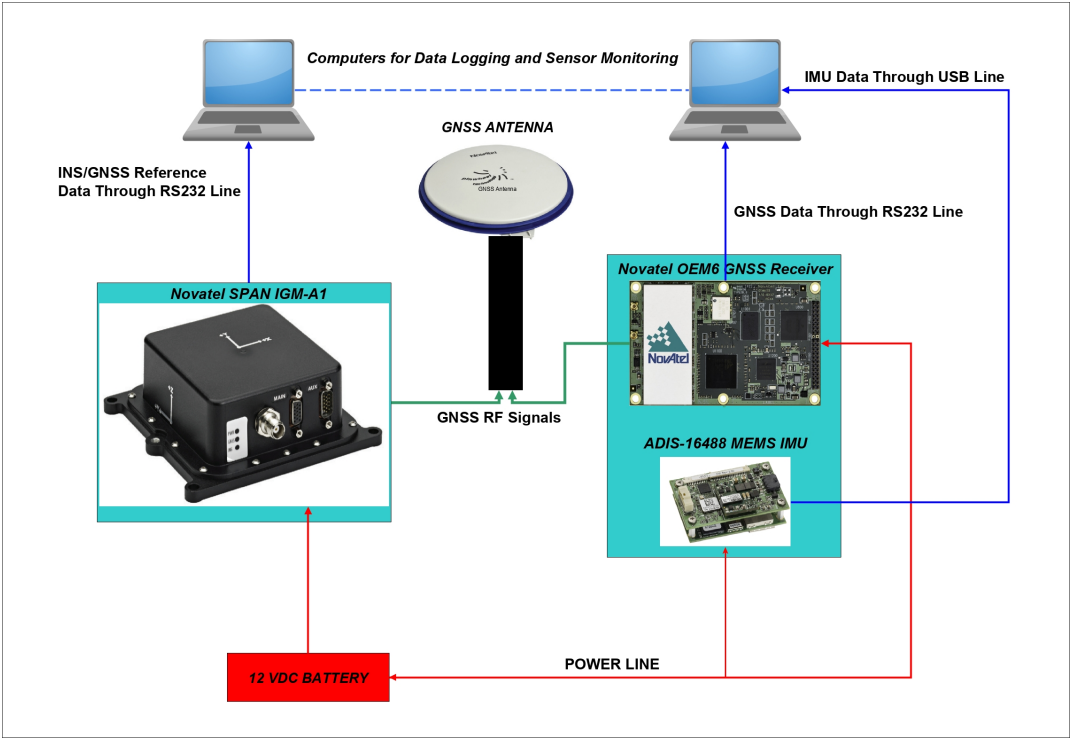


Figure 5.1: Car Trial Test Diagram

As explained earlier, the data collected from all units simultaneously with a car trial at the Middle East Technical University, ANKARA, Turkey. In order to make true measurements, both GNSS receiver connected to the same GNSS antenna by using a GNSS splitter. A 12 VDC battery provided the power through all units and their placement at the car is given in Figure 5.2.



Figure 5.2: Test Setup Placement Before Car Trial

There was a critical measurement before starting tests which were basically matching the phase center of GNSS antenna with the IMU center of measurements i.e. lever arm. This procedure was important since it has an impact on the accuracy of both reference unit and standalone unit's collected data. To get lever arm measurement,

this thesis used a simple method which was taken from [5]. It works by selecting a reference point for measurement of distance of both IMU center and GNSS antenna phase center. After measuring these distances, computation of lever arm was feasible.

The path selected for data collection included some obstacles such as trees, building and a few turns. Data collection trajectory created for this thesis is presented in Figure 5.3:

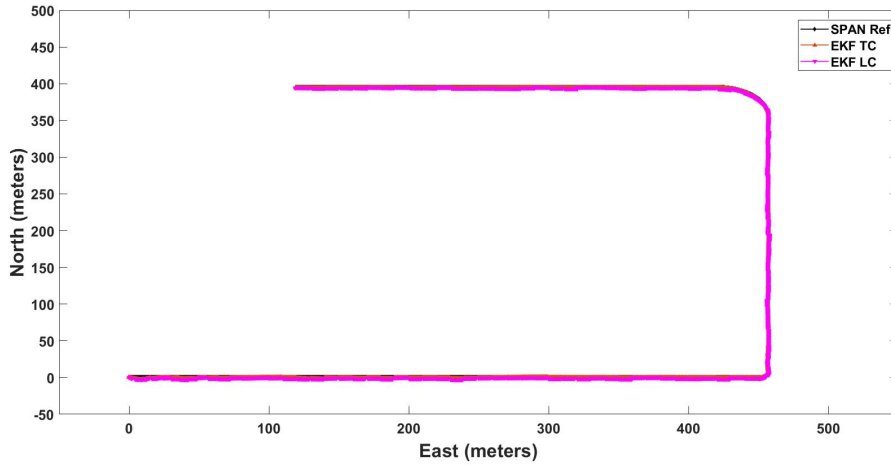


Figure 5.3: Car Trial Path

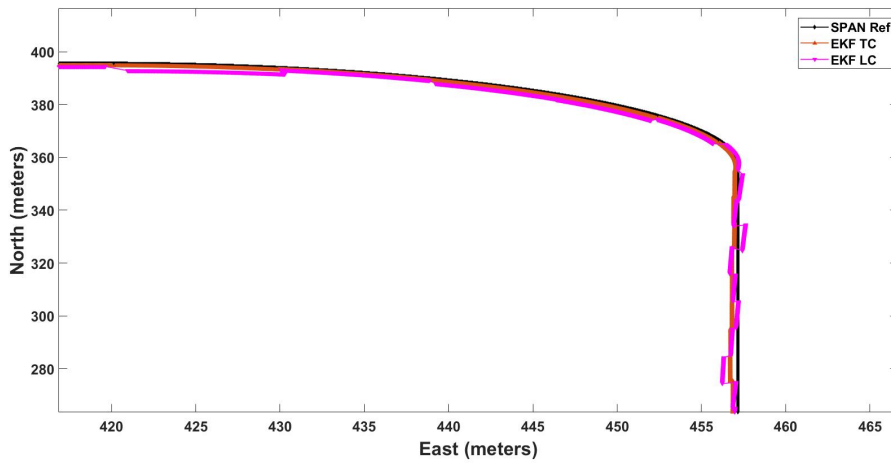
## 5.2 EKF Results with Collected Data

The results with both loosely coupled and tightly coupled EKF are presented in this section. To get error figures about certain parameters, the root-mean-square differences were calculated.

General positioning performance is given below at 1-frame for both integration methods in Figure 5.4. The reference path was created from reference unit collected solution at the same path and only a transformation from geographical coordinates to local level frame was applied.



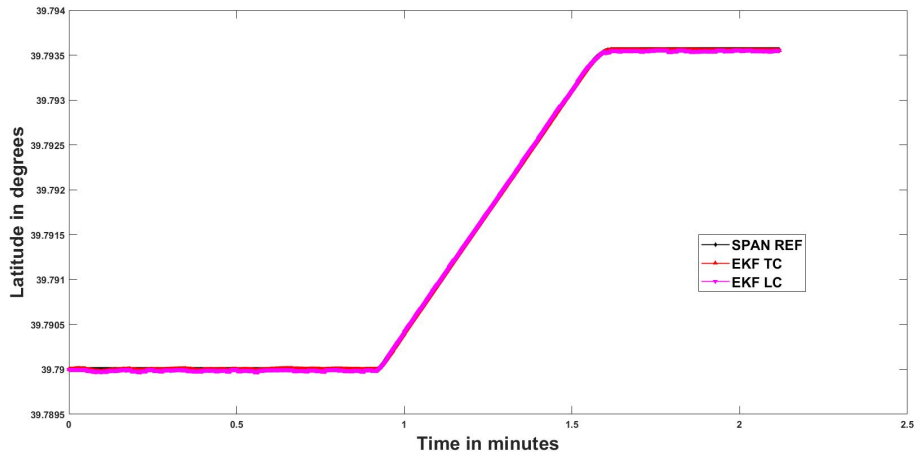
(a) Car Trial Comparison EKF Tightly and Loosely Coupled Integration



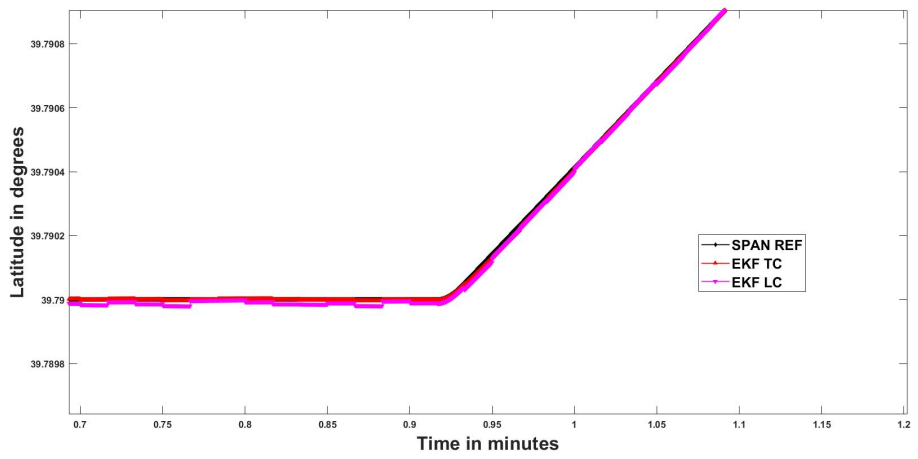
(b) Performance with Closer Look

Figure 5.4: EKF Tightly Coupled and Loosely Coupled Car Test Results

In general, there seems no major differences but when it was inspected closer, the difference between the tightly coupling and loosely coupling was observed. Tightly coupled EKF kept its position computation smoother than the loosely coupled integration. The latitude errors in degrees are provided in Figure 5.5:



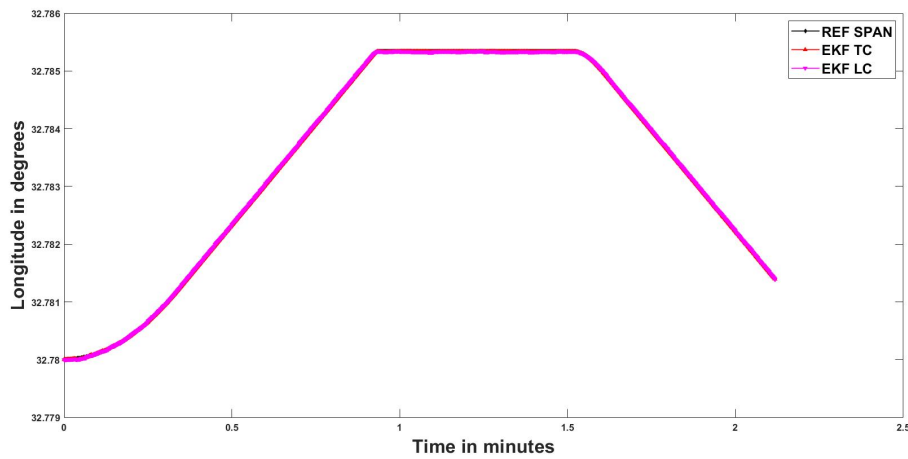
(a) Latitude Comparison of EKF Tightly and Loosely Coupled Integration



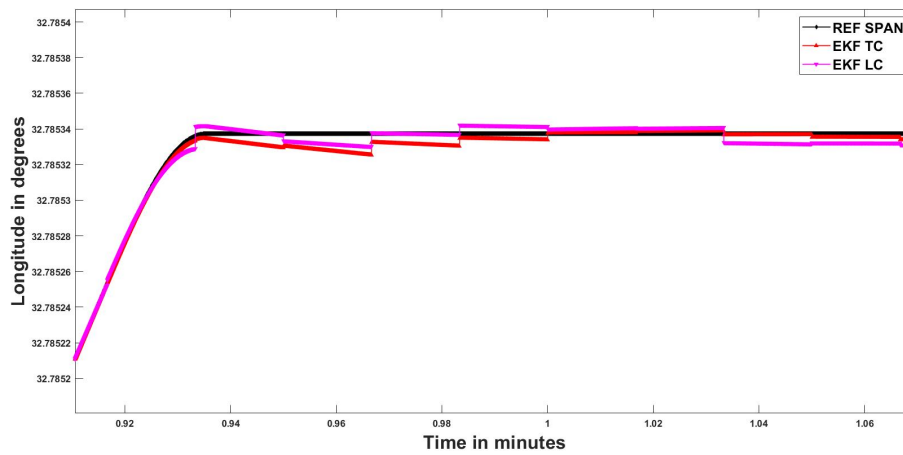
(b) Latitude Performance with Closer Look

Figure 5.5: EKF Tightly Coupled and Loosely Coupled Latitude Performance

Longitude errors in degrees are provided separately in the Figure 5.6:



(a) Longitude Comparison of EKF Tightly and Loosely Coupled Integration



(b) Longitude Performance with Closer Look

Figure 5.6: EKF Tightly Coupled and Loosely Coupled Longitude Performance

Performance difference is easier to observe in Figure 5.5 and Figure 5.6 between tightly and loosely coupling. Positioning performance of EKF tightly coupled and loosely coupled integration is summarized as the error in degrees with respect to reference unit in Figure 5.7:

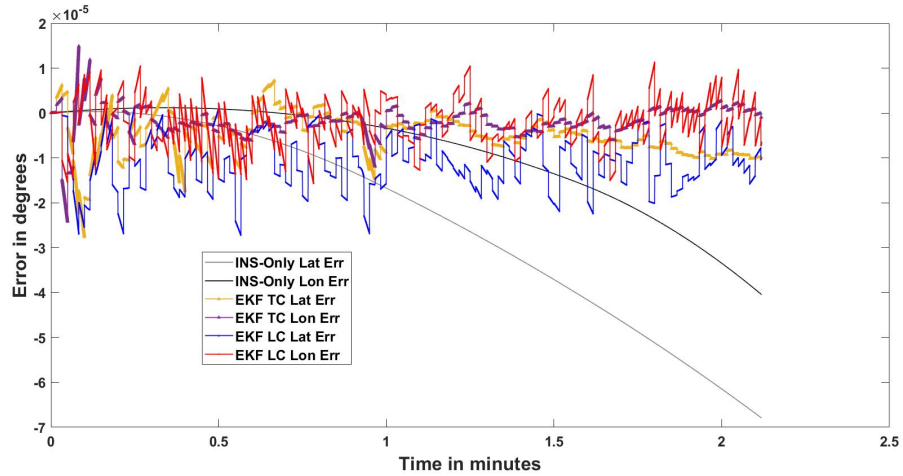


Figure 5.7: EKF Tightly Coupled and Loosely Coupled Integration Positioning Errors

Velocity trend for this car trial can be summarized as below:

- The vehicle was accelerated to 35-36 km/h,
- After acceleration has completed, the vehicle kept on driving with constant velocity until next turn,
- The vehicle turned left with near turn-rate,
- The vehicle kept on going with the level speed at 35-36 km/h and turn left again with slower turn-rate this time,
- Vehicle kept on going with the speed of 30-35 km/h until the end of the trial and data collection was stopped at the finish line.

Velocity error performance for both integration methods is given in Figure 5.8:

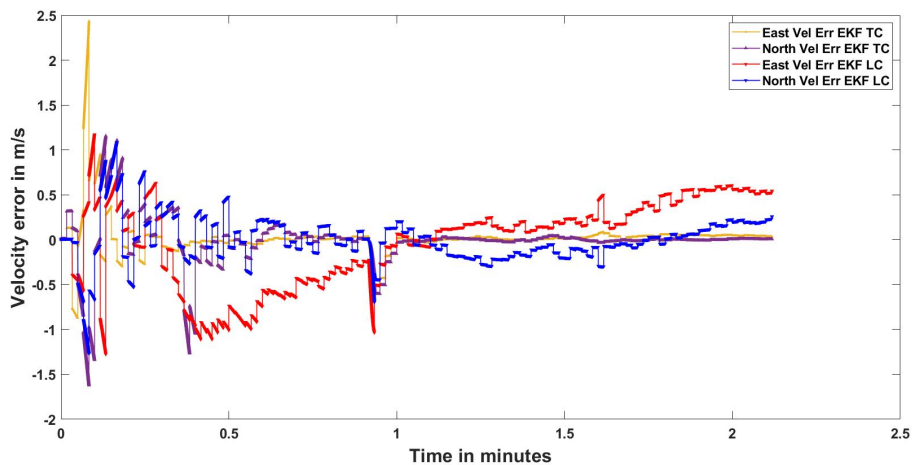


Figure 5.8: EKF Tightly Coupled and Loosely Coupled Integration Velocity Errors

Without the need of detailed inspection, the difference between both integration method can be observed easily. Tightly coupled integration had better performance for velocity.

Attitude (Euler) angles were evaluated in two groups which are pitch/roll errors and heading results. Pitch/roll errors are near 0 for all trial. The error in degrees for both integration method is presented in Figure 5.9:

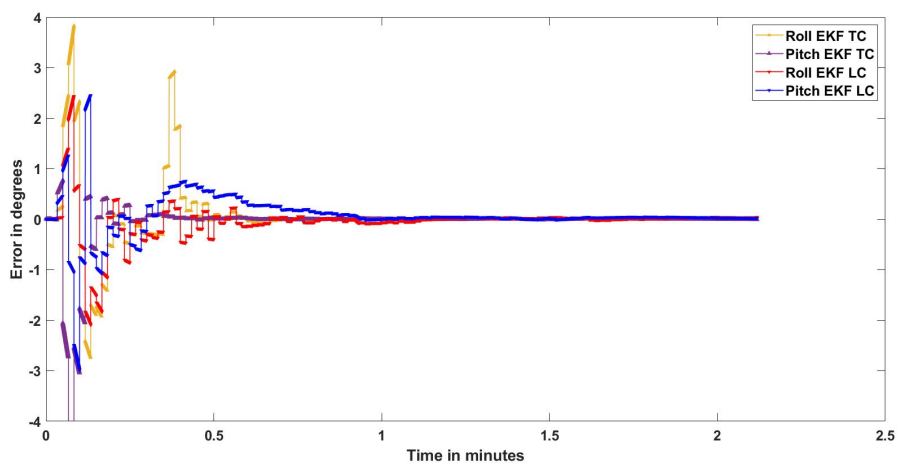


Figure 5.9: EKF Tightly Coupled and Loosely Coupled Integration Roll and Pitch Errors

Pitch and roll need to be estimated from accelerometer data as it was discussed in

Chapter 2. Their estimation takes some time hence, at the beginning of the figures there are bigger error values for both integration method. However, with tightly coupling, alignment for pitch and roll took shorter time and its error rates are closer to zero compared with loosely coupled error values.

On the other side, heading value has interesting results. At the beginning its error was computed as zero because, it cannot produce heading value before computing its roll and pitch values. In addition to that fact, as discussed earlier, both reference unit and standalone selected IMU had same brand and same specifications hence they cannot be statically aligned by measuring Earth's rotation rate. After some acceleration and starting computation of roll and pitch with enough certainty (smaller than  $1^\circ$ ), the computation of heading values was started. At first tightly coupling looked worse but after initialization was completed and the uncertainties of heading started to become small, tightly couple integration outperformed loosely coupled integration. The heading results are given in Figure 5.10:

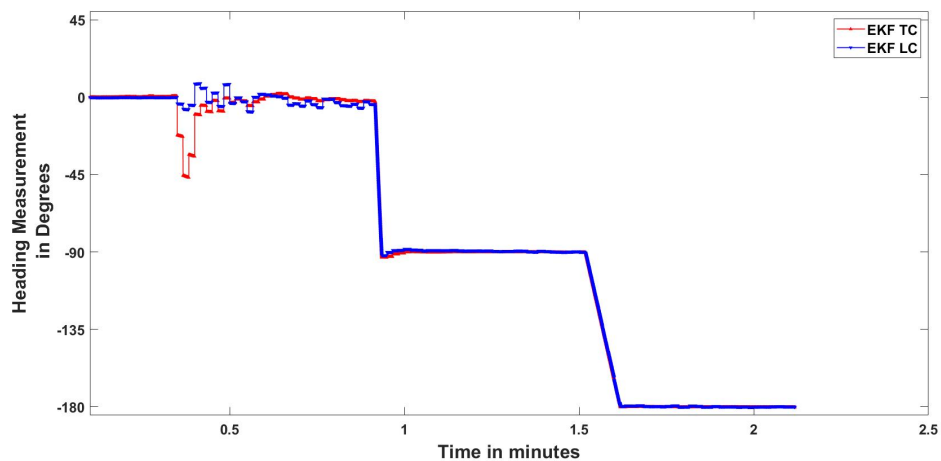


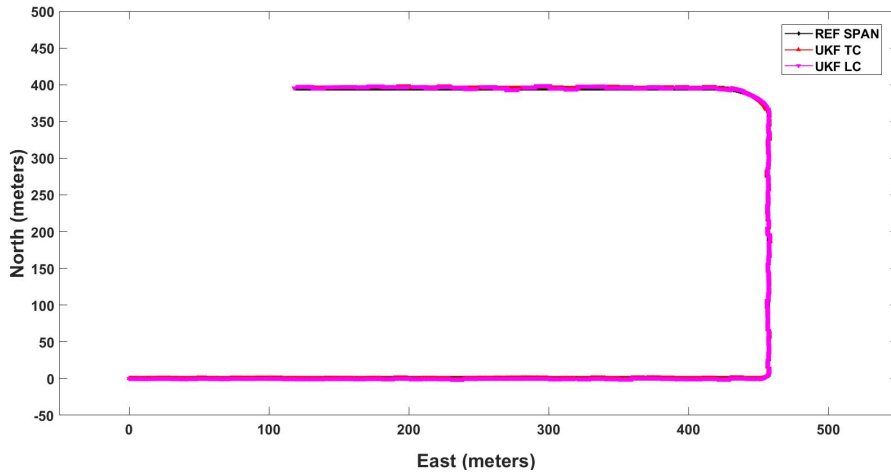
Figure 5.10: EKF Tightly Coupled and Loosely Coupled Integration Heading Results

### 5.3 UKF Result with Collected Data

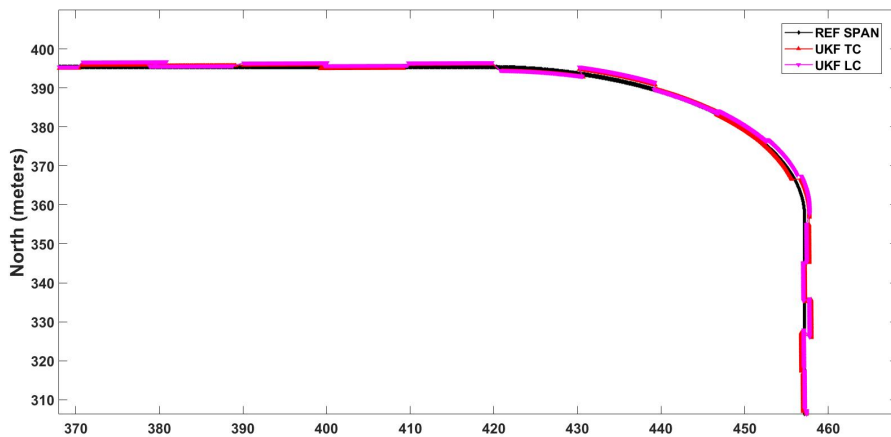
The results with both loosely coupled and tightly coupled UKF are presented in this section with the same order as the previous section.

General positioning performance is given at 1-frame for both integration methods at

Figure 5.15. It was the same logic with the previous section where the reference path was taken from reference unit collected data. It is again difficult to observe easily but when the graph was zoomed at a randomly selected area, the difference between loosely and tightly coupled integration performance became obvious. The tightly coupled integration outperformed loosely coupled integration by computing smoother position solution as it was for EKF.



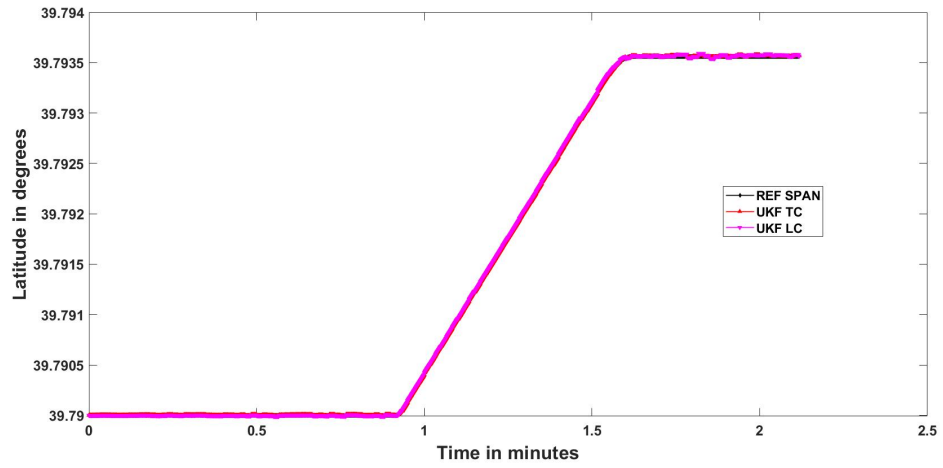
(a) Car Trial Comparison UKF Tightly and Loosely Coupled Integration



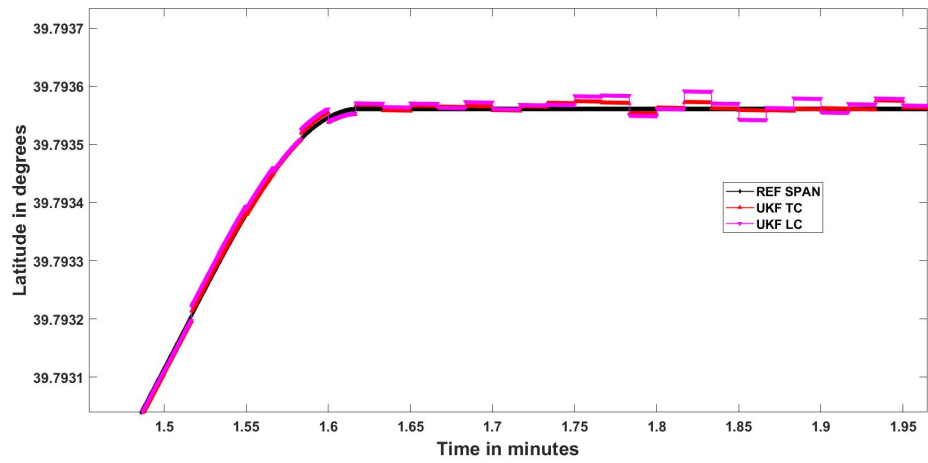
(b) Performance with Closer Look

Figure 5.11: UKF Tightly Coupled and Loosely Coupled Car Test Results

The latitude and longitude errors in degrees are also provided for UKF in Figures 5.12 and 5.13 where the performance difference was observed more directly between tightly and loosely coupled UKF.

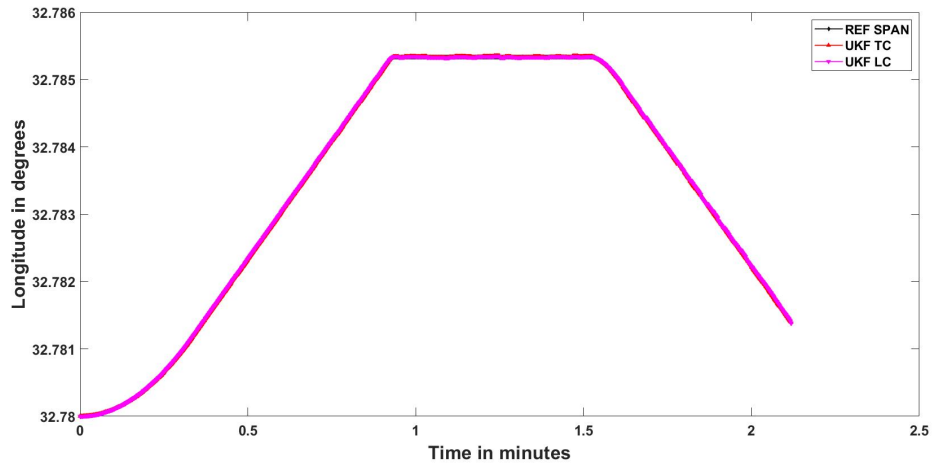


(a) Latitude Comparison of UKF Tightly and Loosely Coupled Integration

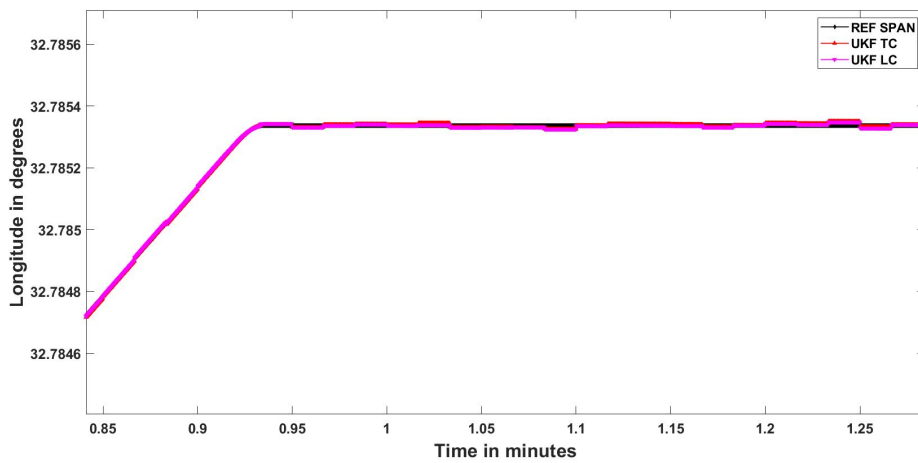


(b) Latitude Performance with Closer Look

Figure 5.12: UKF Tightly Coupled and Loosely Coupled Latitude Performance



(a) Longitude Comparison of UKF Tightly and Loosely Coupled Integration



(b) Longitude Performance with Closer Look

Figure 5.13: UKF Tightly Coupled and Loosely Coupled Longitude Performance

For the vehicle trend given in the previous section, velocity error performance for both integration methods is given in Figure 5.14:

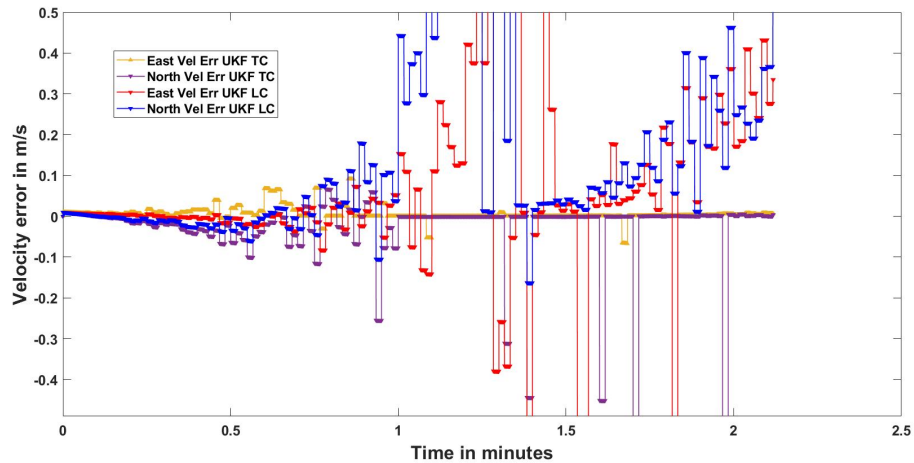


Figure 5.14: UKF Tightly Coupled and Loosely Coupled Integration Velocity Errors

The difference between velocities was observed easily by looking at the values for selected points at the y-axis. It can be seen from here that tightly coupled integration provided better results at velocity. Note that there were some peaks for both tightly coupled and loosely coupled integration computed velocities. They are normally tuned by adjusting scale parameters of UKF normally but they are given here on purpose without adjusting since they were important at comparison between UKF and EKF at Section 5.5.

Attitude (Euler) angles gave interesting results as given in 5.15. The only performance metric that loosely coupled integration was better for UKF was roll and pitch values.

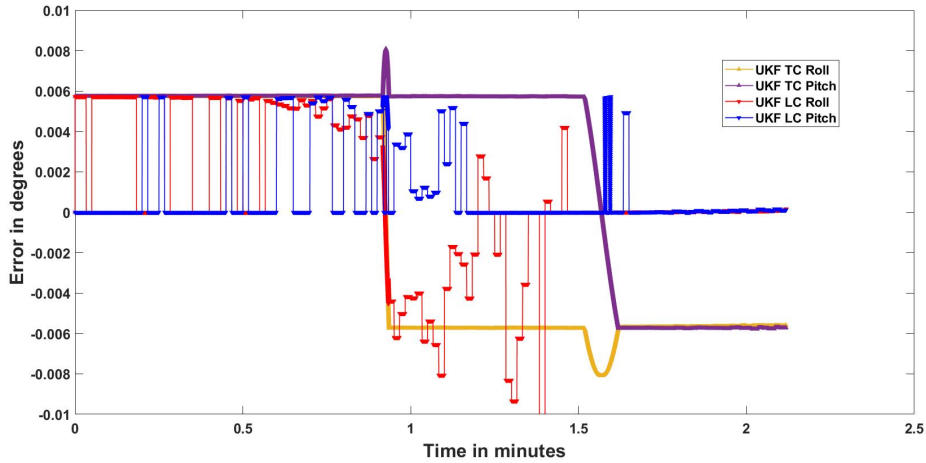


Figure 5.15: UKF Tightly Coupled and Loosely Coupled Integration Roll and Pitch Errors

As can be observed from Figure 5.15, the time for computing roll and pitch was shorter than EKF but it resulted in both attitude values on a constant error value within time. On the other hand, heading results were again similar with EKF as given in Figure 5.16 for UKF. It can be seen from there, especially at the end of car trial, the loosely coupled UKF started to give less accurate heading. The reason for this behaviour can be explained by the possible vulnerability to less dynamic conditions for UKF loosely coupled integration. Especially at the last part where the vehicle started to stop the heading uncertainties started to grow. UKF heading results are given in 5.16:

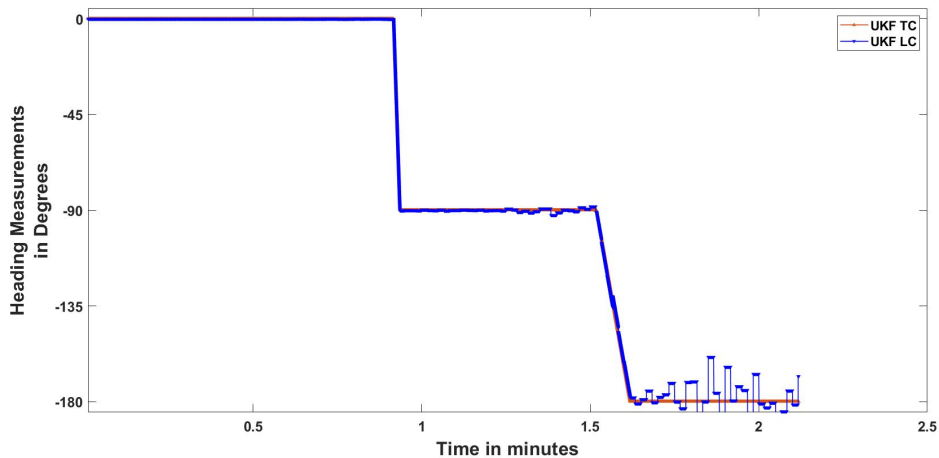


Figure 5.16: UKF Tightly Coupled and Loosely Coupled Integration Heading Results



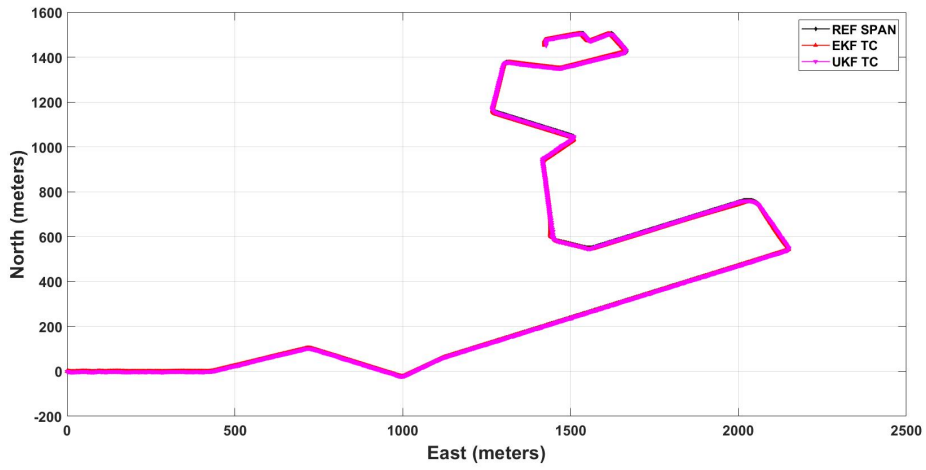


Figure 5.18: Long Car Trial Result of EKF and UKF

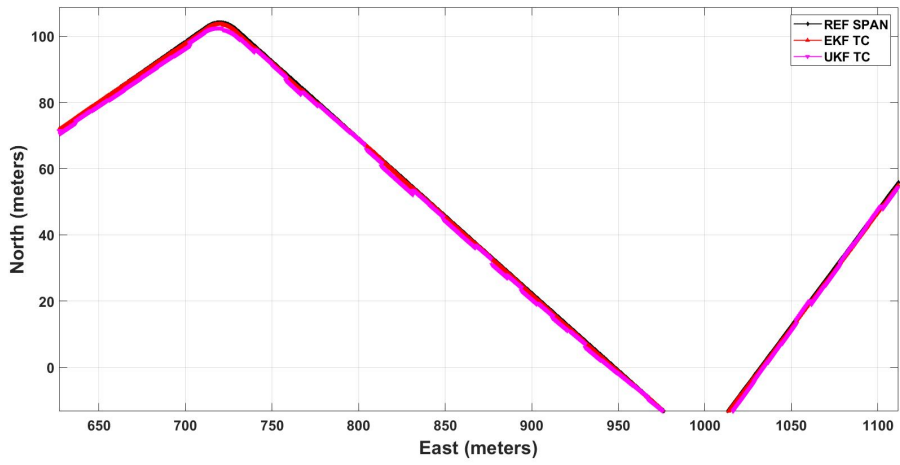


Figure 5.19: Performance with Closer Look to Beginning

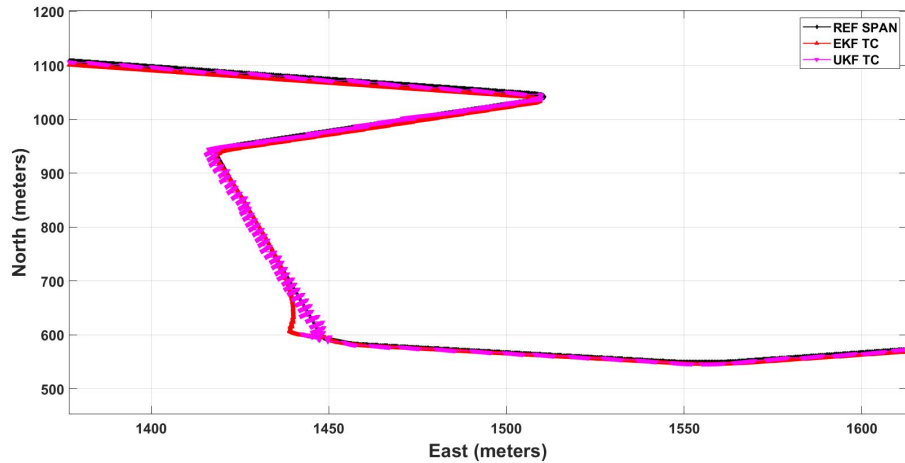


Figure 5.20: Performance with Closer Look to Position with Turns and Intense Trees/Buildings

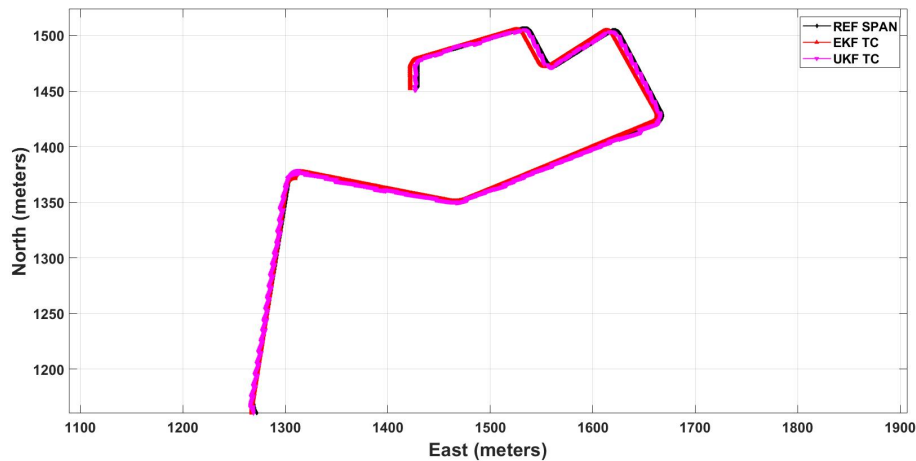


Figure 5.21: EKF and UKF Long Car Trial Test Results

It can be followed from closer looks that at the beginning of trial, both methods worked well with close accuracy to each other. EKF was better for a while. However, after the car went into the road with more trees and buildings, Extended Kalman Filter started to work with more errors. It can be seen in Figure 5.20 that EKF lost track for a short time but it quickly converged to true path. At this time UKF started to diverge with bigger errors until a measurement arrived. The upside down trend of magenta line can be seen in Figure 5.20. At the end of the car trial, there were higher buildings and more turns. Closer look to final part of car trial is given in Figure 5.21.

After investigating GNSS receiver data logs, an expected result was observed. The

GNSS availability, at the time when both filter started computing worse results, was lower than expected. The reason could not be found about it but it may be the result of obstacles or antenna connection at GNSS receivers or a problem within the splitter. When they were worked again at open-sky, there seemed to be no problem in these elements. Hence, with long car trial satellite visibility was tested too. The number of satellites seen for whole trial is given in Figure 5.22:

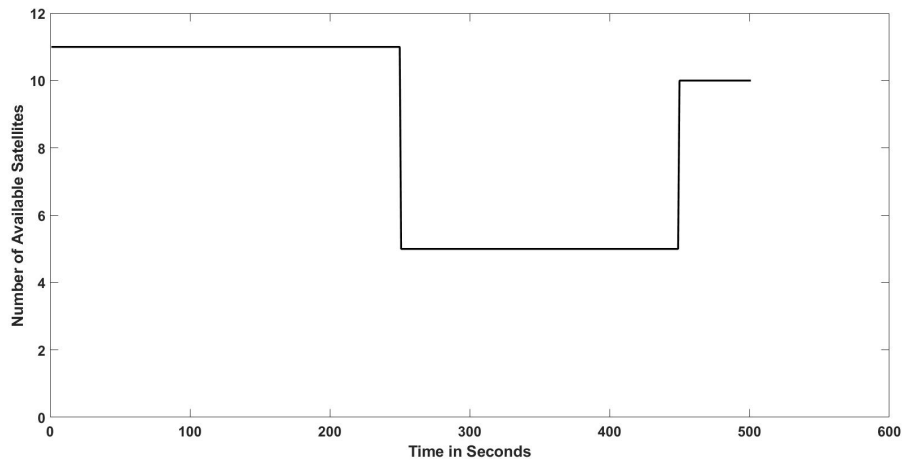
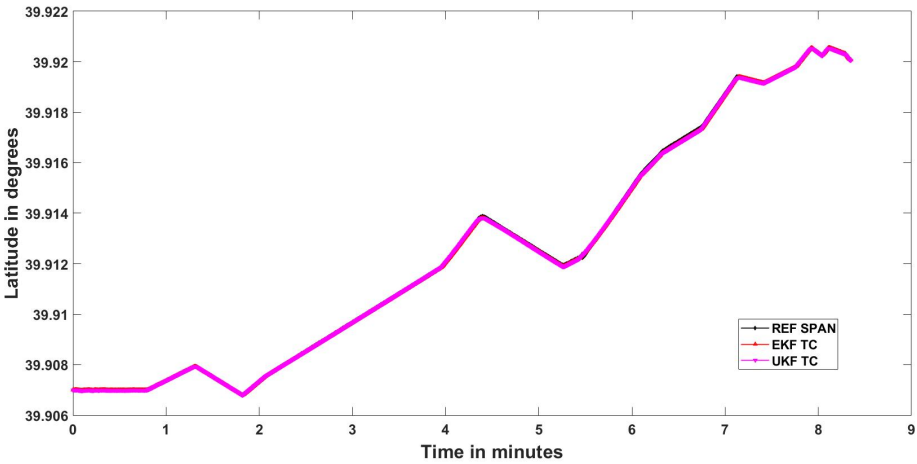


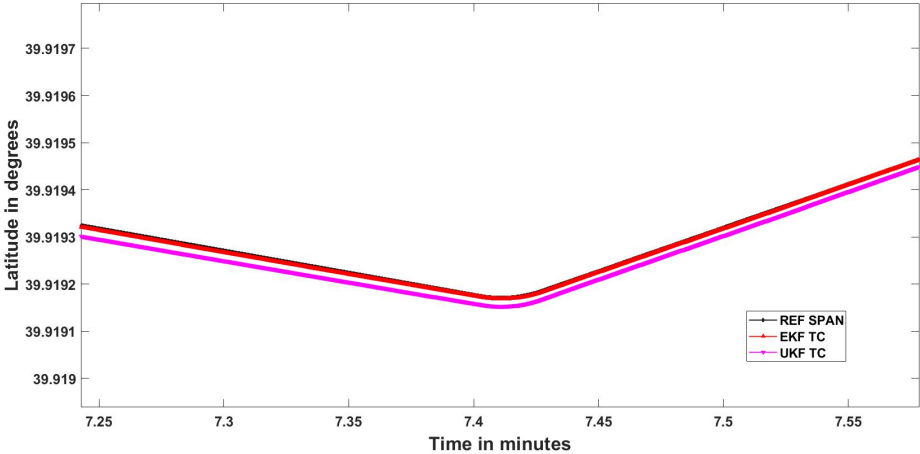
Figure 5.22: EKF and UKF Long Car Trial GNSS Satellite Availability

More information about comparison are given in below figures where latitude, longitude, velocity and attitude comparisons are provided.

The latitude performance was very close to each other but EKF did estimate more smoother latitude results than UKF as given in Figure 5.23.



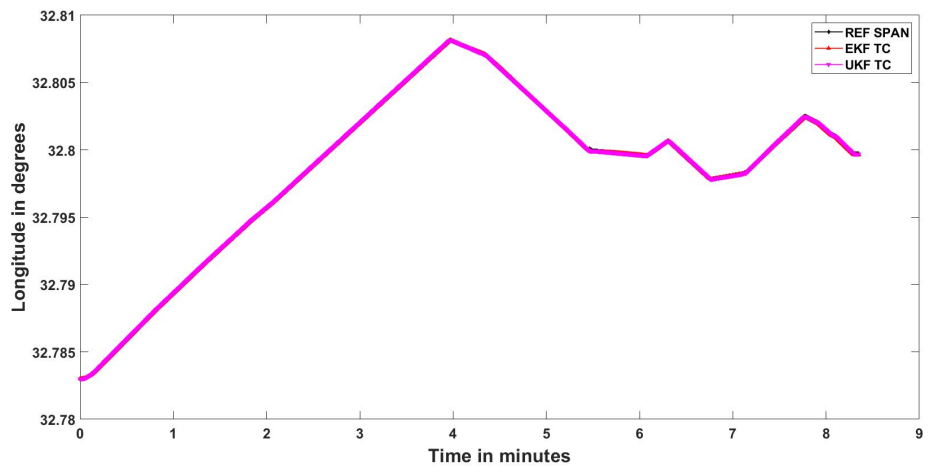
(a) Latitude Comparison of UKF and EKF



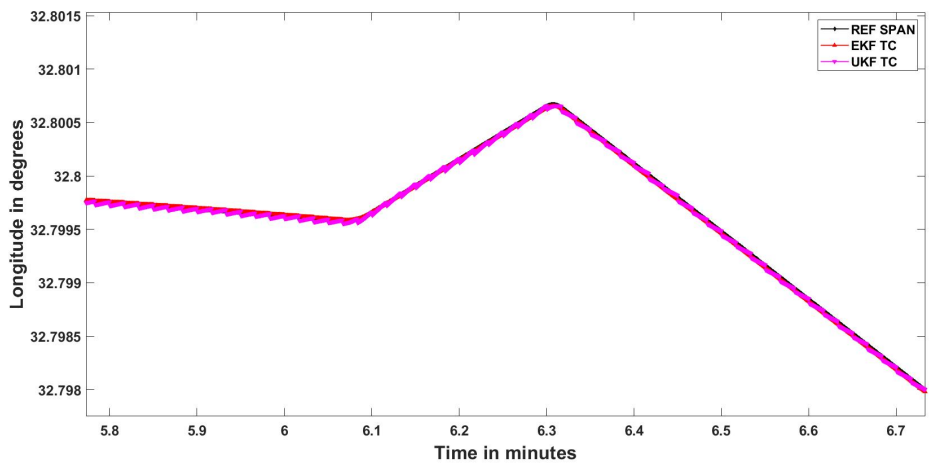
(b) Latitude Performance with Closer Look

Figure 5.23: UKF and EKF Latitude Performance

The longitude performance was very close to each other but EKF did estimate more smoother longitude results than UKF as given in Figure 5.24.



(a) Longitude Comparison of UKF and EKF



(b) Longitude Performance with Closer Look

Figure 5.24: UKF and EKF Longitude Performance

The overall performance of both EKF and UKF with respect to reference unit is given in Figure 5.25 where the satellite availability effects can be observed easily:

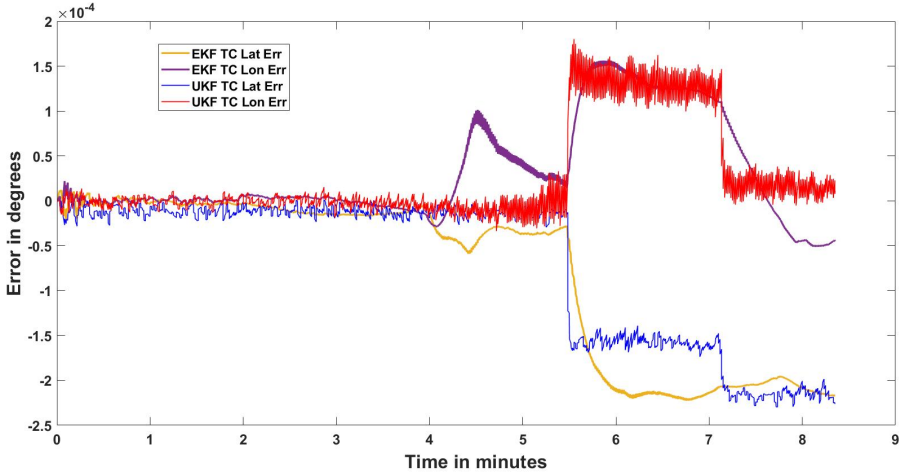


Figure 5.25: EKF and UKF Long Car Trial Positioning Errors

The satellite availability effects are also observed in velocity errors as given in Figure 5.26. Both filters converged well for velocity even under low satellite availability.

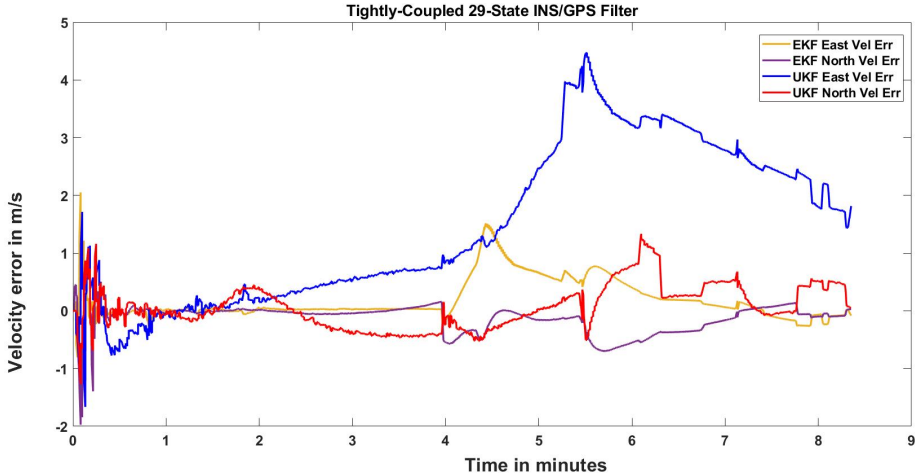


Figure 5.26: EKF and UKF Long Car Trial Velocity Errors

The roll,pitch should not be affected by satellite availability as much as position and velocity estimates did. It can be observed from the roll and pitch errors given in Figure 5.27:

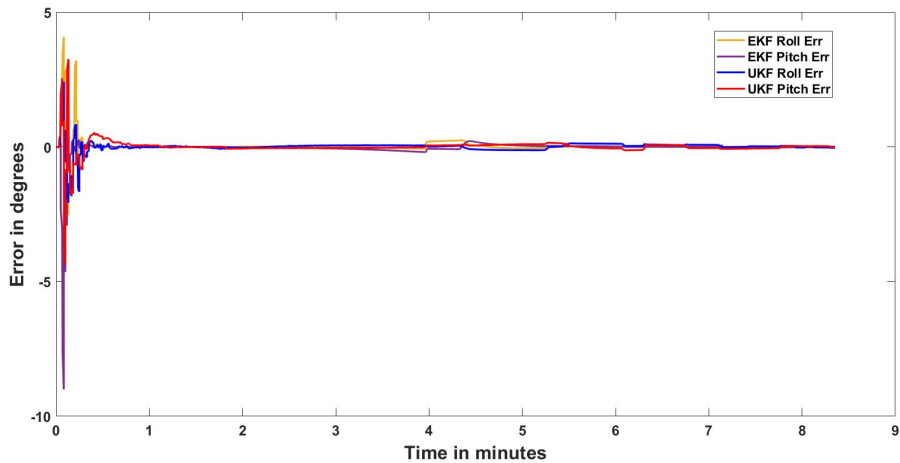


Figure 5.27: EKF and UKF Long Car Trial Roll and Pitch Errors

Heading is vulnerable to low availability of satellites since it is calculated from GNSS velocities when estimated heading’s uncertainty rises. As it can be seen from 5.28, UKF and EKF did very well with heading calculations.

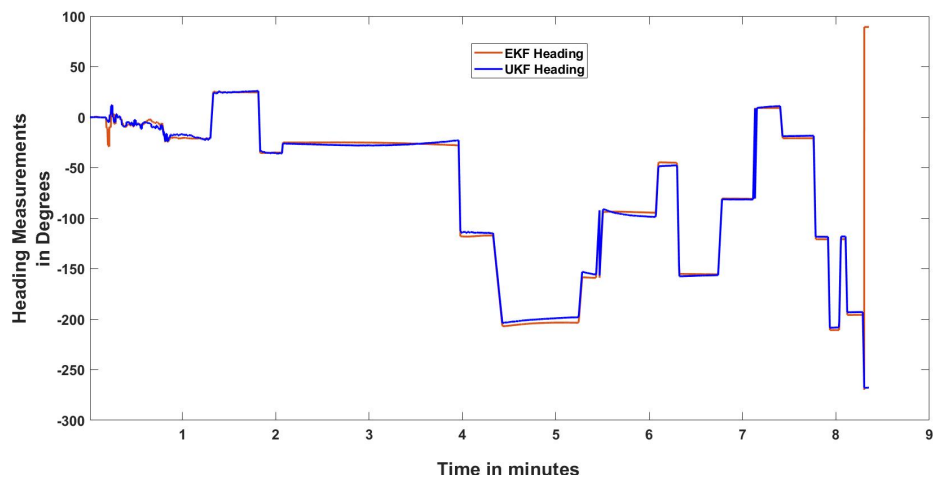


Figure 5.28: EKF and UKF Long Car Trial Heading Results

### 5.5 Overall Results and Filtering Techniques Comparison

In this section, the results provided for both EKF and UKF are discussed. In the both integration methods, tightly coupling method outperforms loosely coupling method. In order to understand if there was a major difference between filtering techniques, one of the designed algorithm’s output that was root mean square differences were

used for all results. With these results comparison tables were created for both EKF and UKF.

Table 5.3 gives the comparison for short car trial:

Table 5.3: RMS Error Comparison for Short Car Trial with high Satellite Availability

	EKF LC	EKF TC	UKF LC	UKF TC
East Pos RMS	2.2732 m	0.5646 m	3.9931	0.6017
North Pos RMS	2.3915 m	0.7682 m	2.4657	0.8291
East Velocity RMS	0.8675 m/s	0.2576 m/s	1.039 m/s	0.0522 m/s
North Velocity RMS	0.2533 m/s	0.2887 m/s	0.2732 m/s	0.2254 m/s
Roll RMS deg	0.3932	0.7094	0.2998	0.0058
Pitch RMS deg	0.4397	0.5435	0.3391	0.0057
Heading RMS deg	1.81	1.82	1.813	1.812

Table 5.4 gives the comparison for long car trial:

Table 5.4: RMS Error Comparison of Long Car Trial with low Satellite Availability

	EKF TC	UKF TC
East Pos RMS	0.9635 m	2.1886 m
North Pos RMS	0.9928 m	2.2775 m
East Velocity RMS	0.4434 m/s	0.4905 m/s
North Velocity RMS	0.2834 m/s	0.3806 m/s
Roll RMS deg	0.3246	0.3323
Pitch RMS deg	0.4502	0.4376
Heading RMS deg	1.7637	1.7772

By looking at the two tables, difference between two filtering techniques: EKF was better than UKF with the applied methods in author-designed algorithms and reference unit selected in this thesis.

The position error rates at Table 5.4 are higher than given tightly coupled error rates at Table 5.3. The reason for this situation was the bad GNSS quality at some part of the route due to low satellite availability. Other than this, roll and pitch errors were less for both tightly and loosely coupled UKF integration in Table 5.3. The main

reason for this situation was that the alignment time for EKF took longer than UKF as discussed earlier. Hence, when longer car trial was applied, the roll and pitch errors are much closer each other for both two filtering technique as given in 5.4.

## 5.6 Effects of Scale Parameters on Scaled UKF

In Chapter 3, scale parameters of UKF were explained. In this chapter, the effect of varying scale parameters of Scaled UKF was examined.

The scaled UKF sigma points and weights were calculated from equations given in Chapter 3.

In below results,  $\beta$  was chosen as 2.  $\kappa$  was chosen as 0. The only variable parameter was  $\alpha$  and for long car-trial results, its effect was investigated.  $\alpha$  takes values between  $10^{-4}$  and 1. The results for 1, 0.75, 0.5, 0.25 and 0.1 are presented in Table 5.5:

Table 5.5: Effects of  $\alpha$  on the performance of UKF

<b>Alpha (<math>\alpha</math>)</b>	1	0.75	0.5	0.25	0.1
East Pos RMS	2.1889 m	2.1888 m	2.1886	2.1956	2.2142
North Pos RMS	2.2810 m	2.2779 m	2.2775	2.2987	2.3290
East Velocity RMS	0.5025 m/s	0.5013 m/s	0.4905 m/s	0.5103 m/s	0.5314
North Velocity RMS	0.3902 m/s	0.3912 m/s	0.3806 m/s	0.3916 m/s	0.4127
Roll RMS deg	0.3411	0.3430	0.3323	0.3542	0.3753
Pitch RMS deg	0.4381	0.4374	0.4376	0.4485	0.4697
Heading RMS deg	1.7792	1.7789	1.7772	1.7987	1.8157

By looking at these results in more detail, the optimum  $\alpha$  is equal to 0.5 which was also the used one in above results.

The other parameter  $\beta$  was also varied by keeping  $\alpha$  constant. No significant changes occurred at the results. Analysis were repeated for different values of  $\alpha$  but the results were same. Hence, the key parameter for an adaptive UKF algorithm is  $\alpha$  for UKF algorithms developed in thesis.

## **5.7 Stability of EKF and UKF**

Both EKF and UKF algorithms did not become unstable with the tests conducted on open field. They remained bounded with the constraints taken from [43]. In order to push limits, there shall be a new test plan where the limits of filter can be pushed. This new test plan should include sharp turns and high variations on accelerations. This type of test will trigger some breaks at small error and small noise assumptions and lead filter to become unstable.



## CHAPTER 6

### CONCLUSIONS AND FUTURE WORK

#### 6.1 Conclusions

This thesis proposed author-designed INS/GNSS integration algorithms by using different coupling and Kalman Filtering methods as a first step in order to accomplish a real-time single box navigation solution for future works. Algorithms developed for this purpose are written clear in MATLAB and they are convertible to an embedded software at the end.

Results of designed integration algorithms were compared by filtering raw data from standalone units. For loosely coupled integration methods, positions and velocity were computed from pseudorange and pseudorange rate data collected from standalone GNSS receiver. For tightly coupled integration methods, pseudo-ranges and pseudorange rate data collected from same receiver was used directly. A car trial scenario and proper test setup were created and each test step was followed carefully. With the given results and methods provided at previous chapters, conclusions can be summarized as below:

1. Tightly coupled integration technique outperforms loosely coupled integration technique for both EKF and UKF.
2. Loosely coupled integration technique is more sensitive to satellite drops, vehicle dynamics and sensor errors compared with tightly coupled integration.
3. 17-State and 29-State EKF and UKF were developed in this thesis. 17-State includes three dimension position, velocity, attitude error estimates and 6 IMU

error estimates and 2 GNSS error estimates. 29-State includes all states in 17-State with the addition of 12 IMU bias and scale factor error states.

4. IMU error modelling is very important for accurate Kalman Filter navigation. In the preliminary design of an INS/GNSS integration project, considering modelling and calibration requirements for low-cost IMUs is important.
5. The system dynamics model and measurement model matrices are very important since they provide non-linearity. For low cost and entry performance IMUs, system dynamics can have more states than expensive and high-performance IMUs.
6. Biases and noises can be modelled easily with the proper selection of models such as Gaussian-Markov, white Gaussian, random constant.
7. Fine alignment and coarse alignment are very important. With wrong alignment, the filter can diverge and compute the wrong navigation solution. The key precaution for this case is to initialize Kalman Filter with accurate and correct values.
8. UKF computation burden is larger than EKF computation. UKF can take more resources than EKF hence, for real-time applications, EKF is preferred.
9. The performance differences between EKF and UKF for both loosely and tightly integration methods are presented. The author designed UKF for this thesis has some outliers and they need to be dealt with in addition to Kalman Filter design.
10. Loosely coupled integration is good enough for open sky and aerial applications since there will not be obstacles or lose of satellites from environmental effects in these applications. For more challenging applications tightly coupled integration is advised.
11. Both UKF and EKF can be used for real-time implementation for especially land application since they both had good performance at bad GNSS quality.
12. For scaled UKF developed in this thesis, parameter  $\alpha$  has impact on navigation solution.

## 6.2 Future Works

With the given conclusions provided at previous section , future works are planned as below:

1. The number of states for both loosely and tightly coupled integration can be increased for more accurate results. For example, non-orthogonality of IMU axes can be modelled as separate error states in the system dynamics model as [8] made in his work.
2. Real-time embedded software can be developed quickly by taking the basis of the methods and algorithms generated for this thesis.
3. For scaled UKF, artificial intelligence can be developed in order to adapt its sigma points and weights more frequently with changing conditions.
4. Motion constraints such as Zero Velocity Updates, height constraint and external velocity aiding can be used for land applications to enable robustness in GNSS denied environments.
5. Different modelling techniques for biases and scale factors can be developed. There are many process models which may fit better than the ones used in this thesis.
6. Instead of modelling the IMU characteristics, a higher performance IMU can be chosen and calibration methods with required equipments can be tested for contribution to less state hence less computational burden.
7. Instead of using only one entry-level IMU, multiple IMUs can be used in order to create a federated filter and the effect of multiple IMUs can be observed on same algorithms.
8. External heading aiding by using a magnetometer or dual-GNSS receiver can be used for faster static alignment or in-motion alignment.
9. The algorithms developed here can be tested for unmanned aerial vehicle application where other motion constraints or external velocity sources such as air-velocity may be inserted to filter input.

10. Effects of more accurate GNSS receivers with RTK, SBAS etc. should be observed in order to minimize inaccuracies coming from satellite navigation.
11. The reference unit used in this thesis was not a high-grade IMU. Hence, a new comparison between developed algorithms and higher grade INS/GNSS unit shall be applied or a path which the coordinates are known exactly can be used for further performance information.
12. In order to see stability performance of two filters, a new field test with harder conditions such as sharp turns, extreme minus and plus accelerations etc. can be applied.

## REFERENCES

- [1] Wrigley, W., "History of Inertial Navigation", *NAVIGATION, Journal of The Institute of Navigation*, Vol. 24, No. 1, Spring 1977, pp. 1-6
- [2] Elliott D. Kaplan, C. J. H. (1997). Understanding GPS. Principles and applications. In *Journal of Atmospheric and Solar-Terrestrial Physics* (Vol. 59). [https://doi.org/10.1016/S1364-6826\(97\)83337-8](https://doi.org/10.1016/S1364-6826(97)83337-8).
- [3] Selve Sargin Güçlü. (2019). *Investigation of the Star Tracker Algorithms and Kalman*. (February).
- [4] Tamer Akça. (2012). *an Adaptive Ukf for Tightly-Coupled Ins/Gps Integration*. (February).
- [5] Infante, E. (2016). *Development and Assessment of Loosely-Coupled Ins Using Smartphone Sensors*.(305). Retrieved from <http://www2.unb.ca/gge/Pubs/TR305.pdf>
- [6] Godha, S. (2006). UCGE Reports Number 20239 Performance Evaluation of Low Cost MEMS-Based IMU Integrated With GPS for Land Vehicle Navigation Application. *Geomatics Calgary*,(20239), 230. Retrieved from <http://plan.geomatics.ucalgary.ca/papers/06.20239.SGodha.pdf>
- [7] Angrisano, A., Prof, S., Petovello, M., Vultaggio, P. M. (2010). *Dipartimento di Scienze Applicate Dottorato di ricerca in Scienze Geodetiche e Topografiche XXIII Ciclo GNSS / INS Integration Methods*.
- [8] Shin, E.H. (2005). Estimation Techniques for Low-Cost Inertial Navigation. *University of Calgary, Ph.D*(20219), 206. Retrieved from <http://www.geomatics.ucalgary.ca/links/GradTheses.html>
- [9] Schultz, C. E. (2006). INS and GPS integration. *Mathematical Modelling*.
- [10] Görkem Sarıkaya (2018). *Technical Analysis and Usage of Satellite Based Navigation Technologies in Aviation*.

- [11] Andrews, A. P. (2007). *Global Positioning Systems , Inertial Navigation , Second Edition*. <https://doi.org/10.1002/0471200719>
- [12] Teunissen, P.J.G. ,A. Kleusberg, eds. (1998). *GPS for Geodesy*. Springer-Verlag, Berlin, Heidelberg, New York, ISBN 3-540-63661-7
- [13] Aourelidin, Aboelmagd, Karamat, Tashfeen, Georgy, Jacques. (2013). *Fundamentals of Inertial Navigation, Satellite-based Positioning and their Integration*. 10.1007/978-3-642-30466-8 10.
- [14] Petovello, M. G. (2004). Real-Time Integration of a Tactical-Grade IMU and GPS for High-Accuracy Positioning and Navigation. *Thesis*,(20173), 242. Retrieved from <http://www.geomatics.ucalgary.ca/links/GradTheses.html>
- [15] Misra, P. and Enge, P. (2011). *Global Positioning System: Signals Measurements, and Performance*,2nd Ed. Ganga-Jamuna press, Lincoln, Massachusetts
- [16] Niu, X., Goodall, C., Nassar, S., El-Sheimy, N. (2006). An efficient method for evaluating the performance of MEMS IMUs. *Record - IEEE PLANS, Position Location and Navigation Symposium, 2006*,766–771. <https://doi.org/10.1109/PLANS.2006.1650673>
- [17] Doğan Yıldız. (2016). *Modelling, Simulation and Testing of Artificial Neural Network Augmented Kalman Filter for INS/GPS and Magnetometer Integration*. (September).
- [18] Gupta, A. K., Koilpillai, R. D., Evani, S. S. S. (2007). A Kalman Filtering Approach for Integrating MEMS Based INS and GPS for Land Vehicle Application *Proceedings of National Conference on Communications*, 1–5. Retrieved from [internal-pdf://142.103.16.79/A Kalman filtering approach for Integrating ME.pdf](internal-pdf://142.103.16.79/A%20Kalman%20filtering%20approach%20for%20Integrating%20ME.pdf)
- [19] Engineering, A. (2007). *Low-Cost INS / GPS Data Fusion with Extended Kalman Filter for Airborne Applications by*. (July).
- [20] Gao, J. (2007). Development of a Precise GPS/INS/On-Board Vehicle Sensors Integrated Vehicular Positioning System. *PhD*,(20255), 218. Retrieved from <http://www.geomatics.ucalgary.ca/links/GradTheses.html>

- [21] NovAtel Inc. “OEM7 SPAN Installation and Operation User Manual v12”.  
<https://docs.novatel.com/OEM7/Content/PDFs>. Last accessed on July 15th, 2019.
- [22] NovAtel Inc. “An Introduction to GNSS – GPS, GLONASS, BeiDou, Galileo and other GNSS Systems”.  
<https://www.novatel.com/assets/Documents/Books/Intro-to-GNSS.pdf> Last accessed on July 1th, 2019.
- [23] NovAtel Inc “Positioning Modes of Operation”.  
<https://www.novatel.com/assets/Documents/Bulletins/apn051.pdf> Last accessed on July 2nd, 2019.
- [24] NovAtel Inc “OEM6 Family Installation and Operation User Manual”.  
<https://www.novatel.com/assets/Documents/Manuals/om-20000128.pdf> Last accessed on July, 25th, 2019.
- [25] NovAtel Inc. “OEM617 Product Sheet”  
<https://www.novatel.com/assets/Documents/Papers/OEM617D19486v1.pdf>  
Last accessed on July, 30th, 2019.
- [26] NovAtel Inc., “SPAN on OEM6”  
<https://www.novatel.com/assets/Documents/Manuals/OM-20000144UM.pdf>  
Last accessed on July, 13th, 2019.
- [27] NovAtel Inc., “IMU Errors and Their Effects”  
<https://www.novatel.com/assets/Documents/Bulletins/APN064.pdf> Last accessed on July, 30th, 2019.
- [28] NovAtel Inc, “SPAN Brochure”  
<https://www.novatel.com/assets/Documents/Papers/SPANBrochure.pdf> Last accessed on July, 30th, 2019.
- [29] Merwe, E. A. W. and R. van der. (1982). Eric A. Wan and Rudolph van der Merwe. *Medizinische Welt*, 33(13), 475–479.
- [30] Simon Julier, J.K.Uhlmann. (2004). Unscented Filtering and Nonlinear Estimation. *Proceedings of the IEEE*, 92(3), 401–422.

- [31] Shin, E., and N. El-Sheimy (2004) “An Unscented Kalman Filter for In-Motion Alignment of Low Cost IMUs,” in *Proceedings of Position Location and Navigation Symposium IEEE*, 26-29 April, pp. 273-279
- [32] Van der Merwe, R., Doucet, A., de Freitas, N., and Wan, E. (2000). *The Unscented Particle Filter. Technical Report CUED/F-INFENG/TR 380*, Cambridge University Engineering Department.
- [33] Wan, E.A. and van der Merwe, R. (2001) *The Unscented Kalman Filter*. In: Haykin, S., Ed., *Kalman Filtering and Neural Networks*, Wiley, New York, 221-280
- [34] Julier, S.J. and Uhlmann, J.K. (2002a). Reduced Sigma Point Filters for the Propagation of Means and Covariances through Nonlinear Transformations. In *Proceedings of the IEEE American Control Conference*, pages 887-892, Anchorage AK, USA
- [35] Julier, S.J. and Uhlmann, J.K. (2002b). The Scaled Unscented Transformation. In *Proceedings of the IEEE American Control Conference*, pages 4555-4559, Anchorage AK, USA
- [36] NovAtel Inc., “Known Solutions” <https://www.novatel.com/support/known-solutions/what-is-the-effect-of-bad-lever-arms-in-the-gnss-filter/> Last accessed on May, 30th, 2019.
- [37] Kraft, M. (1997) Closed Loop Digital Accelerometer Employing Oversampling Conversion *PhD*, School of Engineering, Coventry University, UK.
- [38] Hong, Sinpy/ Hyung Lee, Man, Chun, Ho, Kwon, Sun-Hong, Speyer, Jason. (2006). Experimental study on the estimation of lever arm in GPS/INS *Vehicular Technology, IEEE Transactions on*. 55. 431 - 448, . 10.1109/TVT.2005.863411.
- [39] Novatel Inc., “ADIS-16488 Product Sheet” <https://www.novatel.com/assets/Documents/Papers/OEM-ADIS16488.pdf> Last accessed on June, 30th, 2019. Coventry University, UK.
- [40] Gruyter, W. De, New, B. (2001). *Inertial Navigation Systems with Geodetic Applications*.

- [41] Nassar, S. (2003) Improving the Inertial Navigation System (INS) Error Model for INS and INS/DGPS Applications, *PhD* Thesis, Department of Geomatics Engineering, University of Calgary, Canada, UCGE Report No. 20183.
- [42] Brown, R. G. and P.Y.C. Hwang. (1997). Introduction to random signals and applied Kalman filtering : with MATLAB exercises 4th ed. John Wiley and Sons, ISBN 978-0-470-60969-9.
- [43] Eng, T. J. E., and Sci, C. (2010). Stochastic stability of the discrete-time constrained extended Kalman filter. 18(2). <https://doi.org/10.3906/elk-0812-17>